SYNTHESIS, PHYSICAL PROPERTIES AND APPLICATIONS OF BISANTHENE-BASED NEAR INFRARED DYES AND SEMICONDUCTORS

LI JINLING

(B.Sc., SOOCHOW UNIVERSITY)

A THESIS SUBMITTED

FOR THE DEGREE OF DOCTOR OF PHILOSOPHY

DEPARTMENT OF CHEMISTRY

NATIONAL UNIVERSITY OF SINGAPORE

2011

ACKNOWLEGEMENTS

First of all, I wish to express my deep and sincere gratitude to my supervisor, Dr. Jishan Wu, for his continuous professional guidance and inspiration, as well as unreserved support throughout my Ph.D. study. His wide knowledge, constructive criticisms and insightful comments have provided a fundamental and significant basis for the present thesis. More importantly, his rigorous research methodology, objectivity and enthusiasm in scientific discovery will deeply impact on my life and future career. With sincere thanks, I want to thank Dr. Chunyan Chi for her constant support and suggestion during the years and I gratefully appreciate her kind help and concern.

I am deeply grateful to all the past/current labmates and collaborators in this group, Dr. Xiaojie Zhang, Chongjun Jiao, Jingjing Chang, Dr. Kai Zhang, Dr. Jun Yin, Dr. Jing Luo, Dr. Baomin Zhao, Dr. Weibin Cui, Suvankar Dasgupta, Zhe Sun, Lijun Zhu, Wangdong Zeng, Dr. Xiaobo Huang, Dr. Ding Luo, Hemi Qu, Jinjun Shao, Chenhua Tong, Lu Mao, Qun Ye, Tianyu Lang, Yong Ni, Gaole Dai. Without their help and encouragements, this work could not have been completed on time.

I would like to express my thanks to National University of Singapore for the supply of the research scholarship.

Finally, I would like to express my loving thanks to my parents, my elder brother, my sister in-law, and my lovely nieces and nephew. Their love and encouragement ignited my passion for the accomplishment documented in this thesis.

TABLE OF CONTENTS

Summary

Polycyclic aromatic hydrocarbons (PAHs) represent one of the most widely investigated classes of compounds in synthetic organic chemistry and materials science. In chapter 1, the background of PAHs was first introduced, followed by an introduction to the recent advances on pentacene and perylene-based electronic materials. Then an overview on the development of bisanthene-based molecules and materials was elucidated and the challenges of using bisanthene as a building block for materials were discussed. Under all these backgrounds, a series of bisanthene-based novel PAHs with characteristic structures and unique photophysical and electrochemical properties have been synthesized and investigated in detail in this PhD work.

In chapter 2, three *meso*-substituted bisanthenes as soluble and stable near infrared (NIR) dyes were successfully prepared in a short synthetic route. Compared with the parent bisanthene, these three compounds exhibit largely improved stability and solubility because of the electron-withdrawing or bulky substitutes at the *meso*-positions. The obtained materials also show bathochromic shift of their absorption and emission spectra into the NIR spectral range with high to moderate fluorescence quantum yields, qualifying them as both NIR absorption and fluorescent dyes. These compounds display amphoteric redox behavior with multistep reversible redox processes, and oxidative titration with $SbCl_5$ gave stable radical cations and the process was followed by UV-vis-NIR absorption spectral measurements.

In chapter 3, ovalene-bis(dicarboximide) (ODI) and dicyano-ovalene-

bis(dicarboximide) (ODI-CN) with liquid crystalline character have been successfully synthesized for the first time starting from bisanthene. These new molecules showed ordered self-assembly both in solution and in solid state because of the strong π-π stacking between the large disc-like cores. Due to attachment of electron-withdrawing imide and cyano- groups, ODI-CN exhibited typical n-type semiconducting behavior and high electron mobility up to 0.1 cm^2/Vs under ambient conditions were achieved in solution processing organic field effect transistor (OFET) devices.

In chapter 4, the synthesis of a series of laterally expanded bisanthene compounds *via* Diels-Alder cycloadditon reaction with dienophile at the bay regions of bisanthene have been investigated. The naphthalene-annulated bisanthenes have been successfully prepared, but synthetic efforts towards more extended π-systems met unexpected hydrogenation or Michael addition reaction. The prepared naphthalene-annulated bisanthenes represent new members of largely extended PAHs with small band gap and near infrared absorption/emission with high-to-moderate fluorescent quantum yields. They also showed amphoteric redox behaviour with multiple reversible redox processes. Furthermore, they have non-planar twisted structures due to the steric congestion as supported by density function theory (DFT) calculations. Lastly, their photostability was also measured which showed that these two naphthalene-annulated bisanthenes possessed a relative low photostability because of their large π system and twisted structures.

Lastly, conclusions on the work introduced above have been made. These new synthesized compounds based on bisanthene not only enrich the family of PAHs, but also provide new useful materials for organic electronics.

Keywords: polycyclic aromatic hydrocarbon, near-infrared dye, bisanthene, ovalene, organic field effect transistor, discotic liquid crystal, Diels-Alder cycloadditon

LIST OF TABLES

LIST OF FIGURES

LIST OF SCHEMES

Chapter 1: Introduction

1.1. Polycyclic aromatic hydrocarbons

Polycyclic aromatic hydrocarbons (PAHs), also known as nanographenes, are a class of compounds that have received attention from the fields of organic chemistry, materials chemistry, theoretical chemistry, cancer research, environmental science, and astronomy.[1,2] In particular, PAHs with extended π-conjugation play a significant role as materials on organic electronics, and by appropriate design and chemical modification, their properties could be tuned for applications such as organic light-emitting diodes (OLEDs), organic field effect transistors (OFETs), solar cells, and sensors.[3] Fundamental contributions to the directed synthesis and characterization of PAHs were pioneered by R. Scholl, E. Clar, and M. Zander *et al.*, who achieved the synthesis of numerous aromatic compounds under drastic conditions at high temperatures with strong oxidation.[1] More recently, thanks to modern synthetic methods and analytical techniques, the efficient synthesis of well-defined PAHs under mild condition has been achieved.[4] The unique electronic and optoelectronic properties of PAHs depended on not only the molecular size but also the edge structure. Generally, two main types of edges exist in PAHs: armchair and zigzag.[5] The arm-chair edged PAHs such as hexa-*peri*-hexabenzocoronene (HBC)[3f] (**1-1**, **Figure 1.1**), electron densities of which are rather evenly distributed over the structure, usually exhibit high chemical stability but a large band gap.[5] On the contrary, zigzag edged PAHs with a smaller benzenoid component, would show a low stability but a convergent band gap.[5] The properties of zigzag edged PAHs have been reported as earlier as in 1993 when two theoretical papers predicted localized

electronic states at the zigzag edges.[6]

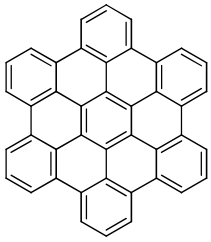

1-1

Figure 1.1 Structure of hexa-*peri*-hexabenzocoronene (HBC) (**1-1**).

One kind of the representative zigzag edged PAHs are acenes (**1-2**, **Figure 1.2**). Acenes and their derivatives are key candidates for organic semiconductors and have attracted great interest from a wide range of researchers.[3b-c,7]

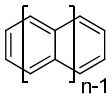

1-2

Figure 1.2 Acene with *n* fused benzene rings, designated as *n*-acene (**1-2**).

Especially, pentacene (n = 5) (**1-2**, **Figure 1.2**), a linear acene consisting of five fused benzene rings, is a benchmark of organic semiconductors with a mobility as high as 5.5 $cm^2\ V^{-1}s^{-1}$ for its polycrystalline thin films.[8] The high performance of the pentacene-based OFETs is generally interpreted by its small reorganization energy (λ) at the molecular level and large intermolecular electronic couplings (transfer integrals, *t*) at the solid-state level.[9] With extension of π-conjugation, λ tends to decrease, whereas *t* increases,[9] and thus much larger acenes than pentacene are expected to be better organic semiconductors. However, pentacene and its higher homologues have drawbacks of poor air-stability owing to their high-lying HOMO energy levels[10] or

chemically labile because of their readily involving chemical reactions, such as Diels-Alder cycloaddition and homodimerization.[11] Thus, it is necessary to introduce bulky substituents for the steric protection from these chemical reactions and yield higher acene derivatives with ambient stability and solution-processability. One successful example is the 6,13-bis(triisopropylsilylethynyl) pentacene (**1-3**, **Figure 1.3**),[12] which is one of the most remarkable soluble p-type semiconductors that has high hole-transport performance: 0.4 cm^2 V^{-1} s^{-1} for its thin film and 1.42 cm^2 V^{-1} s^{-1} for its single crystal nanowires.[13]

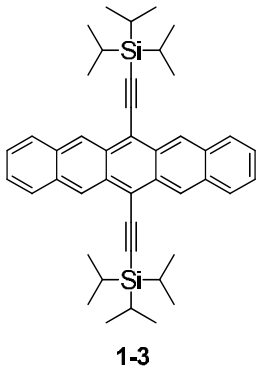

1-3

Figure 1.3 Structure of 6,13-bis(triisopropylsilylethynyl) pentacene **1-3**.

In this molecule, the presence of substituents hinders intermolecular CH-π interaction in the lateral direction, and the molecules show a two-dimensional (2D) π-stack structure instead of a herringbone-type packing, a typical solid-state structure for many molecular organic semiconductors such as pentacene.

Another kind of zigzag edged PAHs is *peri*-fused oligoacenes, namely, *periacene*, such as perylene (**1-4**, **Figure 1.4**), which can be regarded as a *peri*-condensed naphthalene dimer. In the family of colorants, perylene and its derivatives belong to the most important dyes and pigments. Perylene colorants as vat dyes have existed since the beginning of the 20th century,[14] and they are widely commercialized due to

their outstanding chemical, thermal and photochemical stability, their nontoxicity, and low cost.[15] Furthermore, because of their outstanding characters, for example, high molar absorptivities and fluorescence quantum yields, high electron affinities, high electron mobility, and the ready tuning of molecular self-assembly, charge transport as well as air stability by introducing various substituents at the imide N atoms or p-system perylene cores, perylene-3,4:9,10-bis(dicarboximides) (PDIs) has been extensively investigated as active components in organic electronics,[7a,16] especially n-channel organic field-effect transistors (OFETs).[17] Recently, impressive progress has been made by Piliego and co-workers that n-channel OFETs based on *N,N'*-1*H*,1*H*-perfluorobutyl dicyanoperylenecarboxydiimide (**1-6, Figure 1.4**) exhibited a saturation-regime FET mobility of 0.15 cm^2 V^{-1} s^{-1} (0.08 cm^2 V^{-1} s^{-1} in ambient) by solution process.[17d]

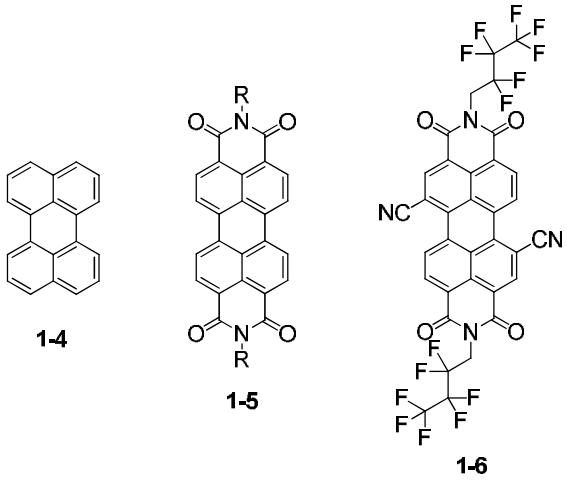

Figure 1.4 Structure of perylene (**1-4**), perylene-3,4:9,10-bis(dicarboximide) (**1-5**) and *N,N'*-1*H*, 1*H*-perfluorobutyl dicyanoperylenecarboxydiimide (**1-6**)

1.2. Overview on the development of bisanthene

Bisanthene, another periacene molecule, could be described as being composed of two anthracene rings conjoined by three single bonds (**1-7**, **Figure 1.5**). However,

compared with pentacene and perylene, research on bisanthene has received insufficient attention in the literature in the past decades. This situation is primarily explained by easy photooxidation of bisanthene molecules in oxygen-containing solution resulting in the formation of a photoproduct with absorption in the shorter wavelength region of the spectrum, which is fully investigated by H. Kuroda and S. M. Arabei *et al.*

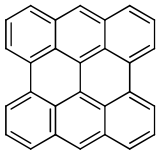

1-7

Figure 1.5 Structure of bisanthene (**1-7**).

In 1960, H. Kuroda reported the absorption spectra of photo-oxide of bisanthene.[18] Previously, they found that the electrical conductivity of an evaporated film of bisanthene increases remarkably as a result of oxygen absorption, which suggested that a charge transfer was taking place between adsorbed oxygen molecules and the surface of the hydrocarbon film. Moreover, the change of the electrical conductivity could be accelerated if the film was illuminated with the visible light, which indicated that some kind of photooxidation take place between oxygen and bisanthene. To approve this hypothesis, accordingly, they did the reaction between oxygen and bisanthene in benzene solution by observing the changes in absorption spectra of bisanthene. The absorption spectra of the oxygen-containing bisanthene solution changed gradually with time, while that of the oxygen-free solution remained unchanged. The intensity of peaks in the wavelength region of 500-700 nm decreased with time when the oxygen–containing solution was illuminated with light. At the same time, the absorption intensity in the region shorter than 400 nm increased. It

seemed obvious that this change was caused by the reaction between bisanthene and the oxygen. Furthermore, they also pointed that the oxygen combined loosely with bisanthene, because the two reactive *meso*-positions of bisanthene were too far apart which was unfavorable for the formation of a stable oxygen addition compound. In addition, they did the reaction between iodine and bisanthene and it showed the similar result as that oxygen-containing bisanthene solution introduced above. Iodine was known to form charge-transfer complex with various polycyclic aromatic hydrocarbons. Therefore, the author asserted that the transformation of the spectra with time was due to the free attachment of an oxygen molecule to the bisanthene and formation of charge transfer complex.

In 2000, Arabei *et al.* reported a detailed analysis of the photochemical oxidation of bisanthene, also by observing the changes in the absorption spectra, and established that the final product of this photo-reaction is bisanthenequinone (**1-11**).[19] Firstly, bisanthene (**1-7**) and bisanthenequinone (**1-11**) were obtained by following the synthetic route as shown in **Scheme 1.1**. Commercially available anthrone (**1-8**) underwent coupling reaction to yield dianthrone (**1-9**), which went through photocycloaddition to give bisanthenequinone (**1-11**) and then it was reduced by zinc to produce bisanthene. Secondly, the absorption and fluorescence spectra of (i) bisanthenequinone in concentrated H_2SO_4, (ii) freshly prepared bisanthene in benzene, and (iii) bisanthene in oxygen-containing benzene under natural illumination for 50 h have been measured for comparison. The spectrum of bisanthenequinone (**1-11**) was measured in concentrated H_2SO_4 because of its very poor solubility in organic solvents. Bisanthene in oxygen-containing benzene under natural illumination, its spectra changed markedly as observed in reference 18, and after two days, the absorption spectrum of this bisanthene solution took the form: the absorption in the

region 500-700 nm disappeared absolutely, while the characteristic absorption bands in the region 350-450 nm came firth. Moreover, the color of the bisanthene solution changed gradually from blue to orange-yellow, and this observed tranformations eventually led to formation of precipitate in the benzene solution. The absorption spectrum of the filtered precipitate dissolved in concentrated H_2SO_4 showed the similar spectrum of bisanthenequinone (**1-11**) in this acid, which allowed the authors to declare unambiguously that the precipitated is nothing more than bisanthenequinone (**1-11**) as the final photoproduct of bisanthene.

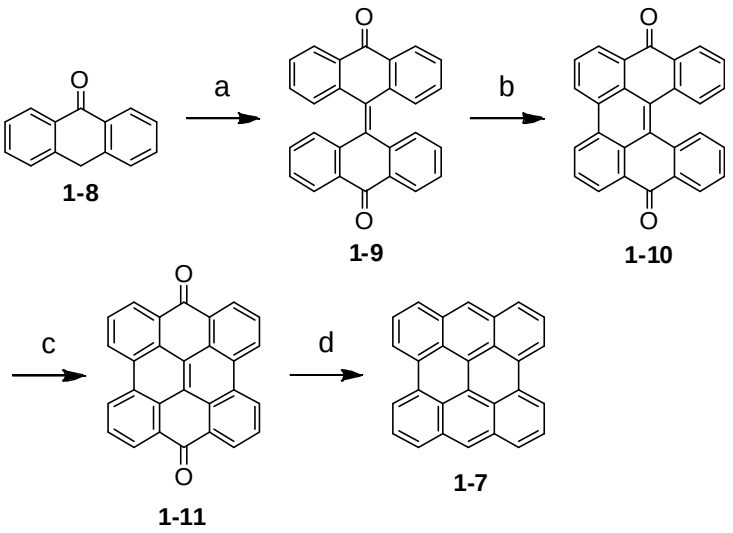

Scheme 1.1 Synthetic route to bisanthene (**1-7**) and bisanthenequinone (**1-11**): (a) Pyridine, piperidine, pyridine-*N*-oxide, $FeSO_4$; (b) *hv*; (c) *hv*; (d) Zn, CH_3COOH, pyridine.

Finally, the possible mechanism of this photooxidation has been proposed as shown in **Scheme 1.2**. Oxygen atoms combine the opposite carbon atoms of the hydrocarbon ring leading to the endomonoperoxide (**1-12**) and endobiperoxide (isomers **1-13** and **1-14**). The endoperoxides **1-12**, **1-13**, **1-14** were very unstable, they can rupture on C-O bond and form compound **1-15** and, finally, bisanthenequinone **1-11**.

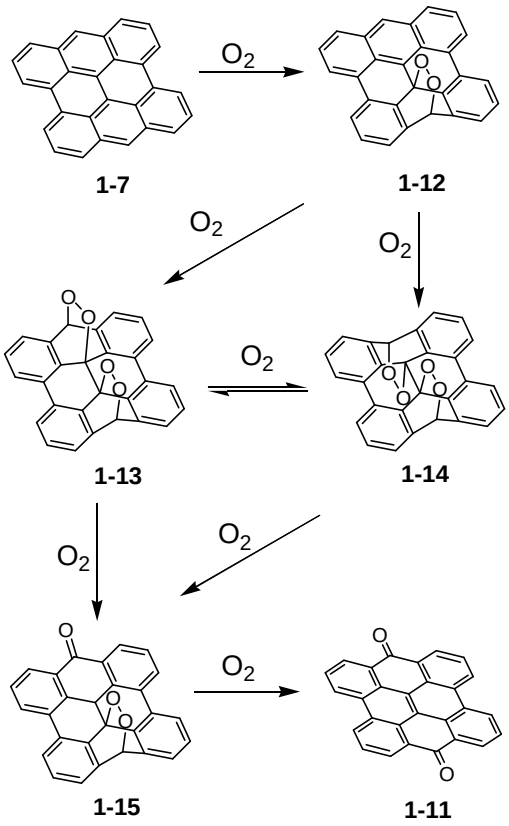

Scheme 1.2 Proposed mechanism for the oxidation of bisanthene (**1-7**).

In 1970, D. R. Maulding reported the photochemical preparation of 4,11-diphenylbisanthene (**1-19**),[20] which have been used as material for phototropic ruby laser Q-switches in 1977.[21] **1-19** was first synthesized through three steps with overall yield of 20% by the sequence from bianthrone (**1-9**) to bisanthenequinone (**1-11**), then to 4,11-dihydroxy-4,11-diphenyl-dihydrobisanthene (**1-21**) (**Scheme 1.3**)[22]. In parallel to this work, the author reported a more convenient approach by the photocyclization of the diphenylbianthracenediol (**1-16**), which can be prepared from bianthrone (**1-9**) in good yield. Ultraviolet irradiation of benzene solution of **1-16** and iodine exposed to the atmosphere produced hydrocarbons **1-19** in 59% yield. The limiting factor in maximizing the yield of **1-19** was the photoinstability of itself, because the photooxidation of **1-19** and oxygen was also occurring during the reacting process. In

addition, varying the amounts of iodine in this reaction had little effect on the yield. Since the decomposition of **1-19** was much slower when irradiated under nitrogen. Therefore, they performed this reaction under nitrogen atmosphere. Surprisingly, the final yield decreased to 5%, and diphenyldibenzoperylene (**1-17**) become the major product, which rapidly converted to photooxide **1-20**, but not **1-19**, when exposed to oxygen. This phenomenon revealed that diol **1-18** and not hydrocarbon **1-17** was responsible for the formation of **1-19**. To confirm this statement, they also did irradiation of benzene solution of **1-18** in the presence of iodine giving **6** in 79% yield. Finally, 10,10'-diphenyl-9,9'-bianthranyl (**1-22**) was not detected in the irradiation from **1-16** to **1-19**, and the possibility is that **1-22** is not an intermediate in this reaction. In this report, the author analyzed the reaction condition and the limiting factors of the yield, as well as the intermediate compounds in the course of irradiation in detail.

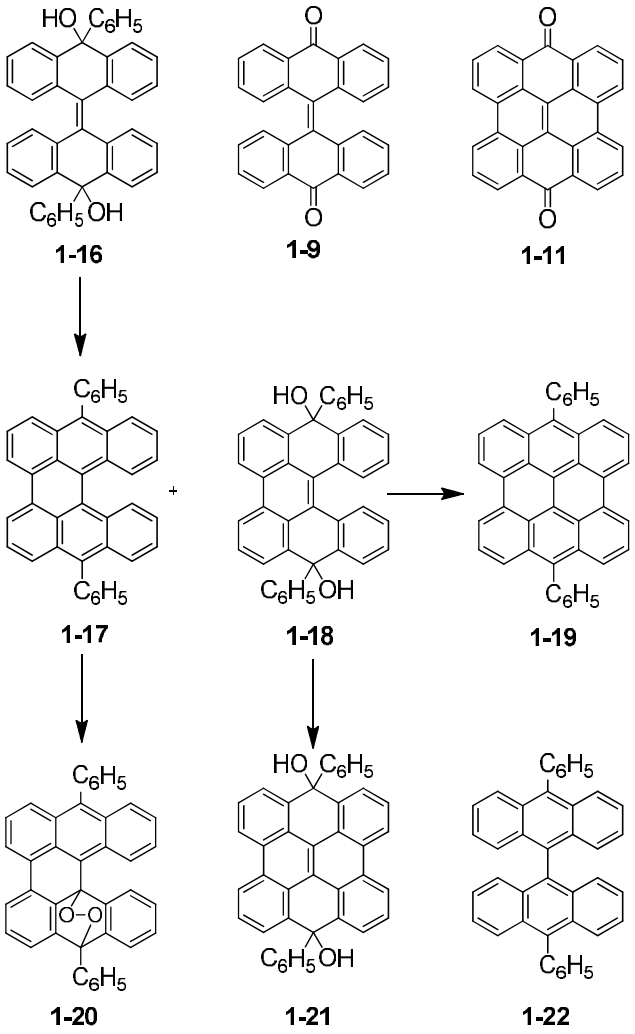

Scheme 1.3 Synthesis route to 4,11-diphenylbisanthene (**1-19**).

Similarly to pentacene, the high reactivity of bisanthene is due to its high-lying HOMO energy level, and it easily undergoes addition reaction with the singlet oxygen in air.[18,19,23] In addition, bisanthene has a poor solubility in organic solvents because of its strong aggregation between molecules, which also contributes much to the insufficient attention that bisanthene received. Actually, bisanthene has far-red absorption at 662 nm, indicating great potential as a building block for near infrared (NIR) dyes. Therefore, our group recently developed different approaches to prepare a series of soluble and stable bisanthene-based near infrared (NIR) dyes: (1)

substitution by electron-withdrawing dicarboxylic imide groups at the zigzag edges;[24] (2) quinoidization along the short-axis.[25]

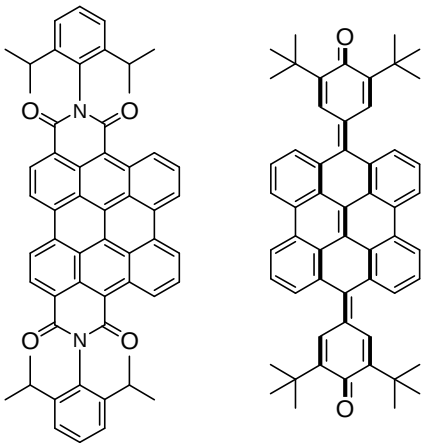

1-23 **1-24**

Figure 1.6 Structures of bisanthene bis(dicarboxylic imides) (**1-23**) and quinoidal bisanthene (**1-24**).

Electron-withdrawing dicarboxylic imides have been attached to zigzag edge of bisanthene (**1-23**) **Figure 1.6**) and the synthetic route is shown in **Scheme 1.4**.[24] The synthesis started from Friedel-Crafts reaction of anthracene (**1-25**) with oxalyl chloride to provide the aceanthrylene-1,2-dione (**1-26**), which was subsequently oxidized, mono-brominated and imidizated to give compound (**1-29**). Compound (**1-30**) was then synthesized by [Ni(cod)$_2$]-mediated Yamamoto homo-coupling of **1-29** in medium yield, which was followed by *t*-BuOK- and DBN-mediated cyclization reaction to give the **1-23** in acceptable yield. The resulting **1-23** has good solubility in organic solvents, and it has a maximum absorption at 830 nm, about 168 nm red-shift compared with the parent bisanthene, which can be ascribed to the substitution by electron-withdrawing dicarboxylic imide groups which lead to a convergence of HOMO-LUMO energy gaps. Consequently, compound **1-27** was an important soluble and stable NIR dyes. Furthermore, the low LUMO level (-4.27 ev) of **1-23** could be

used as building block to construct n-type semiconductors for electronic devices such as n-channel field effect transistors and solar cell.

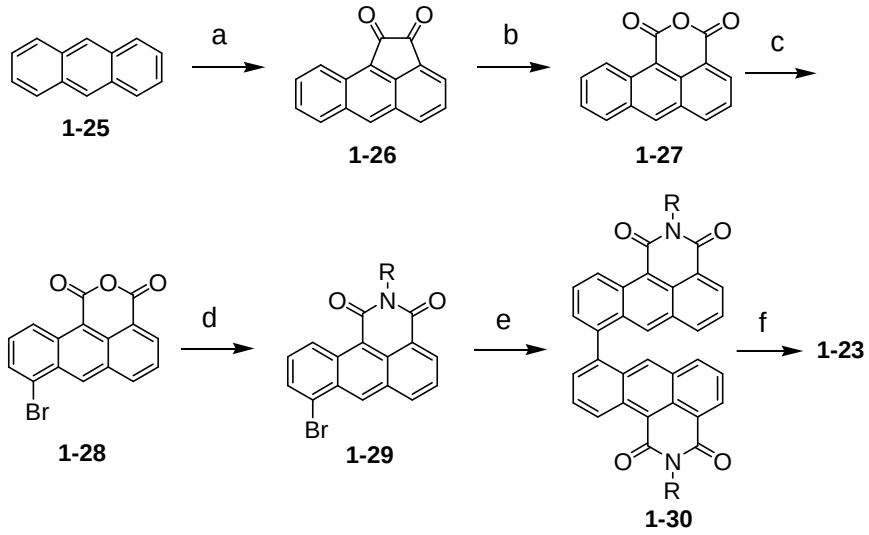

Scheme 1.4 Synthetic route to compounds **1-23**: (a) Oxalyl chloride, $AlCl_3$, CS_2, 0 ^oC, 86%; (b) Oxone, methanol, reflux, 95%; (c) Br_2, conc. H_2SO_4, RT, 50%; (d) 2,6-diisopropylaniline, propionic acid, reflux, 60%; (e) $[Ni(cod)_2]$/COD/BPy, DMF, toluene, 80 ^oC, 60%, BPy = bipyridine; (f) *t*-BuOK, DBN, diglyme, 130 ^oC, 31%.

Quinoidization along the short-axis of bisanthene (**1-24, Figure 1.6**) has been also performed and the synthetic route is shown in **Scheme 1.5**.[25] Bisanthenequinone (**1-11**) reacted with the Grignard reagent of (2,6-di-*tert*-butylphenoxy)trimethylsilane to give diol (**1-31**), which was subsequently desilylated with tetrabutylammonium fluoride (TBAF) and dehydration of the as-formed phenol by $POCl_3$ in pyridine afforded the desired **1-24**. Compound **1-24** shows intense NIR absorption with extended π-conjugation along the short axis, higher solubility than bisanthenequinone, as well as good thermal and photo-stability.[25] In comparison with bisanthene in dichloromethane and bisanthenequinone (**1-11**) in concentrated H_2SO_4, the absorption maximum of this new quinoidal bisanthene (**1-24**) exhibited 28 nm and 128 nm red-shifts, respectively. In addition, **1-24** exhibits clear amphoteric multistage redox behavior on the cyclic

voltammogram, consisting of two reversible one-electron oxidation waves and two reversible one-electron reduction waves. This multistage reversible redox waves provide evidence for the formation of stabilized singly and doubly charged species of quinoidal (**1-24**) as shown **Figure 1.7**, which qualify it a potential ambipolar charge transporting material. **1-24** represents a rare example of quinoidal large polycyclic aromatic hydrocarbons.

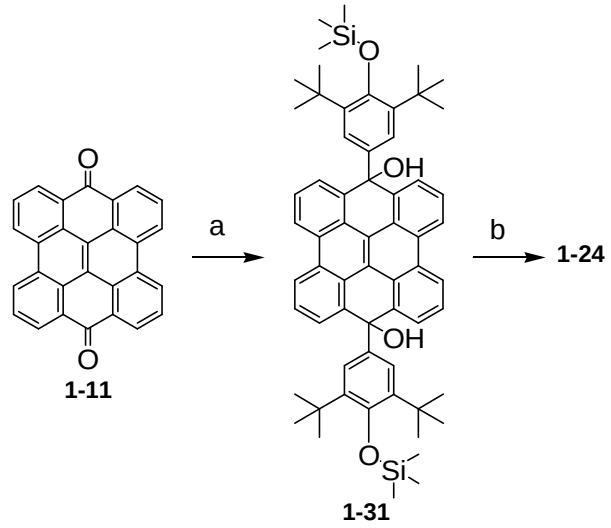

Scheme 1.5 Synthetic route to quinoidal bisanthene (**1-24**): (a) RMgBr, THF, 66%, R = (2,6-di-*tert*-butylphenoxy)trimethylsilane; (b) TBAF, THF; (c) $POCl_3$, pyridine, 20%.

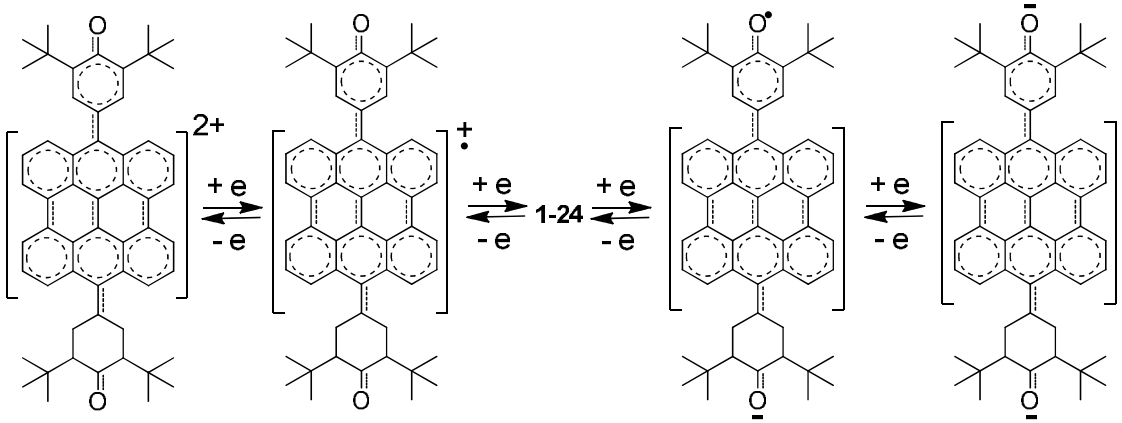

Figure 1.7 Four stable redox states of **1-24** through the amphoteric redox processes.

Besides the modifications on the zigzag edges of bisanthene (**1-7**), Diels-Alder reaction with dienophiles, such as maleic anhydride, also can be performed on bisanthene (**1-7**), because it has a diene character (**1-7-2**) at bay positions as shown in **Figure 1.8** Therefore, bisanthene can be regarded as a building block to build up higher annelated polycyclic aromatic hydrocarbons (benzogenic diene synthesis).

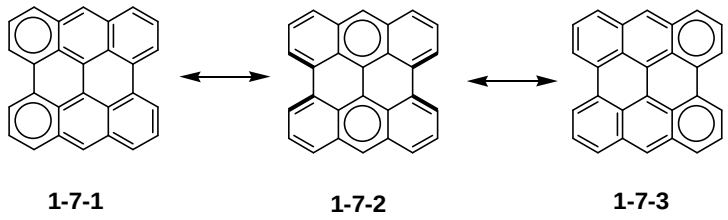

Figure 1.8 The sextet migration resonance structure of bisanthene

In 1948, E. Clar reported that bisanthene (**1-7**) reacted twice with an excess of maleic anhydride in boiling nitrobenzene and yielded the dianhydride (**1-33**), which was decarboxylated by sublimation with soda-lime in vacuum to give the compound ovalene (**1-32**) (**Scheme 1.6**)[26].

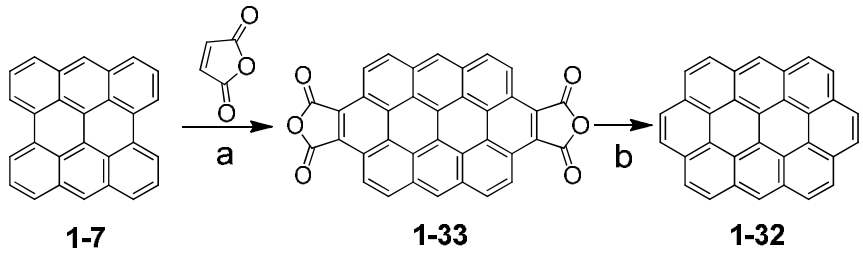

Scheme 1.6 Synthetic route to ovalene (**1-32**) by Clar: (a) nitrobenzene; (b) Soda lime, 400 ^{o}C.

Geometrically, ovalene (**1-32**) may be regarded as a two-dimensional analogue of fullerene C70, since their cross-sections are approximately equivalent. The large aromatic π-system of ovalene (**1-32**), which promise good orbital overlap between

neighboring molecules in the solid state, makes ovelene derivatives interesting candidates for organic opto-electronics, provided that they can be soluble and film-forming. The elliptical shape of the aromatic core means that the introduction of solubilizing substituents may lead to columnar liquid crystalline (LC) self-assembled systems with an associated efficient transport of excitons and charge along the columns.

Therefore, in 2006, based on these considerations, S. Saïdi-Besbes *et al*. reported the soluble benzobisanthene esters (**1-35**) and ovalene esters (**1-36**),[27] derived from anhydride **1-34** and **1-33** since Clar's first synthesis of the insoluble parent hydrocarbons and the carboxylic anhydrides,[26] by an efficient esterification process (**Scheme 1.7)** The author pointed out that the appropriate choice of the alkyl substituents **(**R = 2-ethylhexyl**)** leads to ovalene esters to undergo hexagonal columnar self-assembly at room temperature over extremely large temperature ranges, but with a very high cleaning point above 375 ^{o}C.

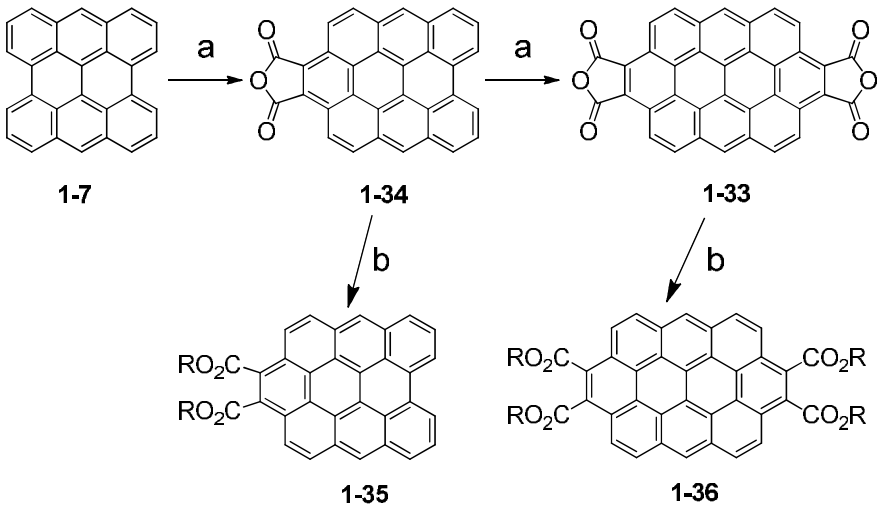

Scheme 1.7 Synthetic route to benzobisanthene esters (**1-35**) and ovalene esters (**1-36**): (a) maleic anhydride, nitrobenzene; (b) RBr, ROH, DBU. DBU = 1,8-diazabicyclo[5.4.0]undec-7-ene**,** R = n-propyl, 2-ethylhexyl.

In 2009 and 2010, H. Eric *et al.* investigated the Diels-Alder cycloaddition of periacenes at bay regions, which provides the implications for metal-free growth of single-chirality carbon nanotubes.[28, 29] Originally, they studied the Diels-Alder reactivity of periacene series phenanthrene, perylene and bisanthene. Phenanthrene itself has never been seen to undergo a bay region Diels-Alder reaction. However, Diels-Alder reaction of *meso*-substituted bisanthene with acetylene,[28] as shown in **Scheme 1.8**, 4,11-dimesitylbisanthene (**1-37**) was chosed because the methyl groups *ortho* to the biaryl bonds were incorporated to force the appendages out-of-plane, thereby enhancing solubility, and also to block any cycloadditions at the central rings of the two anthracene subunits. When **1-37** was heated with diethyl acetylenedicarboxylate in toluene for 24 h at 120 ^{o}C, 1:1 adduct **1-38** and 2:1 adduct **1-39** were obtained, and the 1:1 adduct **1-38** can be easily pushed to completed 2:1 adduct **1-39**. But in the same conditions, only the 1:1 cycloadduct was formed for perylene (**1-4**). These experimental results confirmed that Diels-Alder cycloaddition become progressively easier in the bay regions at the end of periacenes that represent progressively longer strips of amchair nanotube side-walls.

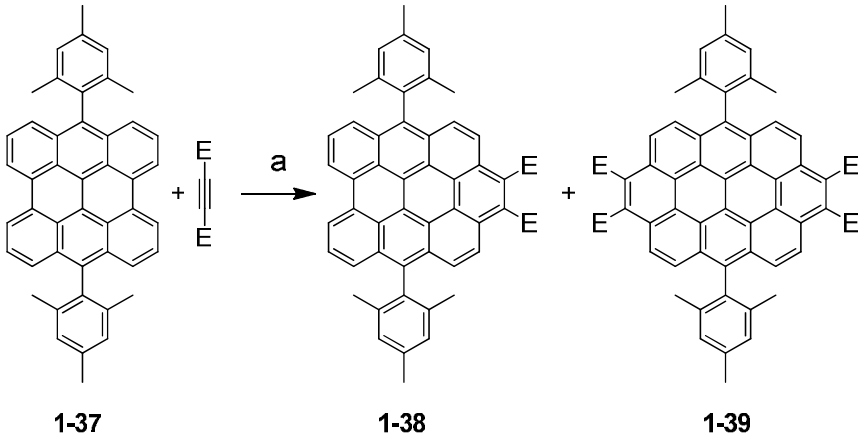

Scheme 1.8 Diels-Alder additions of diethyl acetylenedicarboxylate to 4,11-dimesitylbisanthene (**1-37**): (a) toluene, 120 ^{o}C, 1 day.

For the practical growth of nanotubes from hydrocarbon templates, each Diels-Alder cycloaddition/rearomatization cycle must leave a new unsubstituted benzene ring. Therefore, they subsequently reported one-step conversion of aromatic hydrocarbon bay regions into new unsubstituted benzene rings by nitroethylene, generated *in situ* from 2-nitroethanol by dehydration with phthalic anhydride. As shown in **Scheme 1.9** based on 4,11-dimesitylbisanthene (**1-38**).[29] This work implied the possibility to synthesize single-chirality carbon nanotubes via a metal-free approach from a suitable cylindrical template provide a meaningful guidance for construct finite graphene in the future.

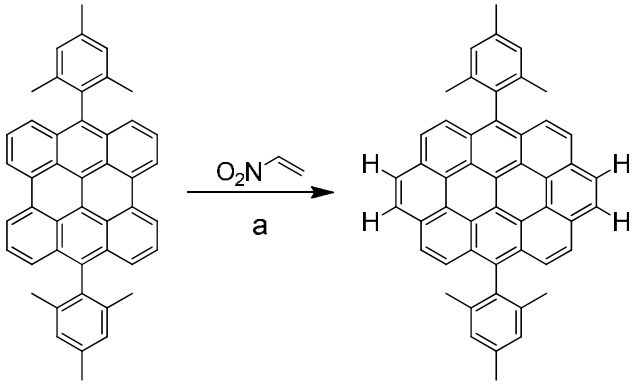

1-37 **1-40**

Scheme 1.9 Diels-Alder addition of nitroethylene to 4,11-dimesitylbisanthene (**1-37**): (a) toluene, 135 ^{o}C.

1.3 Objectives

Although bisanthene has good characters such as small bandgap, planar π system, to be as a good building block for electronics or to construct novel PAHs, the investigation on bisanthene has not been so prosperous because of its photo-unstability and poor solubility. Based on the knowledge above, new soluble and stable bisanthene-based molecules and materials are the major research objectives in this

thesis, which include several aspects:

(1) Synthesis of new soluble and stable NIR dyes based on bisanthene by substitution at its active *meso*-positions with either electron-withdrawing groups or bulky group.

(2) Preparation of n-type cyanated ovalene diimides via Diels-Alder reaction between bisanthene and maleic anhydride and its application on OFET devices.

(3) To construct more extended π systems based on bisanthene via Diels-Alder reaction with dienophiles at the bay regions.

References

1. a) Clar, E. *Polycyclic Hydrocarbons*; Academic Press: New York, 1964; Vol. I/II. b) Clar, E. *The Aromatic Sextet*; Wiley-VCH: London, 1972. c) Scholl, R.; Seer, C.; Weitzenbök, R. *Chem. Ber.* **1910**, *43*, 2202. d) Scholl, R.; Seer, C. *Liebigs Ann. Chem.* **1912**, *394*, 111. e) Scholl, R.; Seer, C. *Chem. Ber.* **1922**, *55*, 330. f) Clar, E.; Stewart, D. G. *J. Am. Chem. Soc.* **1953**, *75*, 2667. g) Clar, E.; Schmidt, W. *Tetrahedron* **1979**, *35*, 2673. h). Zander, M. *Handbook of Polycyclic Aromatic Hydrocarbons*, Marcel Dekker, New York, 1983. Harvey, R. G. in *Polycyclic Aromatic Hydrocarbons*, Wiley-VCH, Wein heim, **1997**.

2. a) Randić, M. *Chem. Rev.* **2003**, *103*, 3449-3605. b) De Proft, F.; Geerlings, P. *Chem. Re*v. **2001**, *101*, 1451. c) Schleyer, P. V. R. *Chem. Rev.* **2001**, *101*, 1115. d) Mitchell, R. H. *Chem. Rev.* **2001**, *101*, 1301. e) Slayden, S. W.; Liebman, J. F. *Chem. Re*v. **2001**, *101*, 1541. f) Goh, S. H.; Harvey, R. G. *J. Am. Chem. Soc.* **1973**, *95*, 242. g) Harvey, R. G.; Zhang, J.-T.; Luna, E.; Pataki, J. *J. Org. Chem.* **1998**, *63*, 6405.

3. a) Bendikov, M.; Wudl, F.; Perepichka, D. F. *Chem. Rev.* **2004**, *104*, 4891 – 4945; b) Anthony, J. E.; *Chem. Rev.* **2006**, *106*, 5028 –5048; c) Anthony, J. E.; *Angew. Chem.* 2008, *120*, 460 –492; *Angew. Chem. Int. Ed.* 2008, *47*, 452 – 483; d) Murphy, A. R.; Fréchet, J. M. J.; *Chem. Rev.* **2007**, *107*, 1066 –1096. e) Wu, J. *Curr. Org. Chem.* **2007**, *11*, 1220. f) Wu, J.; Pisula, W.; Müllen, K. *Chem. Rev.* **2007**, *107*, 718.

4. a) Harvey, R. G. *Polycyclic Aromatic Hydrocarbons*; Wiley-VCH: New York, 1997. b) *Carbon Rich Compounds I/II*; Topics in Current Chemistry; Springer: Berlin, 1998, Vol. 196; 1999, Vol. 201. c) Hagen, S.; Hopf, H. *Top. Curr. Chem.*

1998, *196*, 44. d) Feng, X.; Pisula, W.; Müllen, K. *Pure. Appl. Chem.* **2009**, *81*, 2203-2224.

5. a) Stein, S. E. *Acc. Chem. Res.* **1991**, *24*, 350-356. b)Jiang, D. E.; Sumpter, B. G.; Dai, S. *J. Chem. Phys.* **2007**, *127*, 124703. c) Jiang, D. E.; Dai, S. *Chem. Phys. Lett.* **2008**, *466*, 72. d) Jiang, D. E.; Dai, S. *J. Phys. Chem. A* **2008**, *112*, 332–335. e) Chen, Z. F.; Jiang, D. E.; Lu, X.; Bettinger, H. F.; Dai, S.; von Ragué, Schleyer, P.; Houk, K. N. *Org. Lett.* **2007**, *9*, 5449–5452. f) Liu, Y.; Dobrinsky, A.; Yakobson, B. I. *Phys. Rev. Lett*, **2010**, *105*, 235502.

6. a) Kobayashi, K. *Phys. Rev. B* **1993**, *48*, 1757. b) Klein, D. J. *Chem. Phys. Lett.* **1994**, *217*, 261.

7. a) Dong, H.; Wang, C.; Hu, W. *Chem. Comm.*, **2010**, *46*, 5211-5222. b) Bendikov, M.; Wudl, F. *Chem. Rev.* **2004,** *104*, 4891-4945. c) Bendikov, M.; Duong, H. M.; Starkey,K.; Houk, K. N.; Carter, E. A.; Wudl, F. *J. Am. Chem. Soc.* **2004**, *126*, 7416-7417.

8. Lee, S.; Koo, B.; Shin, J.; Lee, E.; Park, H.; Kim, H. *Appl. Phys. Lett.* **2006**, *88*, 162109.

9. a) Bredas, J.-L.; Beljonne, D.; Coropceanu, V.; Cornil, J. *Chem. Rev*. **2004**, *104*, 4971–5004. b) Coropceanu, V.; Kwon, O.; Wex, B.; Kaafarani, B. R.; Gruhn, N. E.; Durivage, J. C.; Neckers, D. C.; Bredas, J.-L. *Chem. Eur. J.* **2006**, *12*, 2073–2080. c) Valiyev, F.; Hu, W.-S.; Chen, H.-Y.; Kuo, M.-Y.; Chao, I.; Tao, Y.-T. *Chem. Mater*. **2007**, *19*, 3018–3026. d) Niimi, K.; Shinamura, S.; Osaka, I.; Miyazaki, E.; Takimiya, K. *J. Am. Chem. Soc.* **2011**, *133*, 8732–8739

10. Maliakal, A.; Raghavachari, K.; Katz, H.; Chandross, E.; Siegrist, T. *Chem. Mater.*

2004, *16*, 4980–4986.

11. Payne, M. M.; Odom, S. A.; Parkin, S. R.; Anthony, J. E. *Org. Lett.* **2004**, *6*, 3325–3328.

12. a) Anthony, J. E.; Brooks, J. S.; Eaton, D. L.; Parkin, S. R.; *J. Am. Chem. Soc.*, **2001**, *123*, 9482. b) Anthony, J. E.; Eaton, D. L.; Parkin, S. R. *Org. Lett.*, **2002**, *4*, 15, c) Anthony, J. E. *Angew. Chem., Int. Ed.* **2008**, *47*, 452–483.

13. a) Sheraw, C. D.; Jackson, T. N.; Eaton, D. L.; Anthony, J. E. *Adv. Mater.* **2003**, *15*, 2009. b) Kim, D. H.; Lee, D. Y.; Lee, H. S.; Lee, W. H.; Kim, Y. H.; Han, J. I.; Cho, K. *Adv. Mater.* **2007**, *19*, 678.

14. a) Kardos, M.; D.R.P. 276357, **1913**; Kardos, M. *Chem. Abstr.* **1914**, *8*, 22317. b) M. Kardos, D.R.P. 276956, **1913**; Kardos, M. *Chem. Abstr.* **1915**, *9*, 6398.

15. Zollinger, H. *Color Chemistry*, 3rd ed., Wiley-VCH, Weinheim, **2003**.

16. a) Weil, T.; Vosch, T.; Hofkens, J.; Peneva, K.; Müllen, K.; *Angew. Chem. Int. Ed.* **2010**, *49*, 2-28. b) Anthony, J. E.; Facchetti, A.; Heeney, M.; Marder, S. R.; Zhan X. *Adv. Mater.* **2010**, *22*, 3876–3892. c) Li, C.; Liu, M.; Pschirer, N. G.; Baumgarten, M.; Müllen, K. *Chem. Rev.* **2010**, *110*, 6817–6855. d) Wen Y.; Liu, Y. *Adv. Mater.* **2010**, *22*, 1331–1345.

17. a) Jones, B. A.; Ahrens, M. J.; Yoon, M. H.; Facchetti, A.; Marks, T. J.; Wasielewski, M. R. *Angew. Chem. Int. Ed.* **2004**, *43*, 6363; b) Ling, M.; Erk, P.; Gomez, M.; Koenemann, M.; Locklin, J.; Bao, Z. *Adv. Mater.* **2007**, *19*, 1123; c) Weitz, R. T.; Amsharov, K.; Zschieschang, U.; Villas, E. B.; Goswami, D. K.; Burghard, M.; Dosch, H.; Jansen, M.; Kern, K.; Klauk, H. *J. Am. Chem. Soc.* **2008**,

130, 4637; d) Piliego, C.; Jarzab, D.; Gigli, G.; Chen, Z.; Facchetti, A.; Loi, M. A.; *Adv. Mater.* **2009**, *21*, 1573; e) Schmidt, R.; Oh, J. H.; Sun, Y.; Deppisch, M.; Krause, A.; Radacki, K.; Braunschweig, H.; Könemann, M.; Erk, P.; Bao, Z.; Würthner, F. *J. Am. Chem. Soc.* **2009**, *131*, 6215.

18. Kuroda, H. *J. Chem. Phys.* **1960**, *33*, 1586-1587.

19. Arabei, S. M.; Pavich, T. A. ***J. Appl. Spectrosc.*****2000**, *67*, 236-244.

20. Maulding, D. R. *J. Org. Chem.* **1970**, *35*, 1221-1223.

21. Gorelenko, A. Ya.; Tolkachev, V. A.; khalimanovich, D. M. ***J. Appl. Spectrosc.*****1977**, *26*, 710-712.

22. Sauvage, G. *Ann, Chim.* **1947**, *2*, 844.

23. Clar, E. *Chem. Ber*. **1948**, *81*, 52–63.

24. Yao, J. H.; Chi, Ch.; Wu, J. Loh, K-P. *Chem. Eur. J*. **2009**, *15*, 9299 – 9302.

25. Zhang, K.; Huang, K-W.; Li, J. Chi, Ch.; Wu, J. *Org. Lett.* **2009**, *11*, 4854-4857.

26. a) Clar, E. *Nature, Lond*. **1984**, *161*, 238. b) *Chem. Ber.* **1949**, *82*, 55.

27. Saïdi-Besbes, S.; Grelet, É.; Bock, H. *Angew. Chem. Int. Ed.* **2006**, *45*, 1783 – 1786.

28. Fort, E. H.; Nonovan, P. M.; Scott, L. T.; *J. Am. Chem. Soc.* **2009**, *131*, 16006-16007.

29. Fort, E. H.; Scott, L. T.; *Angew. Chem. Int. Ed.* **2010**, *49*, 6626-6628.

Chapter 2: *meso*-Substituted Bisanthenes as Soluble and Stable NIR Dyes

2.1 Introduction

Near infrared (NIR) dyes[1] with absorption and/or emission in the spectral range of 700-1400 nm are of importance for a lot of potential applications such as high-contrast bio-imaging,[2] optical recording,[3] NIR laser filter,[4] NIR photography,[5] solar cells,[6] and optical limiting at telecommunication wavelength.[7] However, many commercially available NIR dyes such as cyanine dyes suffer from inevitable drawbacks due to their insufficient photostability.[8]

Polycyclic aromatic hydrocarbons (PAHs) usually exhibit excellent chemical stability and photostability with respect to the traditional cyanine dyes and one good example is the rylene (oligo-*peri*-naphthalene) which is a type of important stable dye/pigment used in industry.[9] For the design of PAH-based NIR dyes, largely extended π-conjugation is usually required. For example, the alkyl or carboximide-substituted rylene molecules show NIR absorption only when the molecular length reaches four naphthalene units (quaterrylene).[10] Moreover, as introduced in the chapter 1, the band gap of a PAH molecule depended on not only the molecular size, but also the edge structure.[11] The arm-chair edged PAHs usually exhibit high chemical stability but a large band gap. On the other hand, theoretical calculations suggested that zigzag edged PAH molecules with less amount of benzenoid component would show low band gap with near infrared absorption.[12] Zigzag edged, *peri*-fused oligoacenes, namely *periacenes*, are expected to exhibit NIR absorption

and emission.[12] As one member of the periacene family, bisanthene (**2-1**, **Figure 2.1**) was reported to show far-red absorption with absorption maximum at 662 nm.[13] However, the parent bisanthene is a very unstable compound and it decomposes quickly in solution under ambient air and light condition. This is mainly because of its high-lying HOMO level and it is ready to undergo addition reaction with the singlet oxygen in air.[13] Like the zigzag edged pentacene compound,[11b] the reactive sites in bisanthene are the *meso*-positions of the zigzag edges. We recently found that attachment of two electron-withdrawing dicarboxylic imide groups at the zigzag edges of the bisanthene (**2-2**, **Figure 2.1**) not only largely improved its stability but also significantly shifted the absorption to the NIR spectral range with the absorption maximum at 830 nm.[14] In addition, quinoidal bisanthene (**2-3**, **Figure 2.1**) was also prepared and it exhibited good stability with NIR absorption.[15] While these methods are successful, we are looking for alternative approach to prepare soluble and stable bisanthene-based NIR dyes by a short synthetic route. Herein, we report that substitution at the active *meso*-positions of the bisanthene with either aryl or alkyne group is also an efficient way to achieve our target. In this work, two aryl-substituted bisanthenes **2-4** and **2-5** and one triisopropylsilylethynyl-substituted bisanthene **2-6** (**Figure 2.1**) were prepared. The substituents are chosen based on several considerations: (a) conjugation effect: the aryl and alkyne groups are supposed to at least partially extend the π-conjugation with the central bisanthene units so that the absorption and emission spectral can shift into NIR spectral range; at the same time, the extended π-conjugation can also improve the stability of the electron-rich bisanthene unit by extended electron delocalization; (b) steric effect: the bulky substitution at the *meso*-positions can prevent the oxidative addition of singlet oxygen to the bisanthene core; at the meanwhile, the solubility can be also improved due to

diminished intermolecular interactions (especially for compound **2-4**); (c) electronic effect: to form stable bisanthene derivatives, electron withdrawing groups should be attached; herein, three substituents with different electron donating/accepting capabilities are introduced, in particular, the trifluoromethylphenyl in compound **2-5** and the triisopropylsilylethynyl groups in **2-6** are both electron withdrawing groups which are expected to enhance the stability of the electron rich bisanthene. The photophysical properties and electrochemical behavior of compound **2-4** to **2-6** were studied and the effect of the different substituents on their properties was discussed in details. In addition, geometric structure and molecular packing of one of these compounds was studied by crystallographic analysis and their potential as semiconductors in field effect transistor (FET) was also discussed.

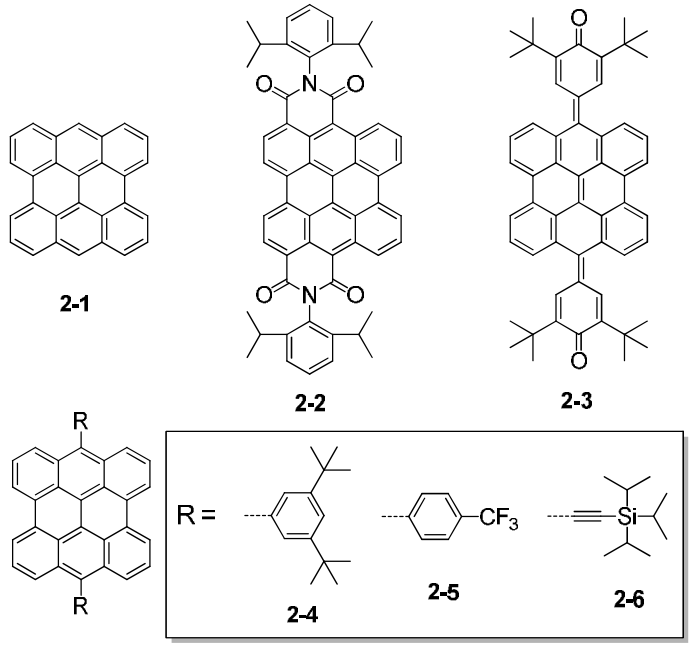

Figure 2.1 Structures of bisanthene (**2-1**) and its derivatives **2-2** - **2-6**.

2.2 Results and Discussions

2.2.1 Synthesis

The synthesis of compounds **2-4**, **2-5** and **2-6** are depicted in **Scheme 2.1**. Bisanthenequinone (**2-7**) was first prepared in gram scale according to literature.[13] The subsequent chemistry is similar to that of pentacenequinone.[16] Compound **2-7** reacted with the Grignard reagent of the respective arenes or the lithium reagent of triisopropylsilylacetylene in anhydrous THF to give the respective alcohols **2-8a-c** in 50-60% yields. This was followed by dehydroxylation and reductive aromatization with NaI/NaH_2PO_2 to afford the target compounds **2-4**, **2-5** and **2-6** in good yields. Actually, this two-step reaction can also be done in one pot without separation of the intermediate compounds **2-8a-c**. Thus this synthetic route is obviously simple and straightforward and the target compounds can be obtained shortly by simple column chromatography purification. Compounds **2-4** to **2-6** have good solubility in normal organic solvents such as chloroform and THF, in particular, the 3,5-di-*tert*-butylphenyl-substituted bisanthene **2-4** shows the highest solubility due to the very bulky substitution. All the intermediate compounds and the final products are well characterized by NMR spectroscopy and high resolution mass spectrometry.

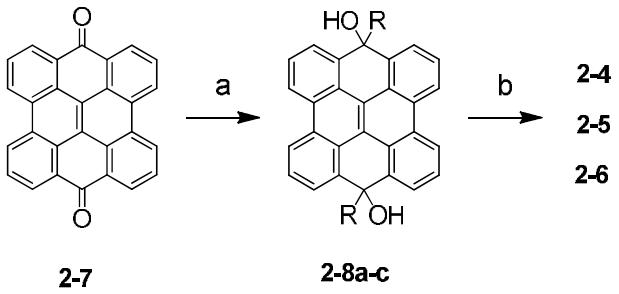

Scheme 2.1 Synthetic route to the *meso*-substituted bisanthenes **2-4**, **2-5** and **2-6**: (a) R-MgBr or R-Li, THF, RT for 2-3 days, 50%-60%; (b) NaI, $NaH_2PO_2 \cdot H_2O$, Acetic acid, 130 ^oC, 70%-72%.

2.2.2 Photophysical Properties and Theoretical Calculations

The UV-vis-NIR absorption and fluorescence spectra of **2-4**, **2-5** and **2-6** recorded in toluene are shown in **Figure 2.2** and the data are collected in **Table 2.1**. Solutions of **2-4** to **2-6** in toluene display a blue color and well-resolved absorption bands between 500 and 800 nm with the maximum peak at 687 (ε = 38438 $M^{-1}cm^{-1}$; ε: molar extinction coefficient in $M^{-1}cm^{-1}$), 683 (ε = 45098 $M^{-1}cm^{-1}$), and 727 (ε = 55690 $M^{-1}cm^{-1}$) nm, respectively. Compared with the absorption spectra of bisanthene,[13] there is about 25, 21 and 65 nm red-shift for **2-4**, **2-5** and **2-6**, respectively. The red-shift for all these compounds indicates that π-conjugation of the bisanthene core is further extended by incorporation of the aryl and triisopropylsilylethynyl moieties. Density function theory (DFT) (B3LYP/6-31G**) calculations of **2-4** to **2-6** were then conducted to further understand their geometric and electronic structures. The optimized structure and the frontier molecular orbital profiles of **2-4** to **2-6** are shown in **Figure 2.3**. The phenyl moieties in **2-4** and **2-5** are twisted about 80^{o} with respect to the bisanthene plane, as a result, only weak electron delocalization between the phenyl ring and the bisanthene units was observed for **2-4** and **2-5**. However, for **2-6**, obvious electron delocalization between the ethynyl moiety and the bisanthene unit was observed. Such a structural difference accounts for the difference in their absorption spectra where the largest red-shift was found for **2-6**. In addition, time-dependant DFT calculations also predict that the absorption maxima for **2-4** to **2-6** are 716.3, 714.4 and 785.6 nm, respectively, and such tendency also agrees well with our experimental results.

Compounds **2-4** to **2-6** also show strong fluorescence with the emission maximum at 701, 699 and 744 nm, respectively (**Figure 2.2** and **Table 2.1**). Their

photoluminescence quantum yields (Φ) were determined according to an optical dilute method (optical density A < 0.05) by using cardiogreen dye ($\lambda_{abs\ (max)}$ = 780 nm, Φ = 0.13 in DMSO) as a standard.[17] The Φ values of 0.81, 0.80 and 0.38 were obtained for **2-4**, **2-5** and **2-6**, respectively. Such high to moderate quantum yields for NIR dye are remarkable given that many NIR absorbing dyes (including the bisanthenes **2-1** to **2-3**) usually exhibit low fluorescence quantum yields.

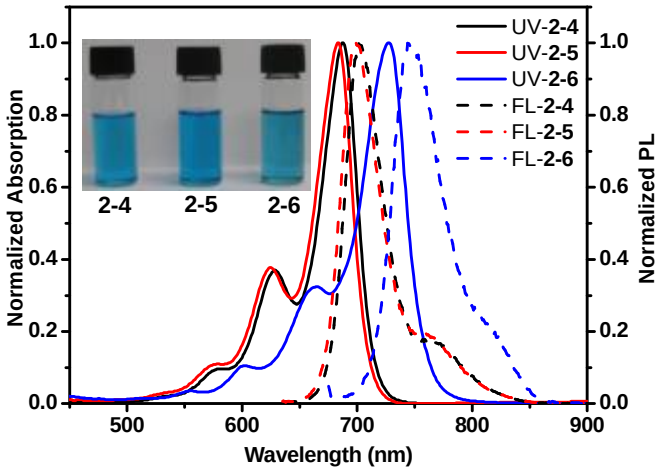

Figure 2.2 Normalized UV-vis-NIR absorption and photoluminescence spectra of compounds **2-4**, **2-5**, and **2-6**. The concentrations for the absorption and emission spectroscopic measurements in toluene are 10^{-5} M and 10^{-6} M, respectively.

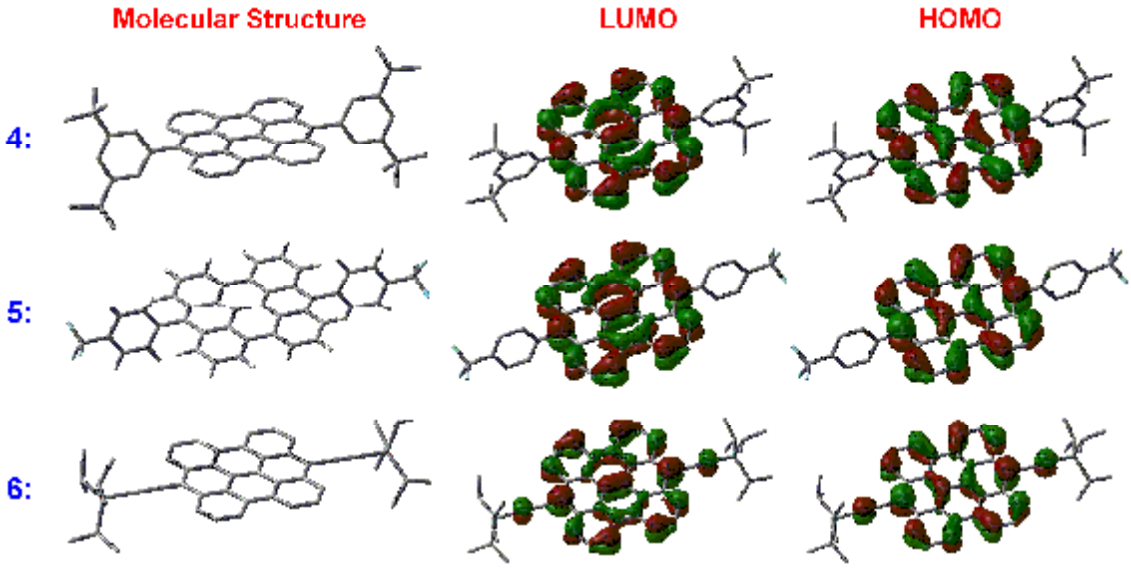

Figure 2.3 Optimized structure and frontier molecular orbital profiles of molecules **2-4** to **2-6** based on DFT (B3LYP/6-31G**) calculations

2.2.3 Photostability and Thermal Stability

In contrast to the very unstable parent bisanthene, the air-saturated solutions of **2-4**, **2-5** and **2-6** in toluene are stable for weeks under ambient conditions without significant change on their UV-vis-NIR absorption spectra. Upon irradiation of white light (100 W), the solutions gradually decomposed with a decrease of the optical intensity at the major absorption band (550-800 nm) and appearance of new absorption band in the shorter wavelength (**Figure 2.4**). The half-times ($t_{1/2}$) of around 618, 674 and 870 minutes were estimated for **2-4**, **2-5** and **2-6**, respectively by plotting the optical density at the absorption maximum with the irradiation time (**Figure 2.4**). While upon irradiation of UV lamp (4 W), the decomposition process became faster and they displayed a half-time ($t_{1/2}$) of about 404, 452 and 586 minutes, respectively (**Figure 2.5**). These results revealed that the photo-stability of the bisanthene-based compounds followed the sequence **2-6** > **2-5** > **2-4** >> **2-1** and it also proved that introduction of phenyl or triisopropylsilylethynyl groups at the *meso*-

positions of the bisanthene unit largely improved the stability of the chromophore. The difference on the stability of the bisanthene **2-1** and its derivatives **2-4** to **2-6** can be explained by a combination of the electronic effect, conjugation effect and steric effect of the substituents. Without any substituent, the parent bisanthene **2-1** with high lying HOMO energy level can be easily oxidized by adding singlet oxygen to the core and eventually a more stable bisanthenequinone **2-7** is formed.[13] However, after substitution by aryl and alkyne at the *meso*-positions, the bulky substituents significantly prohibit the intermolecular interaction between the oxygen and the bisanthene core. Moreover, the extended π-conjugation between the bisanthene and the aryl or alkyne moieties further delocalizes the electron cloud and leads to a more stable extended π-system, in particular, the π-conjugation is more effective in **2-6** with respect to **2-4** and **2-5**. Moreover, electron withdrawing effect also plays important role in the stability of the bisanthene chromophore. For **2-5**, the electron-withdrawing trifluoromethyl group on the phenyl ring reduces the electron density of the bisanthene backbone, so it is less photo-oxidizable than **2-4**. While for **2-6**, the ethynyl group is fully conjugated to the bisanthene π-system (resonance effect) and the sp hybridized ethynyl carbons are modestly more electronegative than sp^2 hybridized carbons to which they are attached (inductive effect), so compound **2-6** is most stable. Such a trend is also in agreement with the observation for *meso*-substituted pentacene derivatives.[18]

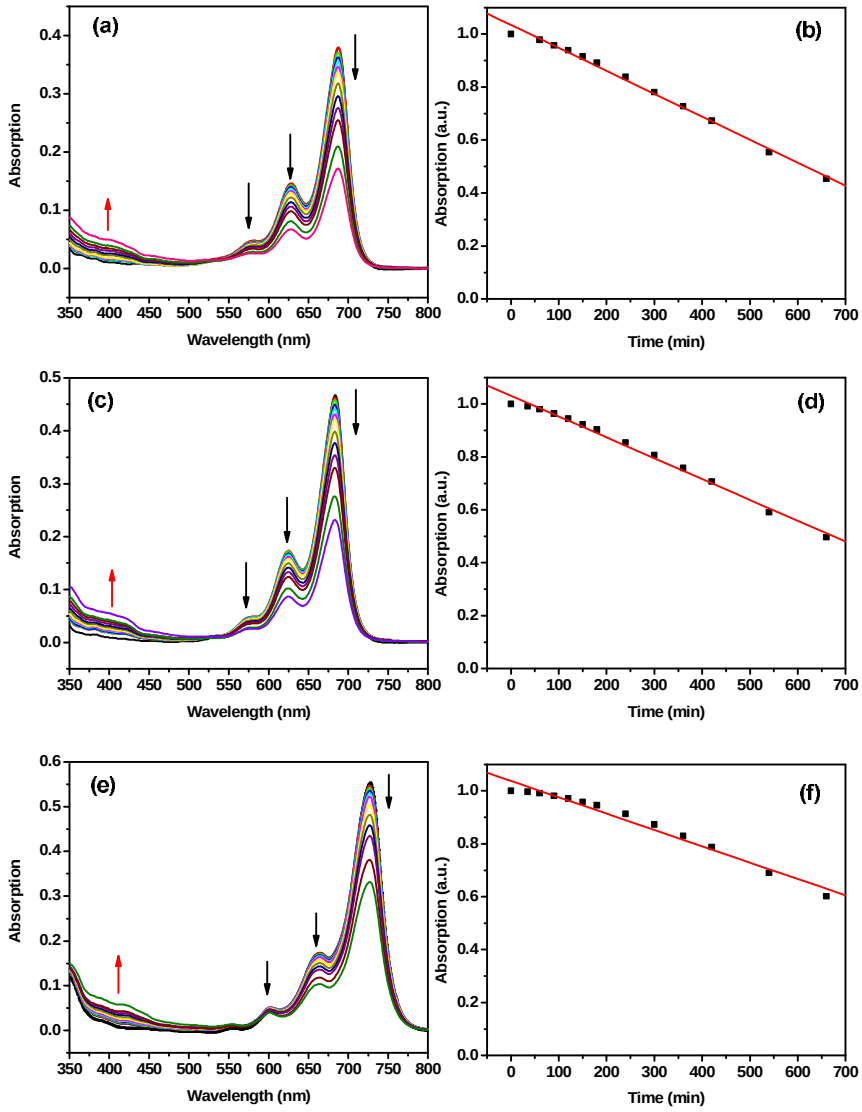

Figure 2.4 Photostability test of compounds **2-4** to **2-6** in toluene upon irradiation of 100 W white light bulb. Left: UV-vis-NIR absorption spectra of **2-4** (a), **2-5** (c) and **2-6** (e) in toluene recorded during the irradiation. The arrows indicate the change of spectral. Right: the change of optical density of **2-4** (b), **2-5** (d) and **2-6** (f) at the absorption maximum wavelength with the irradiation time. The original optical density before irradiation was normalized at the absorption maximum.

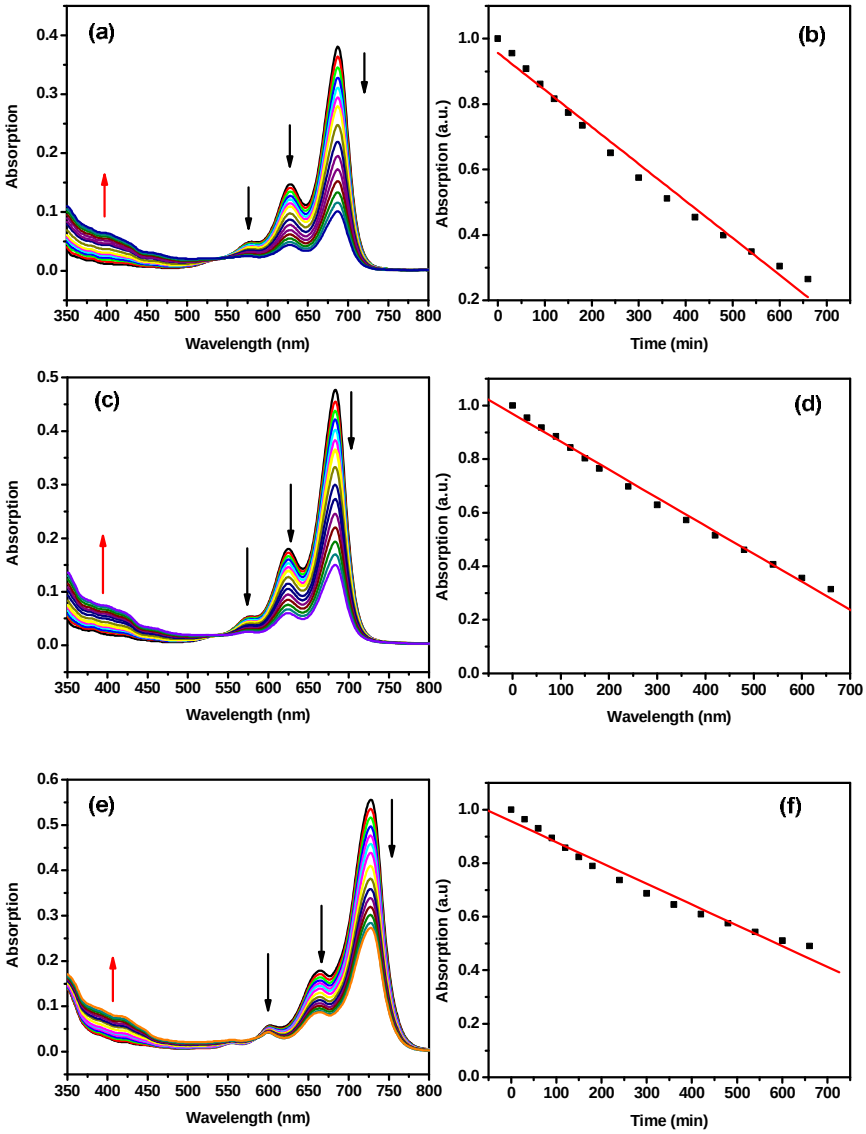

Figure 2.5 Photostability test of compounds **2-4** to **2-6** in toluene upon irradiation of 4 W UV-light. Left: UV-vis-NIR absorption spectra of **2-4** (a), **2-5** (c) and **2-6** (e) in toluene recorded during the irradiation. The arrows indicate the change of spectral. Right: the change of optical density of **2-4** (b), **2-5** (d) and **2-6** (f) at the absorption maximum wavelength with the irradiation time. The original optical density before irradiation was normalized at the absorption maximum.

Thermogravimetric analysis (TGA) measurements reveal that **2-4** and **2-5** are highly stable with a decomposition temperature of about 410 ^{o}C (5 wt% weight loss) in N_2 atmosphere, while for compound **2-6**, its decomposition temperature is about

334 ^{o}C, probably because of the relatively poor thermal stability of C≡C units (**Figure 2.6**). For these three compounds, neither glass transition nor crystal melting point or liquid crystalline-isotropic transition was observed in the temperature range of 25-300 ^{o}C by means of differential scanning calorimetry (DSC). So we can conclude that after substitution at the *meso*-positions of bisanthene, new soluble and stable near infrared absorbing and emitting dyes **2-4** to **2-6** are obtained.

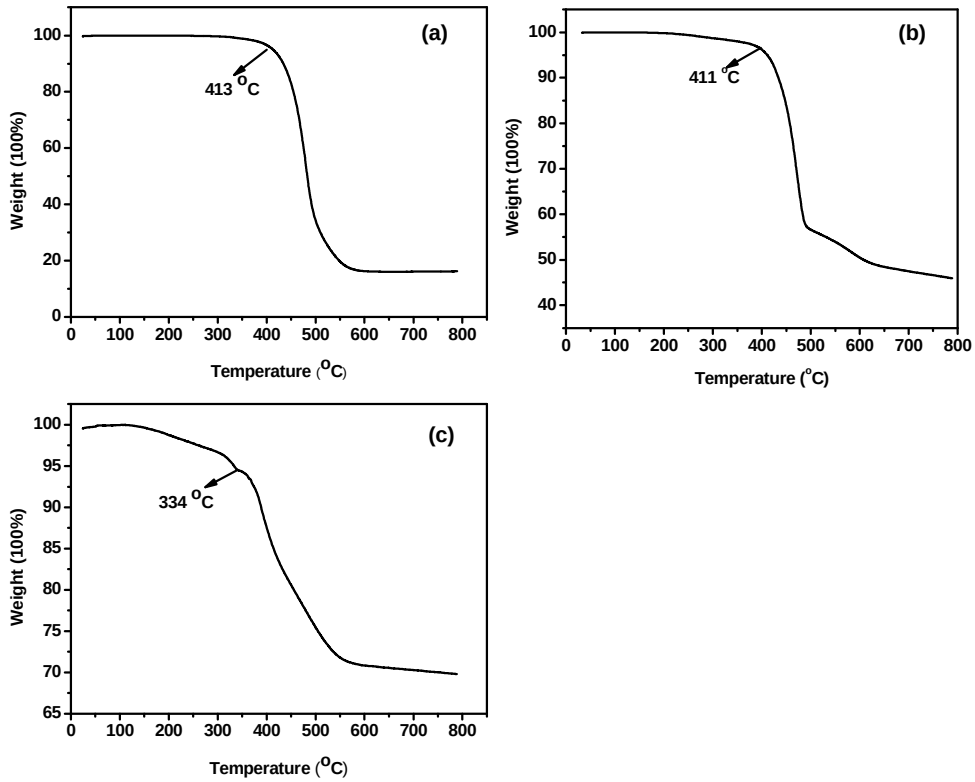

Figure 2.6 Thermogravimetric analysis (TGA) curves of **2-4** (a), **2-5** (b) and **2-6** (c) (heating rate = 10 ^{o}C/min).

2.2.4 Electrochemical Properties and Chemical Oxidation Titration

The electrochemical properties of compounds **2-4** to **2-6** were investigated by cyclic voltammetry (CV) in dry DCM (**Figure 2.7**) and the data are collected in **Table 2.1**. The cyclic voltammograms of **2-4** and **2-5** exhibit two reversible oxidation waves

with half-wave potentials (E_{ox}^{n}) at 0.44 and 1.03 V for **2-4** and 0.53 and 1.14 V for **2-5**, while three oxidative waves were observed for **2-6**, with E_{ox}^{n} at 0.34, 0.72 and 1.20 V (vs. AgCl/Ag). Compounds **2-4**, **2-5** and **2-6** also show two quasi-reversible reduction waves with the half-wave potential of the first reductive waves (E_{red}^{1}) at -1.21, -1.10 and -0.92 V, respectively. Such an amphoteric redox behavior suggests that all these compounds can be reversibly oxidized into respective cationic species (e.g. radical cations and dications) and reduced into corresponding anionic species (e.g. radical anion and dianion) and the charged species can be stabilized by the largely delocalized π-system. The lowest first oxidation potential observed for **2-6** can be explained by the most effective π-conjugation between the bisanthene and the ethynyl moieties as we discussed above. Moreover, more detectable oxidation states can be determined for **2-6**. The first oxidation potential of **2-5** is higher than that for **2-4** due to the electron withdrawing effect of the trifluoromethyl groups.

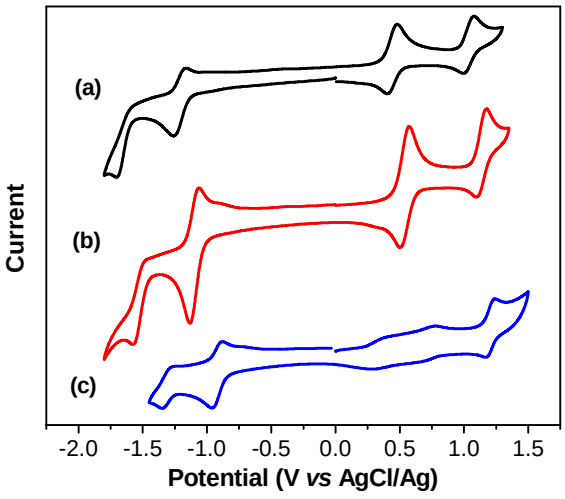

Figure 2.7 Cyclic voltammograms of **2-4** (a), **2-5** (b), and **2-6** (c) in dichloromethane (1 mM) with 0.1 M Bu_4NPF_6 as supporting electrolyte, AgCl/Ag as reference electrode, Au disk as working electrode, Pt wire as counter electrode, and scan rate at 50 mV/s.

Table 2.1 Summary of photophysical and electrochemical properties of compounds **2-4**, **2-5** and **2-6**.

compounds	λ_{abs} (nm)	ε_{max} ($M^{-1}cm^{-1}$)	λ_{em} (nm)	QY	E_{ox}^{1} (V)	E_{ox}^{2} (V)	E_{ox}^{3} (V)	E_{red}^{1} (V)	E_{red}^{2} (V)	HOMO (eV)	LUMO (eV)	E_g^{Opt} (eV)
2-4	687 628 582	3844	701	0.81	0.44	1.03	-	-1.21	-1.65	-4.71	-3.20	1.73
2-5	683 624 580	4510	699	0.80	0.53	1.14	-	-1.10	-1.53	-4.80	-3.31	1.74
2-6	727 662 603 554	5569	747	0.38	0.34	0.72	1.20	-0.92	-1.31	-4.57	-3.47	1.62

E_{ox}^{n} and E_{red}^{n} are half-wave potentials for respective redox waves with AgCl/Ag as reference. HOMO and LUMO energy levels were calculated from the onset potentials of the first oxidation (E_{ox}^{onset}) and the first reduction wave (E_{red}^{onset}) according to equations: HOMO = - (4.8 + E_{ox}^{onset}) and LUMO = - (4.8 + E_{red}^{onset}), where the potentials are referred to $E_{Fc+/Fc}$.

Chemical oxidation titrations of compounds **2-4** to **2-6** were conducted in DCM by using either iodine or $SbCl_5$ as oxidant and the process was followed by UV-vis-NIR absorption spectroscopy. All these compounds can be reversibly oxidized by $SbCl_5$ into stable radical cation with appearance of new characteristic absorption bands in the shorter and longer wavelengths (**Figure 2.8**). Such a phenomenon is common due to the redistribution of frontier molecular orbital energy level in the energy gap and one electron transition at the higher energy and one electron transition at lower energy are allowed in the new energy diagram. The oxidized species can also be reversibly reduced into the neutral state by adding Zn dust to the solution containing oxidized species (**Figure 2.8**). Similar reversible process can be observed for **2-4** and **2-5** when iodine was used as oxidant. However, chemical oxidization of **2-5** by iodine is irreversible likely due to electrophilic addition of I^+ onto the C≡C units (**Figure 2.9**).

The HOMO and LUMO (LUMO = lowest unoccupied molecular orbital) energy levels were deduced from the onset potentials of the first oxidation (E_{ox}^{onset}) and the first reduction wave (E_{red}^{onset}), according to equations: HOMO = -(4.8 + E_{ox}^{onset}) and LUMO = - (4.8 + E_{red}^{onset}), where the potentials are calibrated to $E_{Fc+/Fc}$.[19] Compared with the aryl-substituted bisanthenes (**2-4** and **2-5**), compound **2-6** has a higher lying HOMO energy level (-4.57 eV). However, this compound is still more stable than **2-4**

and **2-5** because of effective electron delocalization. In agreement with the small optical band gap (E_g^{opt}) determined from the absorption spectra, the electrochemcial band gaps are also small due to a convergence of the HOMO and LUMO energy levels. As a result, low band gap materials with NIR absorption and emission are obtained.

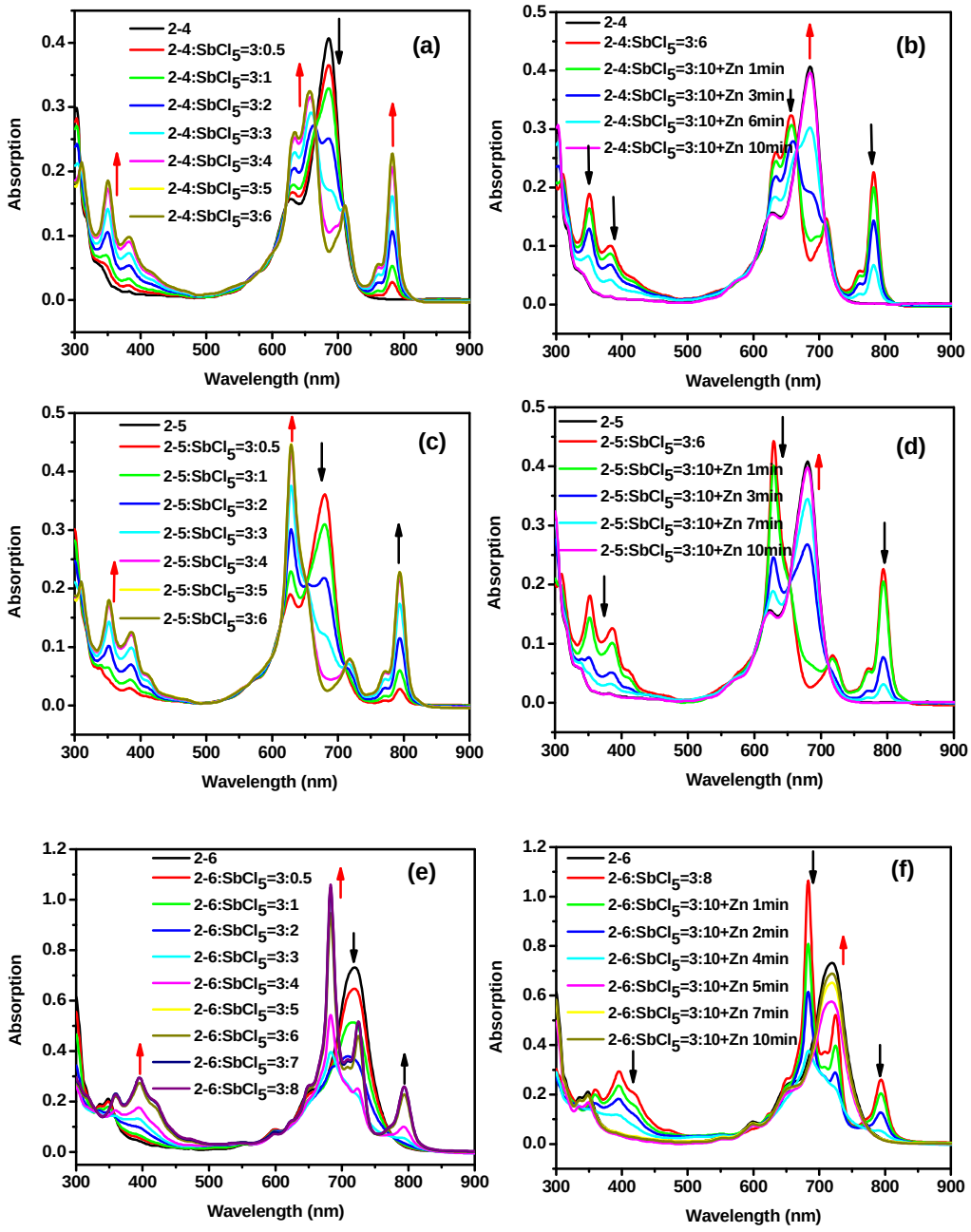

Figure 2.8 Left: UV-vis-NIR absorption spectra of **2-4** (a), **2-5** (c) and **2-6** (e) during the titration with $SbCl_5$ in dry DCM. The arrows show the changes of the spectra during the titration Right: UV-vis-NIR absorption spectra of the oxidized pieces **2-4** (b), **2-5** (d) and **2-6** (f) during reduction by Zn with different contact time. The arrows indicate the changes of the spectra with different contact time with Zn dust.

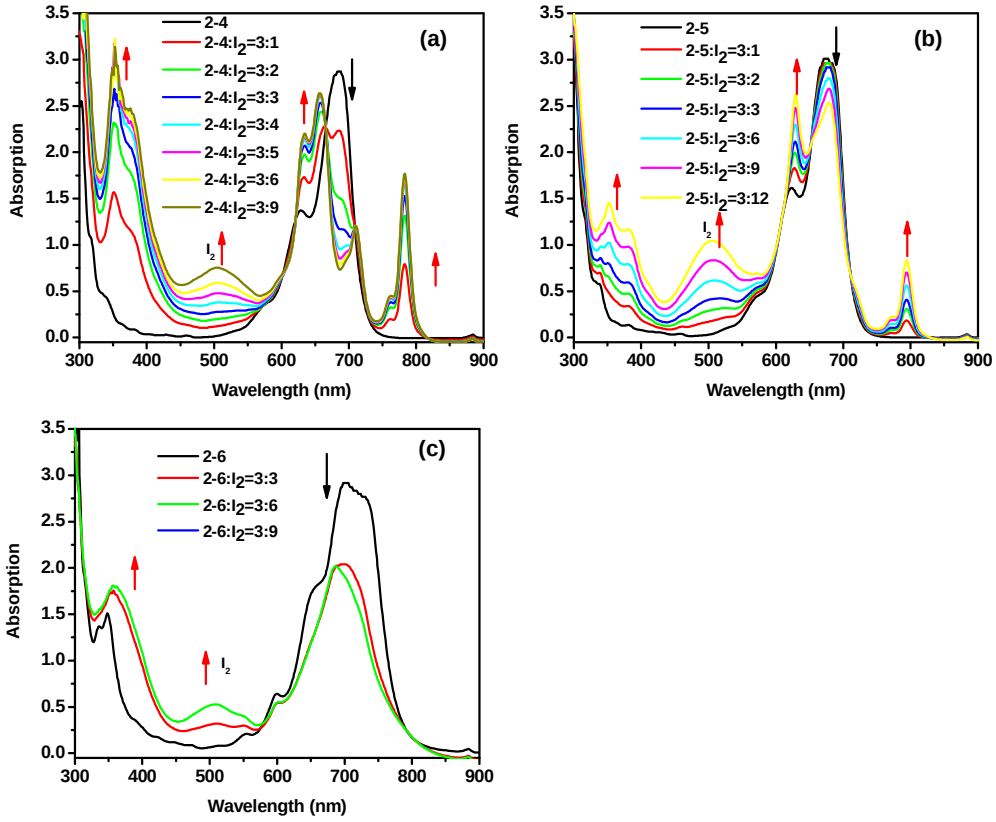

Figure 2.9 UV-vis-NIR absorption spectra of **2-4** (a), **2-5** (b) and **2-6** (c) during the titration by I_2 in dry DCM.

2.2.5 Single-crystal Structure and Molecular Packing

Besides the photophysical and electrochemical properties, molecular structure and solid state packing of these molecules are also of importance when considering of their potential applications as semiconductors in electronic devices such as FET. Single crystal of **2-5** was successfully obtained by slow diffusion of methanol vapor to the chloroform solution. The single-crystal structure and three-dimensional packing of **2-5** are shown in Figure 6.[20] **2-5** has a planar bisanthene unit and the trifluoromethylphenyl groups are twisted from the bisanthene plane with about 80° due to steric congestion (**Figure 2.10 (a)**). Such structure is similar to the phenyl-*meso*-substituted pentacene.[16] Interestingly, **2-5** adopts a layer-like structure (**Figure**

2.10 (b)) and in each layer a herringbone π-stacking motif (**Figure 2.10 (c)**) was observed. Two types of π-π interactions can be distinguished: an offset π-overlap between the bisanthene units with a close contact distance of 3.301 Å and an edge-to-face CH-π interaction with a close contact distance of 2.752 Å. Such a close packing mode with strong intermolecular π-interactions suggests that **2-5** could be a good semiconductor for FET devices.

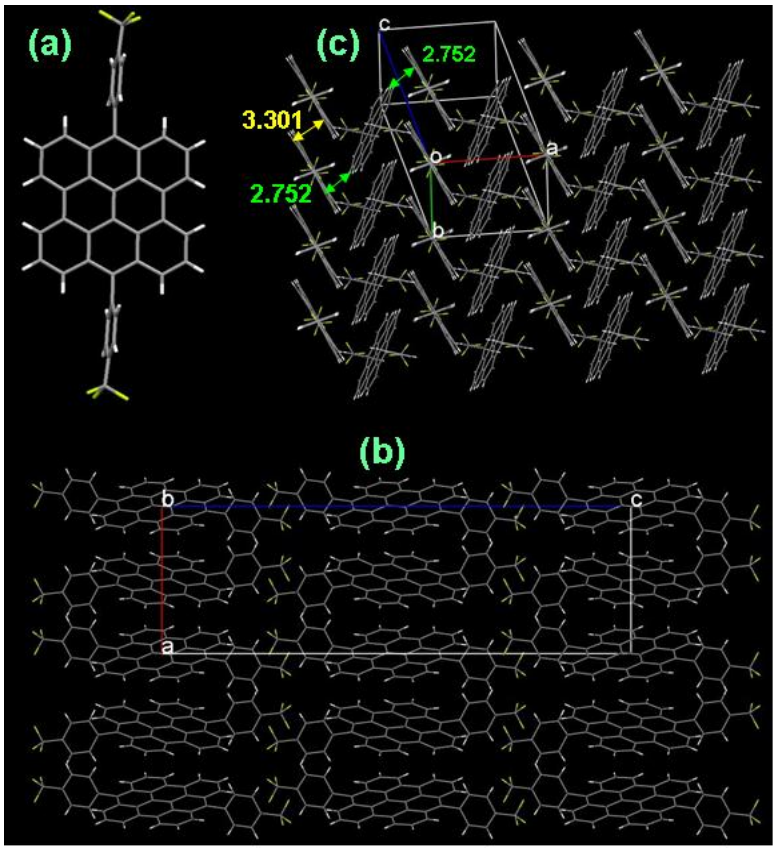

Figure 2.10 Single-crystal structure (a) of compound **2-5**, its three dimensional layer-like packing (b) and the herringbone π-stacking motif in each layer (c).

2.3 Conclusions

In summary, three *meso*-substituted bisanthenes **2-4** to **2-6** were successfully prepared in a short synthetic route. Compared with the parent bisanthene **2-1**, compounds **2-4** to **2-6** exhibit largely improved stability and solubility. The obtained

materials also show bathochromic shift of their absorption and emission spectra into the NIR spectral range with high to moderate fluorescence quantum yields, qualifying them as both NIR absorption and fluorescent dyes. These compounds display amphoteric redox behavior with multi-step reversible redox processes, suggesting that they could be used as both hole and electron transporting materials. In particular, the ordered herringbone π-stacking mode observed in **2-5** indicates that it can be used as potential semiconductor in FETs in the future studies.

2.4 Experimental Section

2.4.1 General Experimental Methods

All reagents and starting materials were obtained from commercial suppliers and used without further purification. Anhydrous tetrahydrofuran (THF) was purified by routine procedure and distilled over sodium under nitrogen before using. The bisanthenequinone **7** was prepared according to literature.[13] Photocyclization reaction was carried out in an Ace 7825 photochemical reactor with irradiation of a 450 W mercury-vapor lamp. Column chromatography was performed on silica gel 60 (Merck 40-60 nm, 230-400 mesh). All NMR spectra were recorded on the Bruker AMX500 spectrometer. All chemical shifts are quoted in ppm, relative to tetramethylsilane, using the residual solvent peak as a reference standard. High resolution mass spectra were recorded on a Finnigan MAT95XL-T with EI ionization source. EI-MS were recorded on Finnigan TSQ 7000 triple stage quadrupole mass spectrometer. UV-vis absorption and fluorescence spectra were recorded in DCM solution on a spectrometer and a fluorometer, respectively. Cyclic voltammetry measurements of compounds **2-4** to **2-6** in DCM (1 mM) was performed on a CHI 620C electrochemical analyzer with a three-electrode cell, using 0.1 M Bu_4NPF_6 as

supporting electrolyte, AgCl/Ag as reference electrode, gold disk as working electrode, Pt wire as counter electrode, and scan rate at 50 mV/s. Thermogravimetric analysis (TGA) was carried out on a TA instrument 2960 at a heating rate of 10 ^{o}C/min under nitrogen flow. Differential scanning calorimetry (DSC) was performed on a TA instrument 2920 at a heating/cooling rate of 10 ^{o}C/min under nitrogen flow. The crystallographic data collection was carried out at 293K on a Bruker-AXS Smart Apex CCD single-crystal diffractometer.

2.4.2 Material Synthesis and Characterization Data

Synthesis of compound 2-8a: Magnesium (82 mg, 3.42 mmol) and a piece of iodine crystal were placed in dry THF (1 mL). To the mixture, 1-bromo-3,5-di-*tert*-butylbenzene (707 mg, 2.62 mmol) in dry THF (10 mL) was added dropwise and the mixture was stirred at room temperature for 2h to generate Grignard reagent. The as-prepared Grignard reagent was transferred into a suspension of bisanthenequinone **2-7** (100 mg, 0.26 mmol) in dry THF (20 mL) and the mixture was stirred at room temperature overnight. The reaction was quenched with water (100 mL) and extracted with diethyl ether. The organic layer was washed by water and dried over anhydrous Na_2SO_4. After removal of solvent, the residue was further purified by column chromatography on silica gel with DCM: hexane = 2:1 (v/v) as eluent to afford **2-8a** (114 mg, 57 %) as a light yellow solid. Melting point: > 300 ^{o}C. ^{1}H NMR (500 MHz, $CDCl_3$), δ ppm = 1.04 (s, 36 H, *t*-Bu), 3.22 (s, 2 H, OH), 7.02 (d, J = 1.25 HZ, 4 H, Ph), 7.07 (t, J = 1.9 Hz, 2 H, Ph), 7.56 (dd, J = 7.86 Hz, 4 H, Ar), 7.89 (d, J = 6.3 Hz, 4 H, Ar), 8.40 (d, J = 7.55 Hz, 4 H, Ar). ^{13}C NMR (125 MHz, $CDCl_3$), δ ppm = 31.35, 34.68, 74.91, 119.25, 120.01, 120.14, 122.05, 123.81, 127.16, 127.36, 128.92, 141.36,

149.45, 149.93. EI MS: m/z = 760.6 ([M]), calculated exact mass: 760.4. HR EI MS: m/z = 760.4257 ([M]), calculated exact mass: 760.4280.

Synthesis of compound 2-4: In absence of light, a mixture of **2-8a** (200 mg, 0.26 mmol), NaI (394 mg, 2.62 mmol), $NaH_2PO_2 \bullet H_2O$ (508 mg, 3.94 mmol) and acetic acid (50 ml) was heated to reflux for 2h. After cooling to room temperature, the deep blue precipitate was collected by filtration, washed with water and methanol, and purified by column chromatography on silica gel with Hexane: Toluene = 1:1 (v/v) as eluent to afford **2-4** (133 mg, 70%) as a deep blue solid. Melting point: > 300 ^oC. ^1H NMR (500 MHz, $CDCl_3$), δ ppm = 1.41 (s, 36 H, *t*-Bu), 7.29 (d, J = 1.9 Hz, 4 H, Ph), 7.34 (dd, J = 8.2 Hz, 4 H, Ar), 7.42 (d, J = 8.8 Hz, 4 H, Ar), 7.56 (t, J = 1.58 Hz, 2 H, Ph), 8.25 (d, J = 7.55 Hz, 4 H, Ar). ^{13}C NMR (125 MHz, $CDCl_3$), δ ppm = 31.62, 35.03, 120.18, 125.51, 126.39, 126.43, 127.10, 132.36, 132.39, 151.02. EI MS: m/z = 726.5 ([M]), calculated exact mass: 726.4. HR EI MS: m/z = 726.4204 ([M]), calculated exact mass: 726.4226.

Synthesis of compound 2-8b: Magnesium (95 mg, 3.94 mmol) and a piece of iodine crystal were placed in dry THF (1 mL). To the mixture, 1-bromo-4-(trifluoromethyl)benzene (591 mg, 2.62 mmol) in dry THF (10 mL) was added dropwise and the mixture was stirred at room temperature for overnight to generate Grignard reagent. The as-prepared Grignard reagent was transferred into a suspension of bisanthenequinone **2-7** (100 mg, 0.26 mmol) in dry THF (20 mL) and the mixture was stirred at room temperature overnight. The reaction was quenched with water (100 mL), and extracted with diethyl ether. The organic layer was washed by water and dried over anhydrous Na_2SO_4. After removal of solvent, the residue was purified by column chromatography on silica gel with DCM: Hexane = 2:1 (v/v) as eluent to

afford **2-8b** (103 mg, 60 %) as a light yellow solid. Melting point: > 300 ^{o}C. ^{1}H NMR (500 MHz, $CDCl_3$), δ ppm = 3.26 (s, 2 H, OH), 7.33 (br, 8 H, Ph), 7.59 (dd, J = 7.58 Hz, 4 H, Ar), 7.83 (d, J = 6.95 Hz, 4 H, Ar), 8.45 (d, J = 7.55 Hz, 4 H, Ar). ^{13}C NMR (125 MHz, $CDCl_3$), δ ppm = 74.09, 119.10, 122.68, 123.60, 124.87, 125.12, 125.15, 127.62, 127.77, 129.11, 140.28, 153.52. EI MS: m/z = 672.3 ([M]), calculated exact mass: 672.2. HR EI MS: m/z = 672.1511 ([M]), calculated exact mass: 672.1524.

Synthesis of compound 2-5: In absence of light, a mixture of **8b** (100 mg, 0.15 mmol), NaI (225 mg, 1.5 mmol), $NaH_2PO_2•H_2O$ (290 mg, 2.25 mmol) and acetic acid (25 ml) was heated to reflux for 2h. After cooling to room temperature, the deep blue precipitate was collected by filtration, washed with water and methanol, and purified by column chromatography on silica gel with Hexane: Toluene = 3:1 (v/v) as eluent to afford **2-5** (68 mg, 72%) as a deep blue solid. Melting point: > 300 ^{o}C. ^{1}H NMR (500 MHz, $CDCl_3$), δ ppm = 7.30 (d, J = 8.85 Hz, 4 H, Ph), 7.39 (dd, J = 7.88 Hz, 4 H, Ar), 7.40 (d, J = 8.3 Hz, 4 H, Ar), 7.92 (d, J = 8.2 Hz, 4 H, Ph), 8.29 (d, J = 7.6 Hz, 4 H, Ar). ^{13}C NMR (75 MHz, $CDCl_3$), δ ppm = 120.65, 125.85, 125.90, 126.37, 127.00, 131.77, 131.99, 132.27, 134.69, 142.90. EI MS: m/z = 638.2 ([M]), calculated exact mass: 638.1. HR EI MS: m/z = 638.1469 ([M]), calculated exact mass: 638.1469.

Synthesis of compound 2-6: To a solution of triisopropylsilylacetylene (479 mg, 2.629 mmol) in anhydrous THF (30 ml) at 0 ^{o}C was added dropwise n-BuLi (1.6 M in hexanes, 1.56 ml, 2.5 mmol). The solution was allowed to stir for 30 min at 0 ^{o}C before bisanthenequinone 7 (100 mg, 0.26 mmol) was added in one portion. The mixture was warmed to room temperature, stirred overnight and then poured into a large amount of water. The mixture was extracted with chloroform, and the organic layer was washed with brine and dried over $MgSO_4$. The solvent was removed by

evaporation and the residue was dried under vacuum. In absence of light, a mixture of the crude product diol **2-8c** (218 mg, 0.26 mmol), NaI (394 mg, 2.62 mmol), $NaH_2PO_2 \bullet H_2O$ (406 mg, 3.15 mmol) and acetic acid (10 ml) was heated to reflux for 2h. After cooling to room temperature, the deep green precipitate was collected by filtration, washed with water and methanol, and purified by column chromatography on silica gel with Hexane: Toluene = 3:1 (v/v) as eluent to afford **2-6** (68 mg, 72%) as a deep green solid. Melting point: > 300 ^{o}C. ^{1}H NMR (500 MHz, $CDCl_3$), δ ppm = 1.32 (br, 6 H, isopropyl), 1.33 (br, 36 H, isopropyl), 7.42 (br, 4 H, Ar), 7.95 (br, 4 H, Ar), 8.19 (br, 4 H, Ar). EI MS: m/z = 710.5 ([M]), calculated exact mass: 710.4. HR EI MS: m/z = 710.3756 ([M]), calculated exact mass: 710.3764.

Appendix:

1. HR-EI mass spectra of 2-4 (a), 2-5 (b), 2-6 (c), 2-8a (d) and 2-8b (e):

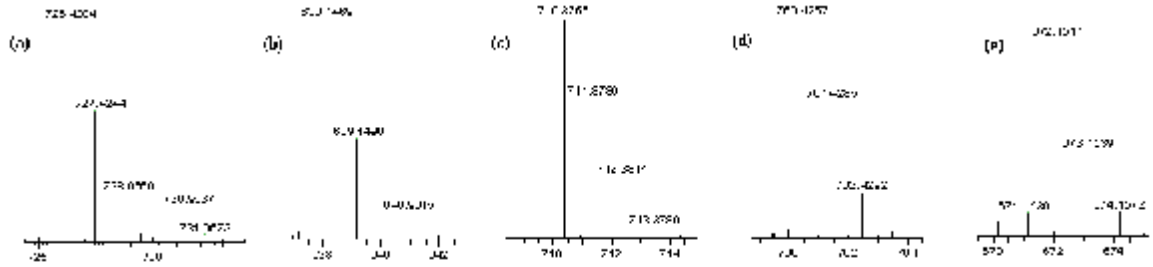

$C_{56}H_{54}$ $C_{42}H_{20}F_6$ $C_{50}H_{54}Si_2$ $C_{56}H_{56}O_2$ $C_{42}H_{22}F_6O_2$

2. ^{1}H NMR and ^{13}C NMR spectra of compounds 2-4, 2-5 and 2-6:

^{1}H NMR spectrum of compound **2-4** in $CDCl_3$ (75 MHz):

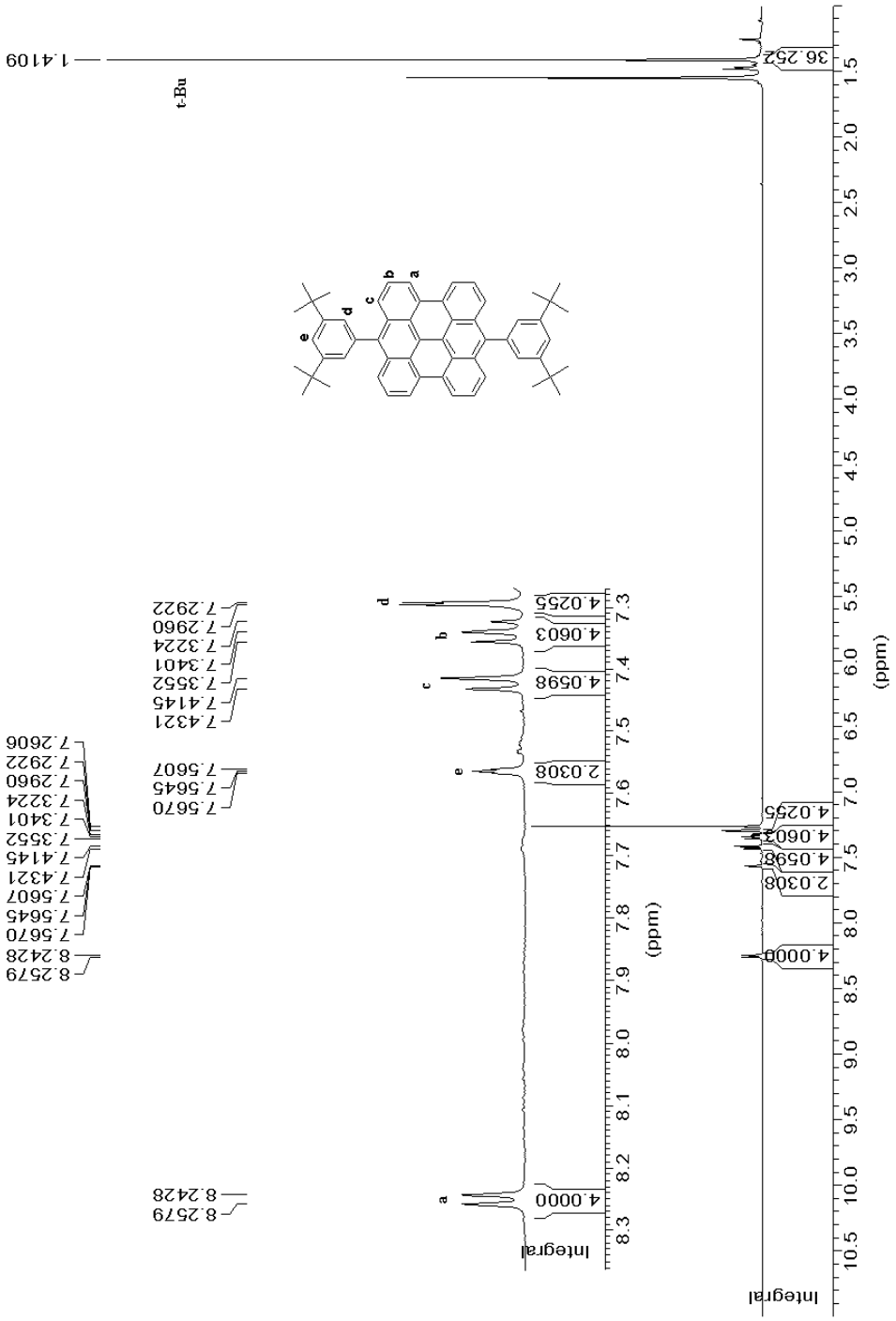

^{13}C NMR spectrum of compound **2-4** in $CDCl_3$ (125 MHz):

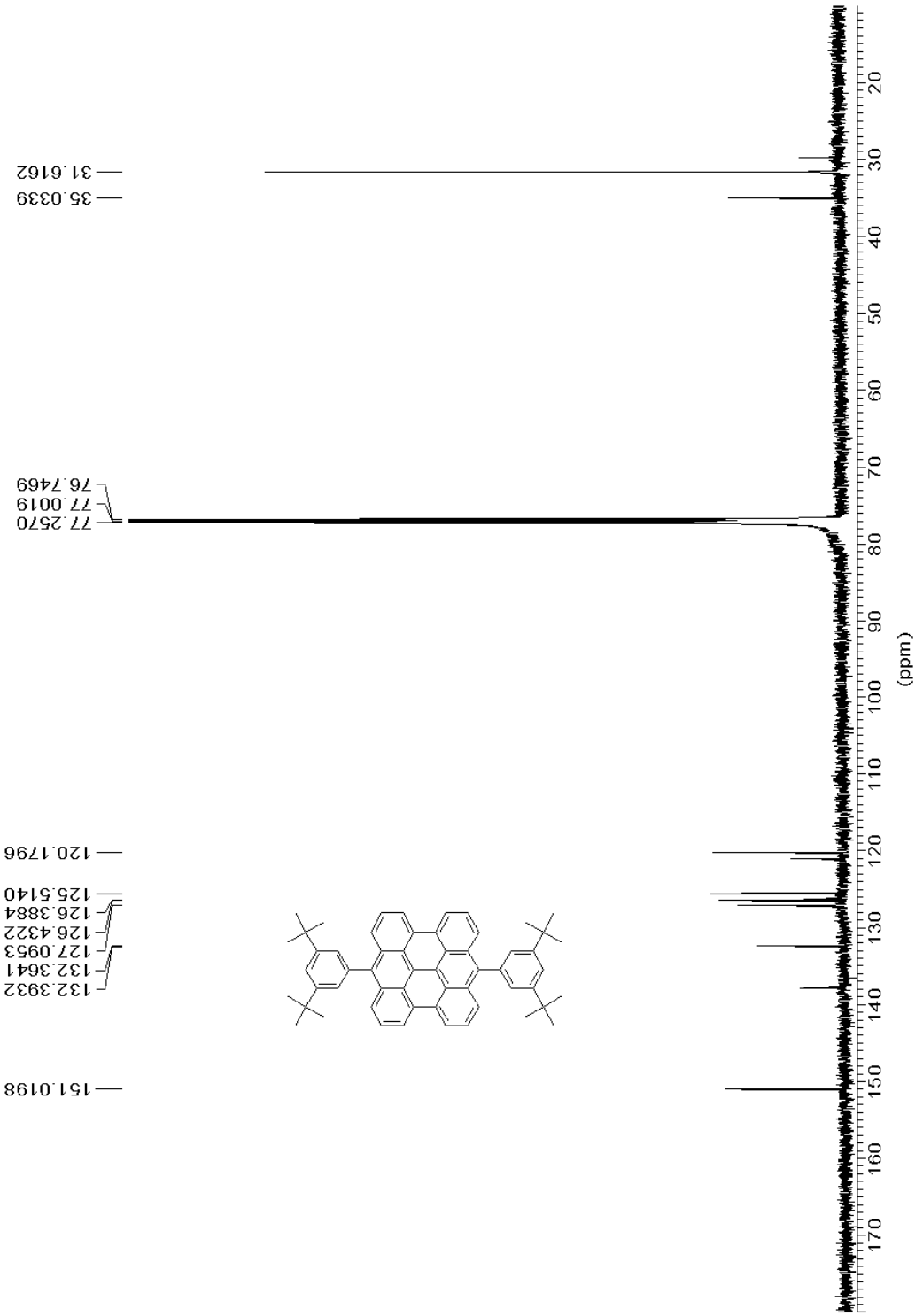

^{1}H NMR spectrum of compound **2-5** in $CDCl_3$ (75 MHz):

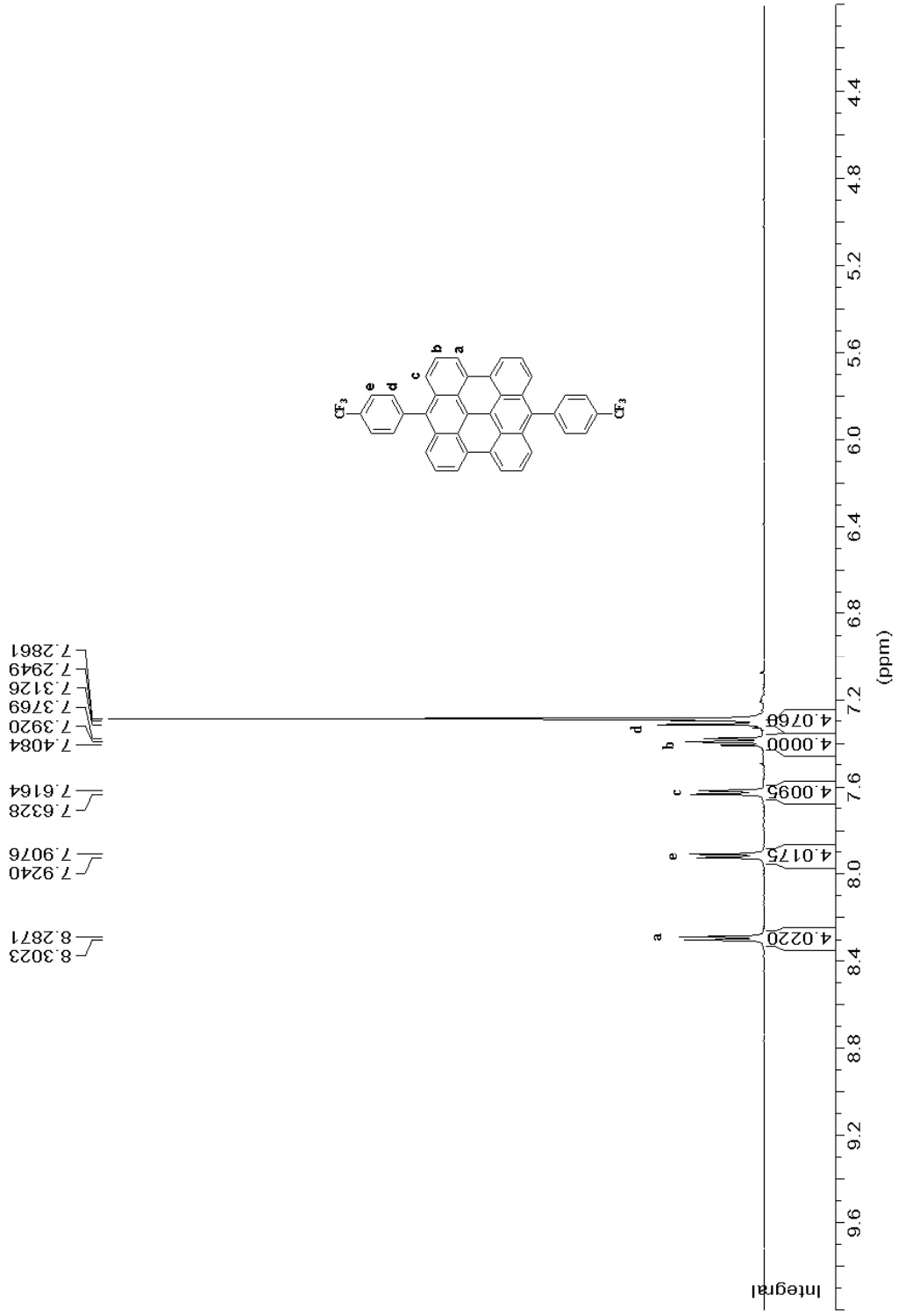

^{13}C NMR spectrum of compound **2-5** in $CDCl_3$ (125 MHz):

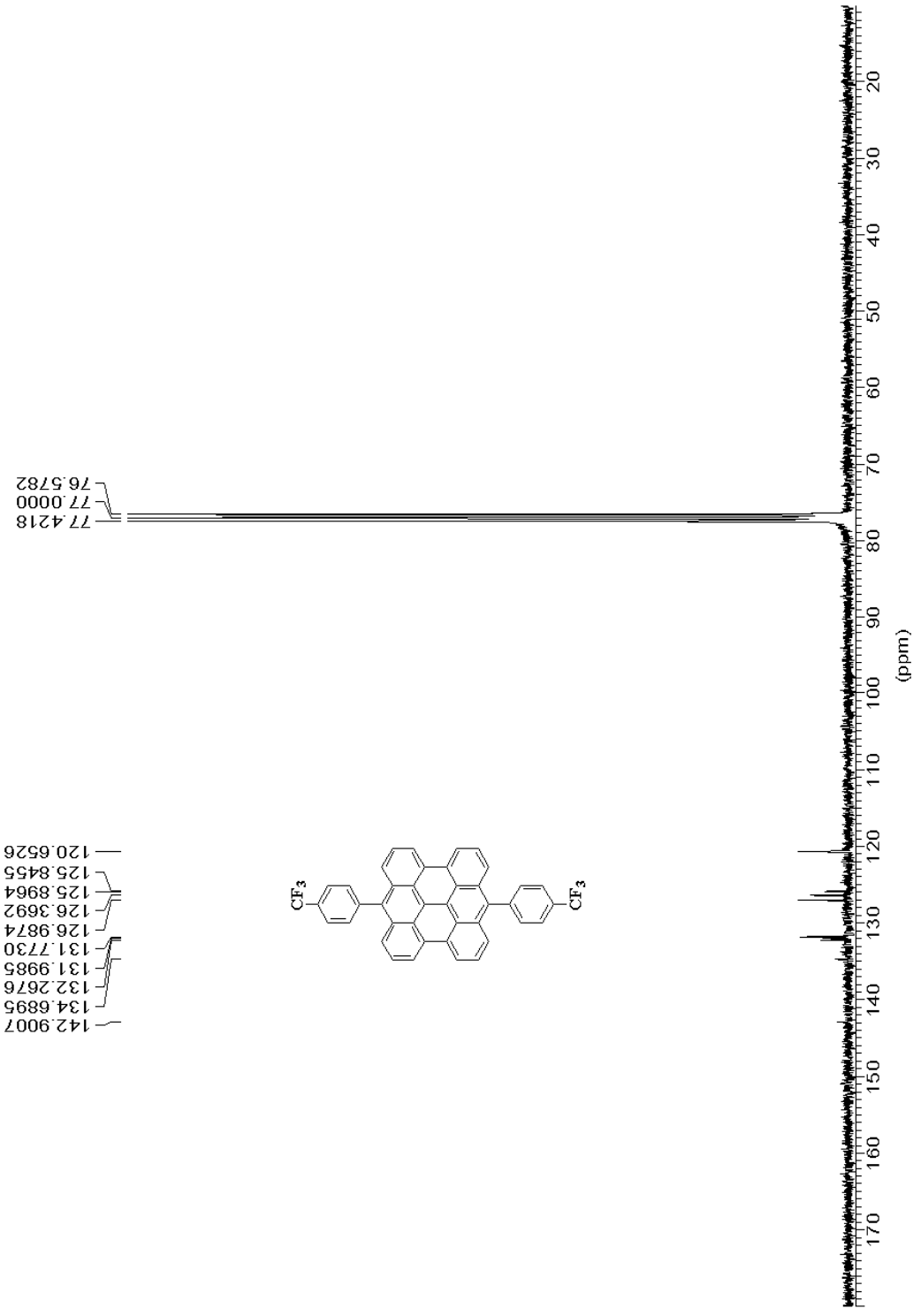

^{1}H NMR spectrum of compound **2-6** in $CDCl_3$ (75 MHz):

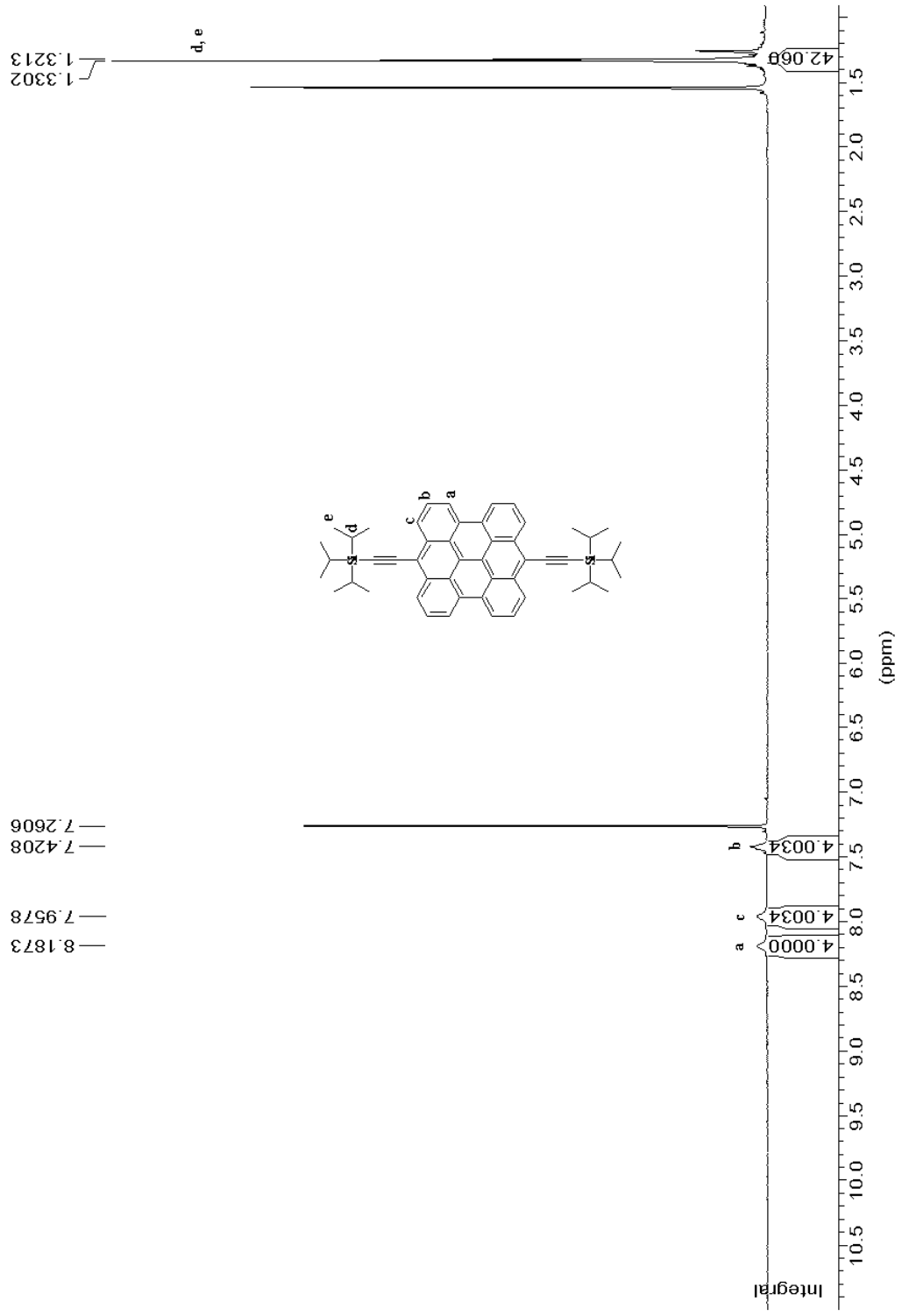

References and notes

1. (a) Fabian, J.; Nakanzumi, H.; Matsuoka, M. *Chem. Rev.* **1992**, *92*, 1197-1226. (b) Fabian, J.; Zahradnik, R. *Angew Chem., Int. Ed. Engl.* **1989,** *28*, 677-828.

2. (a) Kiyose, K.; Kojima, H.; Nagano, T. *Chem. Asian J.* **2008**, *3*, 506-515. (b) Amiot, C. L.; Xu, S. P.; Liang, S.; Pan, L. Y.; Zhao, X. J. *Sensors* **2008**, *8*, 3082-3105.

3. Emmelius, M.; Pawlowski, G.; Vollmann, H. W. *Angew. Chem. Int. Ed. Engl.* **1989**, *28*, 1445-1470.

4. Kololuoma, T.; Oksanen, J.A.I.; Raerinne P.; Rantala, J.T. *J. Mater. Res.* **2001**, *16*, 2186-2188.

5. Tani, T.; Kikuchi, S. *Photogr. Sci. Eng.* **1967**, *11*, 129-144.

6. (a) Imahori, H.; Umeyama, T.; Ito, S. *Acc. Chem. Res.* **2009**, ASAP, DOI: 10.1021/ar900034t. (b) Reddy, P. Y.; Gribabu, L.; Lyness, C.; Snaith, H. J.; Vijaykumar, C.; Chandrasekharam, M.; Lakshmikantam, M.; Yum, J.-H.; Kalyanasundaram, K.; Grätzel, M.; Nazeeruddin, M. K. *Angew. Chem. Int. Ed.* **2007**, *46*, 373 –376.

7. (a) Beverina, L.; Fu, J.; Leclercq, A.; Zojer, E.; Pacher, P.; Barlow, S.; Van Stryland, E.W.; Hagan, D. J.; Brédas, J. -L.; Marder, S. R. *J. Am. Chem. Soc.* **2005**, *127*, 7282-7283. (b) Bouit, P. A.; Wetzel, G.; Berginc, G.; Loiseaux, B.; Toupet, L.; Feneyrou, P.; Bretonnière, Y.; Kamada, K.; Maury, O.; Andraud, C. *Chem. Mater.* **2007**, *19*, 5325-5335.

8. Gregory, P. *High-Technology Applications of Organic Colorants*, Plenum, New York, **1991**.

9. (a) Herrmann, A.; Müllen, K. *Chem. Lett.* **2006**, *35*, 978-985. (b) Pschirer, N. G.; Kohl, C.; Nolde, F.; Qu, J.; Müllen, K. *Angew. Chem., Int. Ed.* **2006**, *45*, 1401-1404. (c) Sinks, L. E.; Rybtchinski, B.; Iimura, M.; Jones, B. A.; Goshe, A. J.; Zuo, X. B.; Tiede, D. M.; Li, X.-Y.; Wasielewski, M. R. *Chem. Mater.* **2005**, *17*, 6295-6303. (d) Hortrup, F. O.; Müller, G. R. J.; Quante, H.; de Feyter, S.; de Schryver, F. C.; Müllen, K. *Chem. Eur. J.* **1997**, *3*, 219–225.

10. (a) Quante, H.; Müllen, K. *Angew. Chem., Int. Ed. Engl.* **1995**, *34*, 1323-1325. (b) Geerts, Y.; Quante, H.; Platz, H.; Mahrt, R.; Hopmeier, M.; Böhm, A.; Müllen, K. *J. Mater. Chem.* **1998**, *8*, 2357-2369. (c) Langhals, H.; Büttner, J.; Blanke, P. *Synthesis* **2005**, 364-366. (d) Jiao, C. J.; Huang, K. W.; Luo, J.; Zhang, K.; Chi, C. Y.; Wu, J. *Org. Lett.* **2009**, *11*, 4508-4511.

11. (a) Wu, J.; Pisula, W.; Müllen, K. *Chem. Rev.* **2007**, *107*, 718-747. (b) Anthony, J. E. *Angew. Chem. Int. Ed.* **2008**, *47*, 452-483.

12. (a) Jiang, D.E.; Sumpter, B. G.; Dai, S. *J. Chem. Phys.* **2007**, *127*, 124703; (b) Jiang, D. E.; Dai, S. *Chem. Phys. Lett.* **2008**, *466*, 72-75. (c) Jiang, D. E.; Dai, S. *J. Phys. Chem. A* **2008**, *112*, 332-335. (d) Chen, Z. F.; Jiang, D. E.; Lu, X.; Bettinger, H. F.; Dai, S.; von Ragué, Schleyer, P.; Houk, K. N. *Org. Lett.* **2007**, *9*, 5449-5452.

13. (a) Arabei, S. M.; Pavich, T. A. *J. Appl. Spectr.* **2000**, *67*, 236-244; (b) Kuroda, H. *J. Chem. Soc.* **1960**, 1856-1857; (c) Clar, E. *Chem. Ber.* **1948**, *81*, 52-63.

14. Yao, J.; Chi, C.; Wu, J.; Loh, K. *Chem. Eur. J.* **2009**, *15*, 9299-9302.

15. Zhang, K.; Huang, K. W.; Li, J. L.; Luo, J.; Chi, C. Y.; Wu, J. *Org. Lett.* **2009**, *11*, 4854-4857.

16. (a) Allen, C. F. H.; Bell, A. *J. Am. Chem. Soc.* **1942**, *64*, 1253-1261. (b) Funk, R. L.; Young, E. R. R.; Williams, R. M.; Flanagan, M. F.; Cecil, T. L. *J. Am. Chem. Soc.* **1996**, *118*, 3291-3292. (c) Miller, G. P.; Mack, J.; Briggs, J. *Org. Lett.* **2000**, *2*, 3983-3286. (d) Anthony, J. E.; Eaton, D. L.; Parkin S. R. *Org. Lett.* **2002**, *4*, 15-18. (e) Jiang, J. Y.; Kaafarani, B. R.; Neckers, D. C. *J. Org. Chem.* **2006**, *71*, 2155-2158. (f) Wudl, F.; Perepichka, D. F. *Chem. Rev.* **2004**, *104*, 4891 –4945.

17. Licha, K.; Riefke, B.; Ntziachristos, V.; Becker, A.; Chance, B.; Semmler, W. *Photochem. Photobiol.* **2000**, *72*, 392-398.

18. Kaur, I.; Jia, W.-L.; Kopreski, R.-P.; Selvarasah, S.; Dokmeci, M.-R.; Pramanil, C.; McGruer, N.-E.; Miller, G.-P. *J. Am. Chem. Soc.* **2008**, *130*, 16274-16286.

19. (a) Chi, C.; Wegner, G. *Macromol. Rapid Comm.* **2005**, *26*, 1532-1537. (b) Pommerehne, J.; Vestweber, H.; Guss, W.; Mahrt, R. F.; Bassler, H.; Porsch, M.; Daub, J. *Adv. Mater.* **1995**, *7*, 551-554.

20. Single crystal data for **2-5**: $C_{42}H_{20}F_6$, orthorhombic, space group: Pbca, unit cell parameters: a = 10.9112(9) Å, b = 7.7032(7) Å, c = 34.108(3) Å, α = 90°, β = 90°, γ = 90°, volume = 2866.8(4) $Å^3$, Z = 4, density = 1.480 Mg/m^3, R1 = 0.0775, wR2 = 0.1543

Chapter 3: Disc-like 7,14-Dicyano-ovalene-3,4:10,11-bis(dicarboximide): Synthesis and Application as Solution Processible n-Type Semiconductor for Air Stable Field-Effect Transistors

3.1 Introduction

Organic semiconductors have attracted intensive academic and commercial interest due to their intriguing optoelectronic properties and potential applications for electronics.[1] Although successes have been achieved for p-type semiconductors,[2] development of n-type semiconductors, despite recent impressive progress,[3,4] have lagged far behind that of p-type materials. One general approach towards n-type semiconductors is to attach electron-withdrawing carbonyl and cyano groups or perfluorinated alkyl chains onto the typical p-type semiconductors such as oligothiophenes,[5] polythiophenes[6] and oligoacenes.[3a,7] Another approach is substitution of an atom in an extended π-system with an more electro-negative atom.[3b,8] Among various building blocks for organic semiconductors, discotic liquid crystals (DLCs) typically comprising a rigid aromatic core and flexible peripheral chains have attracted growing attention.[1c, 9] These disc-like molecules offer the ability to self-assemble into columnar superstructures together with the self-healing of structural defects in mesophases, leading to high one-dimensional charge-carrier mobility along columns, while potentially being more readily processed from solution or from an isotropic melt. Various DLCs based on triphenylene,[10] hexabenzocoronene

(HBC),[11] porphyrin,[12] and phthalocyanine[13] have been investigated and used as p-type semiconductors in electronic devices. N-type semiconductors based on disc-like molecules can be obtained by using similar design concept and naphthalene diimide [14] and perylene diimde (PDI) derivatives [15] have been successfully used for n-channel organic field-effect transistors (OFETs). However, in most cases, the thin films were made by vapor deposition technique and only recently, FET electron mobility of 0.08 cm^2/Vs was achieved for PDIs by solution processing.[15d] Larger size coronene diimide derivatives were also prepared and high space charge limited current (SCLC) mobilities were measured, but no FET mobility was reported.[16] It has been also proposed that increased core sizes could lead to stronger intermolecular interactions, and, hence, possibly increase charge carrier mobility.[17, 18] Therefore, we are interested in exploring the potential of an even larger sized aromatic molecule, namely ovalene, as a building block for solution processible n-type semiconductors.

The oval-shaped ovalene[19] is an insoluble material due to strong intermolecular interactions. Soluble ovalene tetraester exhibited hexagonal columnar LC phase,[20] but no OFET devices and charge carrier mobility data have been reported so far. Herein, we report the synthesis, physical characterizations and FET applications of ovalene-3,4:10,11-bis(dicarboximide) (**ODI**) and 7,14-dicyano-ovalene-3,4:10,11-bis(dicarboximide) (**ODI-CN**) (**Scheme 3.1**). In particular, the **ODI-CN** is supposed to be an appropriate n-type semiconductor based on the following considerations: (1) attachment of strong electron-withdrawing –CN and dicarboximide groups will significantly enhance the electron affinity; (2) introduction of branched dove-tailed alkyl chains will not only solubilize the insoluble ovalene core, but also lead to highly ordered columnar LC materials; (3) unlike other high-symmetry DLCs substituted by insulating aliphatic chains (e.g. six-fold symmetric alkylated HBCs),[11] **ODI-CN** has a

C_2 symmetry and this makes inter-column charge transport more feasible. Our studies demonstrated that OFET devices based on thin films of **ODI-CN** processed from solution showed high electron mobility up to 0.1 $cm^2 V^{-1} s^{-1}$ at ambient atmosphere.

3.2 Results and Discussions

3.2.1 Synthesis

The synthesis of **ODI** and **ODI-CN** is outlined in **Scheme 3.1**. Treatment of bisanthenequinone **3-1**[21] with zinc dust and acetic acid in refluxing pyridine gave a mixture of bisanthene **3-2a** and hydrogenated bisanthene **3-2b**, which were used directly in the subsequent Diels-Alder reaction with maleic anhydride in reluxing nitrobenzene to give crude ovalene dicarboxylic anhydride **3-3** as an insoluble material. Imidization of the ovalene dianhydride **3** with 2-decyltetradecan-1-amine afforded the **ODI** in overall 82% yield for three steps. Bromination of **ODI** selectively took place at the most reactive 7, 14- positions and gave the 7,14-dibromo-ovalene diimide (**ODI-Br**) in 85% yield. $Pd(OAc)_2$-mediated cyanation of **ODI-Br** successfully afforded **ODI-CN** in 86% yield.

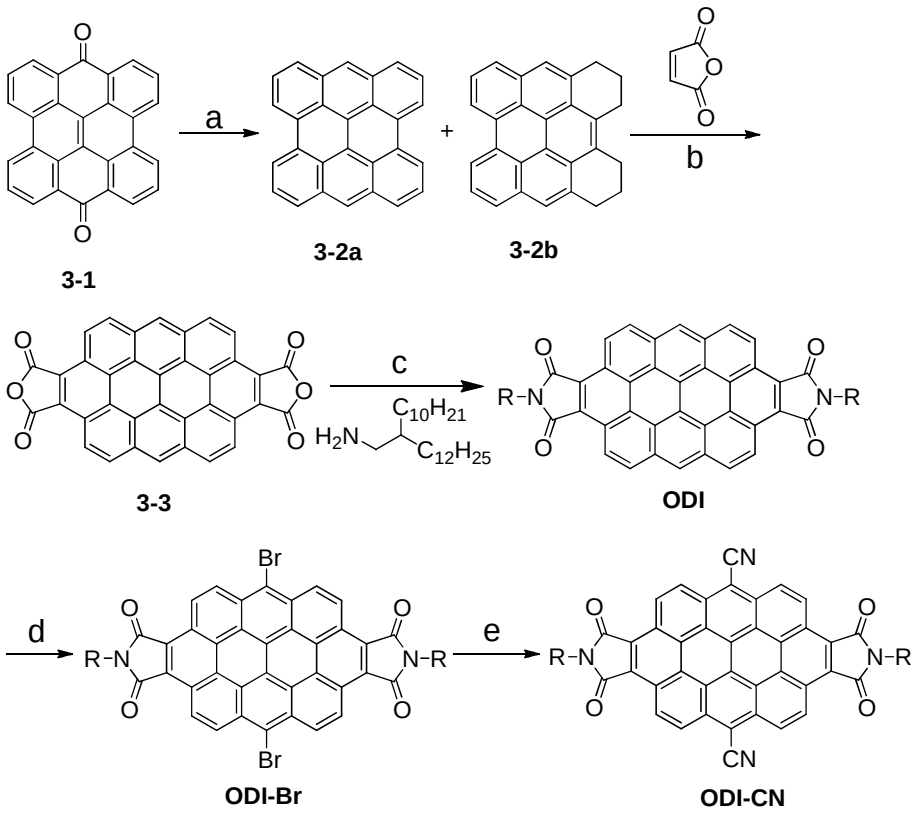

Scheme 3.1 Synthetic route to **ODI** and **ODI-CN**: (a) Zn, pyridine, HOAC, reflux; (b) Nitrobenzene, 240 ^{o}C; (c) DMF, 170 ^{o}C, 82% from **3-1**; (d) Br_2, $CHCl_3$, RT, 85%; (e) CuCN, $Pd_2(dba)_3$.dppf, dioxane, 120 ^{o}C, 86%.

3.2.2 Photophysical and Electrochemical Properties

ODI exhibits good solubility in normal organic solvents such as chloroform, toluene, THF and chlorobenzene *etc*.. **ODI-CN** shows relatively poor solubility in these common solvents at room temperature but it can be easily dissolved at elevated temperature. The longest absorption maxima of **ODI** and **ODI-CN** in chloroform are located at 560 and 548 nm, respectively **(Figure 3.1 and Table 3.1).** The fluorescence spectrum of **ODI-CN** also showed similar blue-shift in compared with **ODI** due to the introduction of electron-accepting -CN groups. Cyclic voltammetry (**Figure 3.2 and Table 3.1**) revealed a low lying LUMO energy level (-3.90 eV) for **ODI-CN**, which is 0.76 eV lower than that for **ODI** (-3.14 eV).

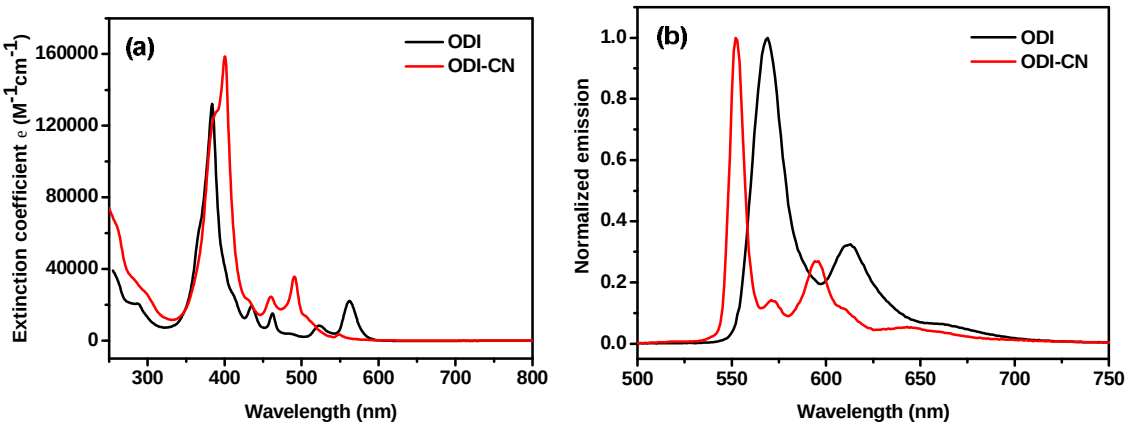

Figure 3.1 UV-vis absorption (a) and fluorescence spectra (b) of **ODI** and **ODI-CN** in dilute chloroform solutions (concentration = $1x10^{-5}$ M for absorption spectra and $1x10^{-6}$ M for emission spectra; excitation wavelenghth was 521 nm and 491 nm for **ODI** and **ODI-CN**, respectively).

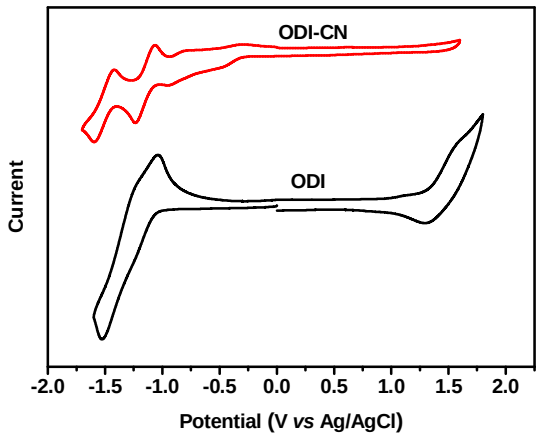

Figure 3.2 Cyclic voltammograms of **ODI** and **ODI-CN** in chlorobenzene with 0.1 M Bu_4NPF_6 as the supporting electrolyte.

Table 3.1 Summary of photophysical and electrochemical properties of **ODI** and **ODI-CN**.

Compounds	λ_{abs} (nm)	λ_{em}(nm)	E_{ox}^{1} (V)	E_{red}^{1} (V)	E_{red}^{2} (V)	E_{red}^{3} (V)	E_{red}^{4} (V)	HOMO (eV)	LUMO (eV)	E_g^{opt} (eV)
ODI	560, 521, 462, 435	384, 568, 612	1.1	-1.17	-1.40	-	-	-5.54	-3.14	2.14
ODI-CN	548, 491, 460, 431	401, 552, 595	-	-0.43	-0.85	-1.14	-1.51	-6.13	-3.90	2.23

E_{ox}^{n} and E_{red}^{n} are half-wave potentials for respective redox waves with AgCl/Ag as reference. HOMO and LUMO energy levels were calculated from the onset potentials of the first oxidation (E_{ox}^{onset}) and the first reduction wave (E_{red}^{onset}) according to the following equations: HOMO = -(4.8 + E_{ox}^{onset}) and LUMO = -(4.8 + E_{red}^{onset}), where the potentials are referred to $E_{Fc+/Fc}$. The HOMO level of **ODI-CN** was calculated from the optical energy gap (E_g^{opt}).

3.2.3 Aggregation in Solution

Both **ODI** and **ODI-CN** have strong tendency to aggregate in solution as revealed by variable-temperature ^{1}H NMR measurements (**Figure 3.3**). In particular, ^{1}H NMR spectrum of **ODI-CN** only shows broad resonances in the aromatic region at room temperature and the peaks are gradually shifted to low field and become well-split upon heating to higher temperatures. This is a good sign that **ODI-CN** molecules have strong intermolecular association *via* π-π interactions in solution.

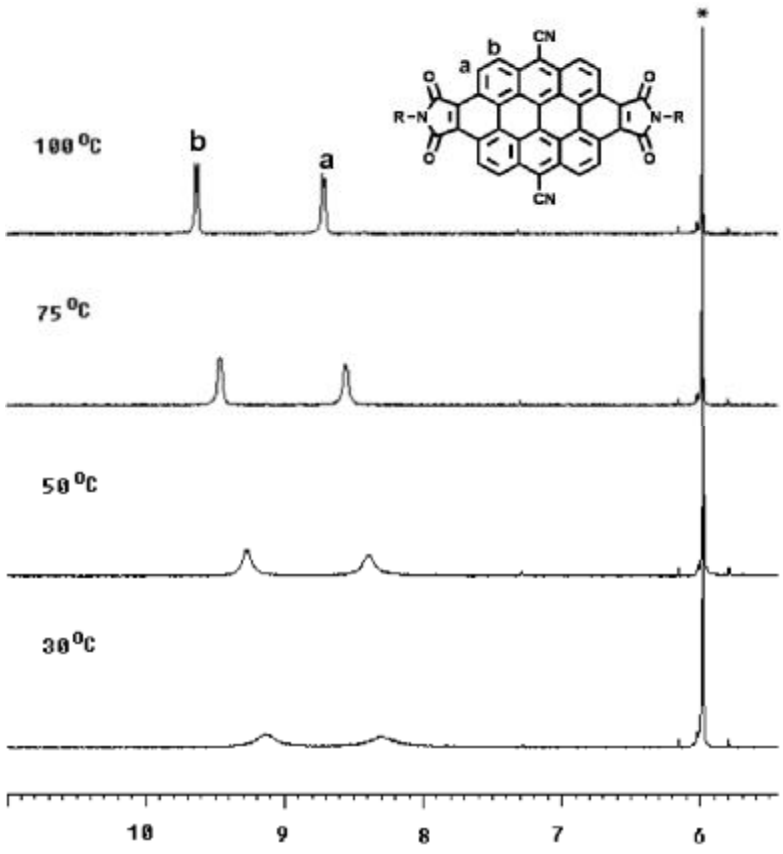

Figure 3.3 Variable-temperature ^{1}H NMR (500 MHz) spectra (aromatic region) of **ODI-CN** in [D2]tetrachloroethane.

3.2.4. Thermal Behavior and Molecular Packing

The thermal behavior of **ODI** and **ODI-CN** were investigated by combination of thermogravimetric analysis, differential scanning calorimetry, polarizing optical microscopy, and X-ray powder diffraction (XRD). **ODI** exhibited a higher thermal stability (decomposition temperature (T_d) = 443 ^{o}C) than **ODI-CN** (T_d = 345 ^{o}C) in N_2 atmosphere probably due to the relatively poor thermal stability of –CN group (**Figure 3.4**). **ODI** showed a monoclinic plastic crystalline phase (a = 4.85 nm, b = 3.01 nm, γ = 134^{o}) at room temperature and a hexagonal ordered columnar liquid crystalline phase (a = b = 2.62 nm, γ = 120^{o}) between 98 and 116 ^{o}C (**Figure 3.5**, **3.7**). The intense reflection peak at 3.48 Å can be correlated to long range ordered π-

stacking along the short axis of the discs. Another columnar LC phase was observed above 116 ^{o}C, which was supported by the fan-type texture observed at 350 ^{o}C (**Figure 3.5**). **ODI-CN** displayed a transition from polycrystalline to liquid crystalline phase at 236 ^{o}C (**Figure 3.6**). XRD pattern measured at room temperature showed a series of reflection peaks which can be correlated to a lamellar structure with inter-layer distance of 3.42 nm (**Figure 3.7**). Both **ODI** and **ODI-CN** do not enter isotropic phase below 500 ^{o}C, indicating very strong interactions between these large size ovalene molecules.

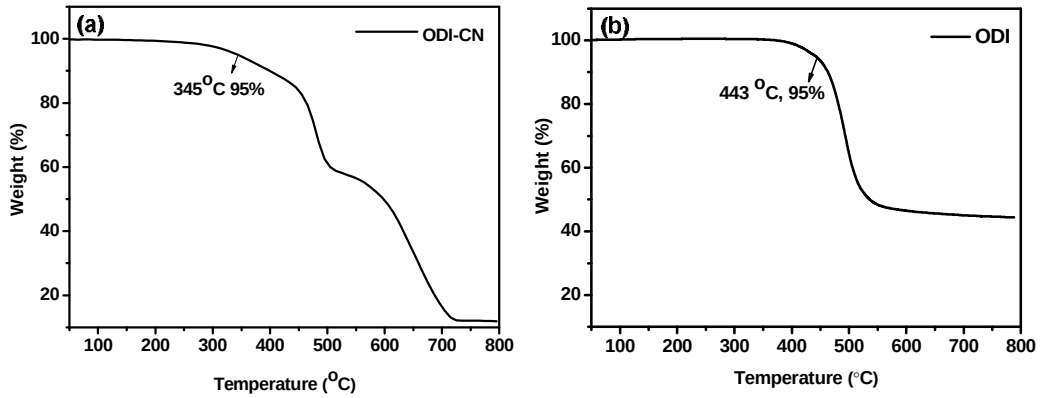

Figure 3.4 Thermogravimetric analysis (TGA) curves of **ODI** (a) and **ODI-CN** (b) (heating rate = 10 ^{o}C/min).

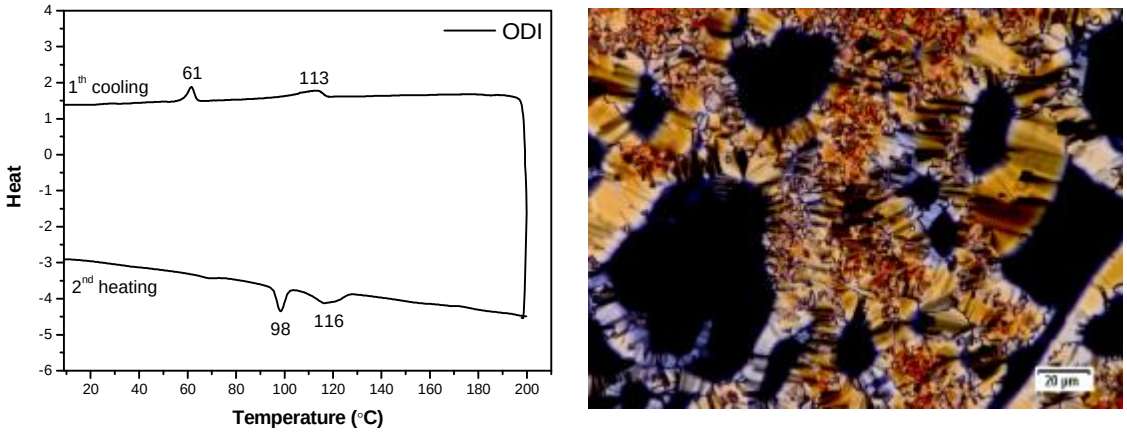

Figure 3.5 Differential scanning calorimetry (DSC) thermograms of **ODI** (second heating and first cooling scans are given, 10 ^{o}C min^{-1} under N_2, left) and polarizing optical microscopy (POM) image of **ODI-CN** at 350 ^{o}C during heating.

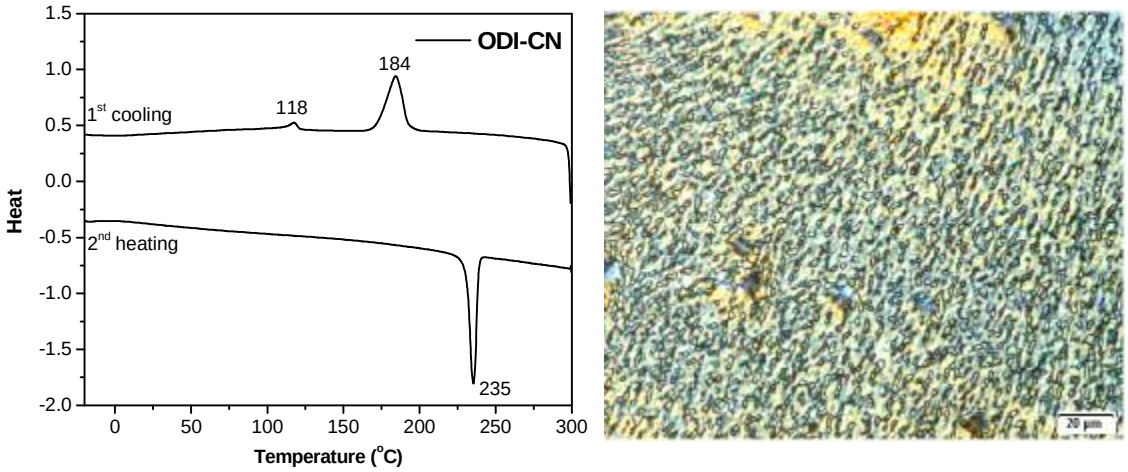

Figure 3.6 Differential scanning calorimetry (DSC) thermograms of **ODI-CN** (second heating and first cooling scans are given, 10 ^{o}C min^{-1} under N_2, left) and polarizing optical microscopy image of **ODI-CN** at 300 ^{o}C during heating.

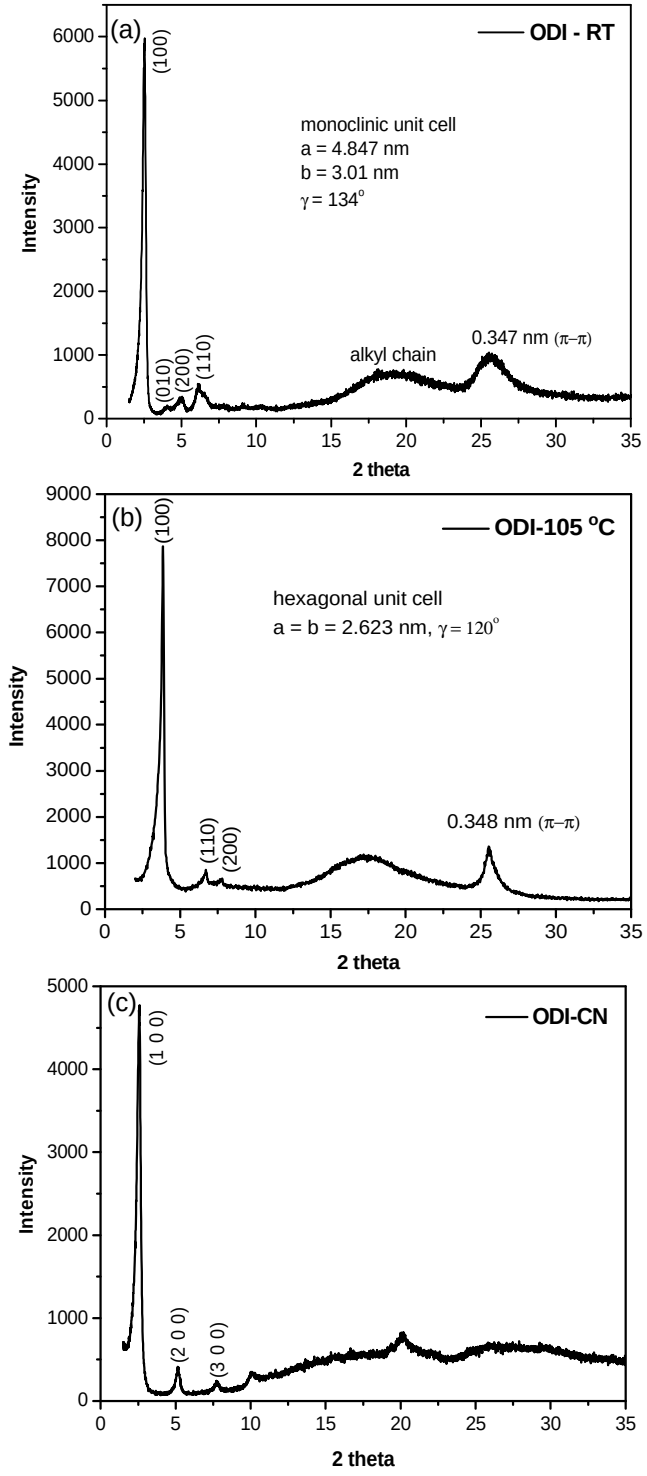

Figure 3.7 Powder X-ray diffraction (XRD) patterns of (a) **ODI** at room temperature; (b) **ODI** at 105 ^{o}C and (c) **ODI-CN** at room temperature.

3.2.5 Device Characterization

Charge transport properties of **ODI** and **ODI-CN** were investigated in OFETs. **ODI**, although showing ordered self-assembly, did not show FET activity in air. However, OFETs based on **ODI-CN** showed typical n-channel character in air. The devices were fabricated and measured with both top-contact and bottom-contact geometries under ambient conditions. In both cases, the thin films were prepared by spin-coating from chloroform solutions or drop-casting from 1,2-dichlorobenzene (DCB) solution. The dielectric surfaces (SiO_2) were either modified by octyltrichlorosilane (OTS) or unmodified. The devices were annealed in liquid crystalline phase of **ODI-CN** at 250 ^oC. Typical output and transfer characteristics are shown in **Figure 3.8**. The FET mobility was extracted using the following equation in the saturation regime from the gate sweep:

$$I_D = \frac{W}{2L} C_i \mu (V_G - V_T)^2$$

where I_D is the drain current in the saturated regime, μ is the field-effect mobility, C_i is the capacitance per unit area of the gate dielectric layer (SiO_2, 200 nm, C_i = 17.25 nF cm^{-2}), and V_G and V_T are gate voltage and threshold voltage, respectively. W and L are channel width and length, respectively. All the devices showed n-type behavior, and the top-contact devices exhibited an average mobility of 0.01-0.1 $cm^2V^{-1}s^{-1}$, and current on/off ratio of 10^5-10^6 (**Table 3.2**). The bottom-contact devices showed relatively lower mobility. For top-contact devices, the devices fabricated on unmodified substrate exhibited higher mobility than that made on OTS-modified SiO_2 substrate. For all devices, annealing at 250 ^oC improved FET mobility due to the self-healing property of **ODI-CN** in liquid crystalline phase.

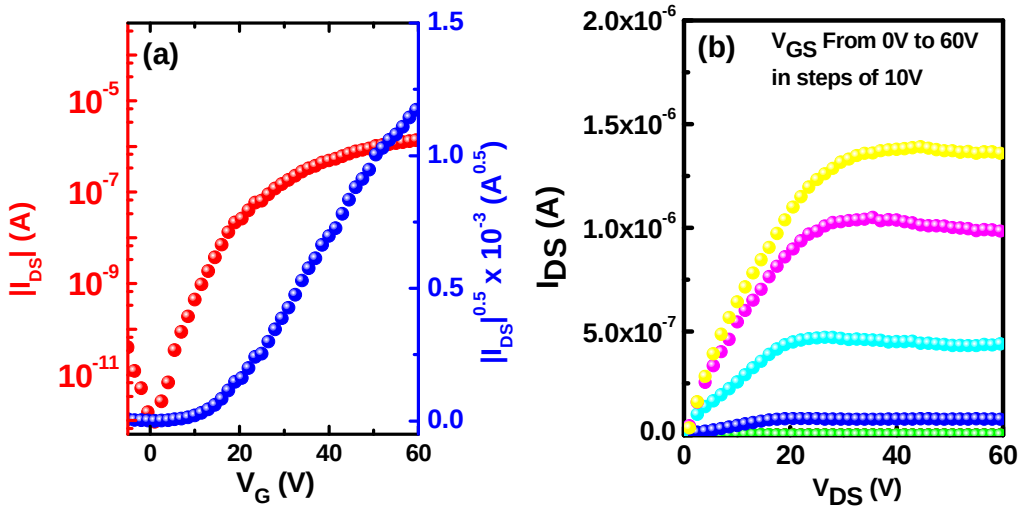

Figure 3.8 Transfer (a) and output (b) characteristic of the OFETs (bottom-contact) based on **ODI-CN**. The thin film was prepared from DCB solution on OTS treated SiO_2/Si substrate followed by annealing at 250 ^oC.

Table 3.2 Characteristics of **ODI-CN** based FET devices.

Run	solvents	Surface treatment	T_A[°C][a]	electrodes	μ_{sat}[cm^2/Vs]	V_T[V]	On/Off
1	$CHCl_3$	OTS	250	Au	0.014	15.5	1.08×10^{6}
2	$CHCl_3$	Bare[b]	250	Au	0.036	14.0	8.62×10^{5}
3	DCB	OTS	250	Au	0.03	13.8	5.96×10^{5}
4	DCB	bare	250	Au	0.1	13.7	8.27×10^{5}
5	$CHCl_3$	OTS	250	Au	0.004[c]	16.8	7.19×10^{4}
6	$CHCl_3$	Bare	250	Au	0.008[c]	17.8	4.84×10^{4}
7	DCB	OTS	250	Au	0.012[c]	17.4	8.07×10^{4}
8	DCB	OTS	250	Au	0.003[d]	21.4	2.46×10^{5}
9	DCB	Bare	250	Au	0.007[d]	15.4	5.28×10^{5}
10	DCB/$CHCl_3$[e]	Bare	250	Au	0.002[d]	21.9	1.13×10^{5}
11	DCB/$CHCl_3$[e]	OTS	250	Au	0.01[d]	17.7	6.20×10^{5}

[a] Annealing temperature. [b] Without treatment with OTS. [c] Test after storing in air for two months. [d] Bottom-contact geometry. [e] Drop-casted from DCB solution, then the film was annealed , and then spin-coated with chloroform solution.

The AFM image of the annealed thin film of **ODI-CN** spin-coated from chloroform showed uniform grains that are orderly connected to each other (**Figure 3.9a-b**). While the annealed thin film drop-casted from DCB revealed large crystalline grains of over one micrometer in size (**Figure 3.9c-d**). The large polycrystalline grains should facilitate charge carrier transport and in fact devices

fabricated from DCB solution showed higher FET mobility than that from chloroform solution on bare SiO_2/Si substrate. In addition, although the grains become larger after annealing, they are less connected or poorly contacted, which could lead to a decreasing performance. Therefore, thin films were also prepared by drop-casting from DCB solution followed by annealing and then chloroform solution was spin-coated to fill the cracks and voids between grains. Improved performance was achieved for devices with OTS-modified substrate. The XRD patterns of the thin films after annealing exhibited intense Bragg's diffraction peaks (**Figure 3.10**), indicating the formation of large crystals on the surface of the substrate. A typical lamellar structure can be easily assigned based on a series of (100), (200) and (300) reflection peaks, which are correlated to a layer-like packing mode with an interlayer distance of 3.35 nm. These data also suggest that the molecules possess a stacking orientation nearly upright to the surface (**Figure 3.10, insert**) and such a dense packing mode facilitates efficient charge transport along the π-stacked columns and gave high FET mobility. Moreover, the devices also displayed relatively good air stability due to the low-lying LUMO energy level (-3.9 eV).[22] The device still showed high mobility up to 0.012 $cm^2V^{-1}s^{-1}$ even after storing in air for two months (**Table 3.2,** run 7). The kinetic stability of the highly crystalline dense packing could be another contributor to the air stability.[23]

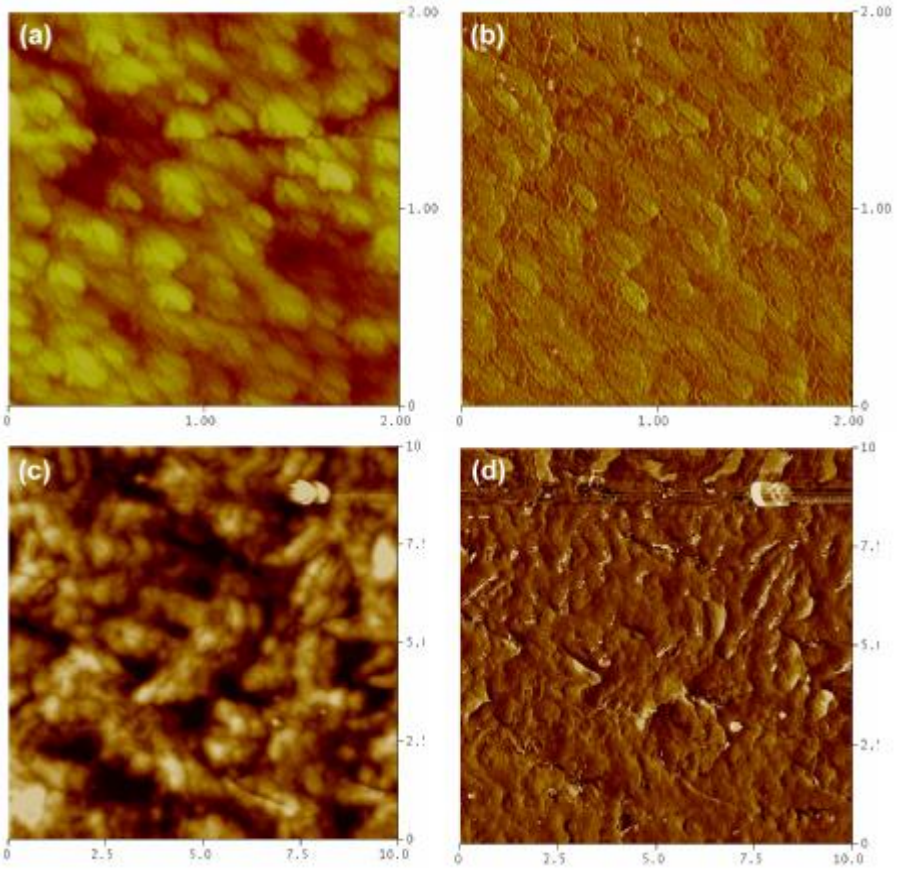

Figure 3.9 Tapping mode AFM images of the thin films of **ODI-CN** on SiO_2/Si substrate prepared by different methods. (a) and (b): spin-coated from chloroform solution followed by annealing at 250 ^oC (scan area 2×2 μm^2); (c) and (d): drop-casted from DCB solution followed by annealing at 250 ^oC (scan area 10×10 μm^2). (a) and (c): height mode; (b) and (d): phase mode.

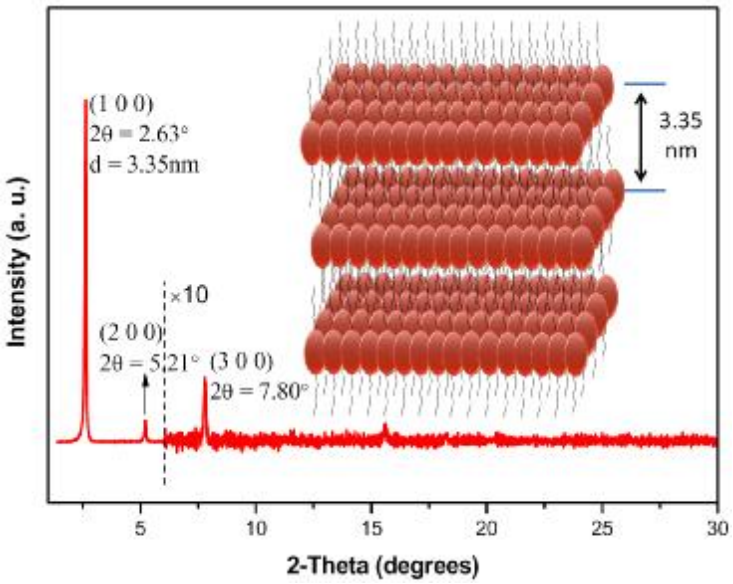

Figure 3.10 XRD pattern of **ODI-CN** thin film prepared by drop-coating from DCB solution onto OTS treated substrate followed by annealing. Insert is the proposed packing mode.

3.3 Conclusions

In summary, large disc-like ovalene diimides were prepared for the first time. These new molecules showed ordered self-assembly both in solution and in solid state. Due to attachment of electron-withdrawing imide and cyano- groups, **ODI-CN** exhibited typical n-type semiconducting behavior and high electron mobility up to 0.1 cm^2/Vs were achieved in solution processing OFET devices. The device also displayed good air stability. Further investigation on uniaxial alignment of these molecules between source and drain electrodes with intention to increase the charge carrier mobility is under way in our laboratories.

3.4 Experimental Section

3.4.1 Device Fabrication

Top-contact, bottom-gate FET devices were prepared under ambient conditions. A

heavily p-doped silicon wafer with a 200-nm thermal SiO_2 layer was used as the substrate/gate electrode. The SiO_2/Si substrate was cleaned with acetone, then immerse in a piranha solution for 8 minutes, followed by rinsing with deionized water, and then re-immersed in a solution of OTS in toluene at 65 °C for 20 minutes. The semiconductor layer was deposited on top of the OTS-modified and untreated SiO_2 surface by spin-coating the solution of **ODI-CN** in chloroform (6 mg/mL) at 1500 rpm for 60 seconds or drop-casting the solution in dichlorobenzene (4 mg/mL). Subsequently, gold source/drain electrode pairs were deposited by thermal evaporation through a metal shadow mask to create a series of FETs with various channel length (L = 100 or 150 μm) and width (W = 1 or 4 mm) dimensions. The bottom-contact devices were fabricated using standard photolithography technique followed by evaporation of 95 nm gold on 5 nm titanium was used to define source and drain electrodes of 30-100 μm channel lengths and 10 mm channel widths. The SiO_2 dielectric was modified by OTS. The Au electrode was modified by 1-octanethiol. The semiconductor layer was deposited on top of the OTS-modified SiO_2 surface by same solution process. The thin films were annealed at 250 °C under vacuum for 1h. The FET devices were then characterized using a Keithley SCS-4200 probe station under ambient conditions in the dark.

3.4.2 General Experimental Methods

All reagents and starting materials were obtained from commercial suppliers and used without further purification. Tetrahydrofuran (THF) was purified by routine procedure and distilled over sodium under nitrogen before using. Bisanthenequinone was prepared according to literature (Arabei, S. M.; Pavich, T. A. *J. Appl. Spectr.* **2000**, *67*, 236). 2-Decyltetradecan-1-amine was prepared according to previous report

(Zhan X. W. et al. *J. Am. Chem. Soc.* **2007**, *129*, 7246). Column chromatography was performed on silica gel 60 (Merck 40-60 nm, 230-400 mesh). All NMR spectra were recorded on the Bruker AMX500 spectrometer. All chemical shifts are quoted in ppm, relative to tetramethylsilane, using the residual solvent peak as a reference standard. MALDI-TOF MS spectra were measured on a Bruker Autoflex MALDI-TOF instrument, using 1,8,9-trihydroxyanthracene as a matrix. UV-vis absorption was recorded on Shimadzu UV-1700 spectrometer. The solvents used for UV-vis and PL measurements are of HPLC grade (Merck). The electrochemical measurements were carried out in anhydrous chlorobenzene with 0.1 M tetrabutylammonium hexafluorophosphate (Bu_4NPF_6) as the supporting electrolyte at a scan rate of 0.05 V/s at room temperature under the protection of nitrogen. A gold disk was used as working electrode, platinum wire was used as counter electrode, and Ag/AgCl (3M KCl solution) was used as reference electrode. Thermogravimetric analysis (TGA) was carried out on a TA instrument 2960 at a heating rate of 10 ^{o}C/min under nitrogen flow. Differential scanning calorimetry (DSC) was performed on a TA instrument 2920 at a heating /cooling rate of 10 ^{o}C/min under nitrogen flow. Polarizing optical microscope (POM) measurements were conducted on the OLYMPUS BX51equipped with the Linkam TP94 programmable hot stage. X-ray diffraction (XRD) patterns of the thin film and powder were measured on a Bruker-AXS D8 DISCOVER with GADDS X-ray diffractometer. Copper Kα line was used as a radiation source with λ = 1.5406 Å. Tapping-mode AFM was performed on a Nanoscope V microscope (Veeco Inc.).

3.4.3 Material Synthesis and Characterization Data

Synthesis of compound 3-3: Four portion of zinc powder (4 x 6 g) and 80% acetic acid (4 x 10 mL) were added in 30-minute intervals to a refluxing suspension of bisanthenequinone in pyridine (200 mL). The yellow suspension became green, then brown. After 5 h, the solution was cooled to room temperature, the zinc power filtered off, and water (1 L) added. The precipitate thus formed was filtered off and dried under vacuum to yield 1.6 g of a yellow insoluble solid. This solid was heated at relux for 12 h with maleic anhydride (5 g) in nitrobenzene (60 mL). A color change from greenish yellow via blue and violet to brown was observed during warming and the first 30 minutes at reflux. Chloroform was added to the cooled solution, and the insoluble solid was filtered off, washed with chloroform, and dried under vacuum to yield crude dianhydried **3-3** as an insoluble material.

Synthesis of compound ODI: Crude dianhydride **3-3** (1 g, 1.86 mmol), 2-decyltetradecan-1-amine (3.28 g, 9.28 mmol), and 200 mL of DMF were heated under nitrogen at 175 ^{o}C overnight. The reaction mixture was cooled to room temperature and 200 mL of methanol was added. The red solid was collected by vacuum filtration and washed with methanol for several times, dried under vacuum, and then further purified by column chromatography on silica gel with DCM: Hexane = 1:1 (v/v) as eluent to afford **ODI** (1.84 g, 82%) as deep red solid. ^{1}H NMR (500 MHz, $Cl_2CDCDCl_2$, 100 ^{o}C), δ ppm = 0.96 (m, 12H, -CH_3), 1.34-1.74 (m, 80H, -CH_2), 2.31 (br, 2H, -CH)， 4.01 (d, *J* = 6.9 Hz, 4H, -CH_2), 7.60 (d, *J* = 8.2 Hz, 4 H, Ar), 7.65 (s, 2 H Ar), 8.73 (d, *J* = 8.2 Hz, 4 H Ar). ^{13}C NMR (125 MHz, $Cl_2CDCDCl_2$, 100 ^{o}C), δ ppm = 13.52, 13.55, 22.21, 22.25, 26.49, 28.94, 29.00, 29.32, 29.40, 29.45, 29.48, 29.99, 31.55, 31.60, 32.07, 37.60, 42.68, 114.91, 115.00, 119.48, 121.09, 121.74, 121.79, 123.14, 126.03, 127.63, 168.99. MS (MALDI-TOF): m/z = 1209.51; High

resolution (HR) MS (MALDI-TOF): m/z = 1208.8250, calculated for $C_{84}H_{108}N_2O_4$: 1208.8304 (error = -4.44 ppm).

Synthesis of compound ODI-Br: ODI (500 mg, 0.41 mmol), bromine (0.1 mL) in 100 mL of $CHCl_3$ was reacted at room temperature for 5 days. The organic layer was extracted with $CHCl_3$ and washed with Na_2SO_3 aqueous solution for several times. The organic layer was concentrated and further purified by column chromatography on silica gel with $CDCl_3$: Hexane = 1:2 (v/v) as eluent to afford **ODI-Br** as deep red solid in 85% yield. ^{1}H NMR (500 MHz, $Cl_2CDCDCl_2$, 100 ^{o}C), δ ppm = 0.99 (m, 12H, -CH_3), 1.34-1.62 (m, 80H, -CH_2), 2.17 (br, 2H, -CH), 3.82 (br, 4H, -CH_2), 7.35 (br, 4 H, Ar), 8.21 (br, 4 H, Ar). ^{13}C NMR (125 MHz, $Cl_2CDCDCl_2$, 100 ^{o}C), δ ppm = 13.61, 13.63, 22.29, 22.32, 26.31, 29.01, 29.06, 29.29, 29.39, 29.46, 29.49, 29.99, 31.62, 31.66, 31.86, 37.45, 42.57, 113.19, 116.75, 119.78, 120.77, 121.67, 122.22, 123.15, 126.35, 167.87. MS (MALDI-TOF): m/z = 1367.24; HR MS (MALDI-TOF): m/z = 1364.6447, calculated for $C_{84}H_{106}Br_2N_2O_4$: 1364.6514 (error = -4.90 ppm).

Synthesis of compound ODI-CN: ODI-Br (100 mg, 0.07 mmol), zinc cyanide (65 mg, 0.73 mmol), 1,1'-bis(diphenylphosphino)-ferrocene (12.7 mg, 0.02 mmol), tris(dibenzylideneacetone)-dipalladium (5.4 mg, 0.01 mmol) were combined in dry *p*-dioxane (20 mL) and refluxed for 2 days under nitrogen atmosphere. The crude product was filtered through glass funnel, and washed with methanol, and then further purified by column chromatography on silica gel with hot $CHCl_3$ as eluent to afford **ODI-CN** (78 mg, 86%) as red solid. ^{1}H NMR (500 MHz, $Cl_2CDCDCl_2$, 100 ^{o}C), δ ppm = 0.92 (m, 12H, -CH_3), 1.33-1.73 (m, 80H, -CH_2), 2.37 (br, 2H, -CH), 4.18 (d, *J* = 6.3 Hz, 4H, -CH_2), 8.34 (d, *J* = 8.85 Hz, 4H, Ar), 9.33 (d, *J* = 8.85 Hz, 4H, Ar). ^{13}C NMR (125 MHz, $Cl_2CDCDCl_2$, 100 ^{o}C), δ ppm = 13.52, 13.55, 22.21, 22.25, 26.40,

26.42, 28.93, 28.99, 29.31, 29.37, 29.38, 29.43, 29.92, 31.54, 31.59, 32.00, 37.62, 43.37, 105.10, 114.08, 114.83, 116.45, 118.61, 121.44, 124.29, 125.32, 125.40, 127.17, 167.85. MS (MALDI-TOF): m/z = 1259.18; HR MS (MALDI-TOF): m/z = 1258.8221, calculated for $C_{86}H_{108}N_4O_4$: 1258.8209 (error = 0.98 ppm).

Appendix:

1. MALDI-TOF mass spectra of ODI, ODI-Br and ODI-CN.

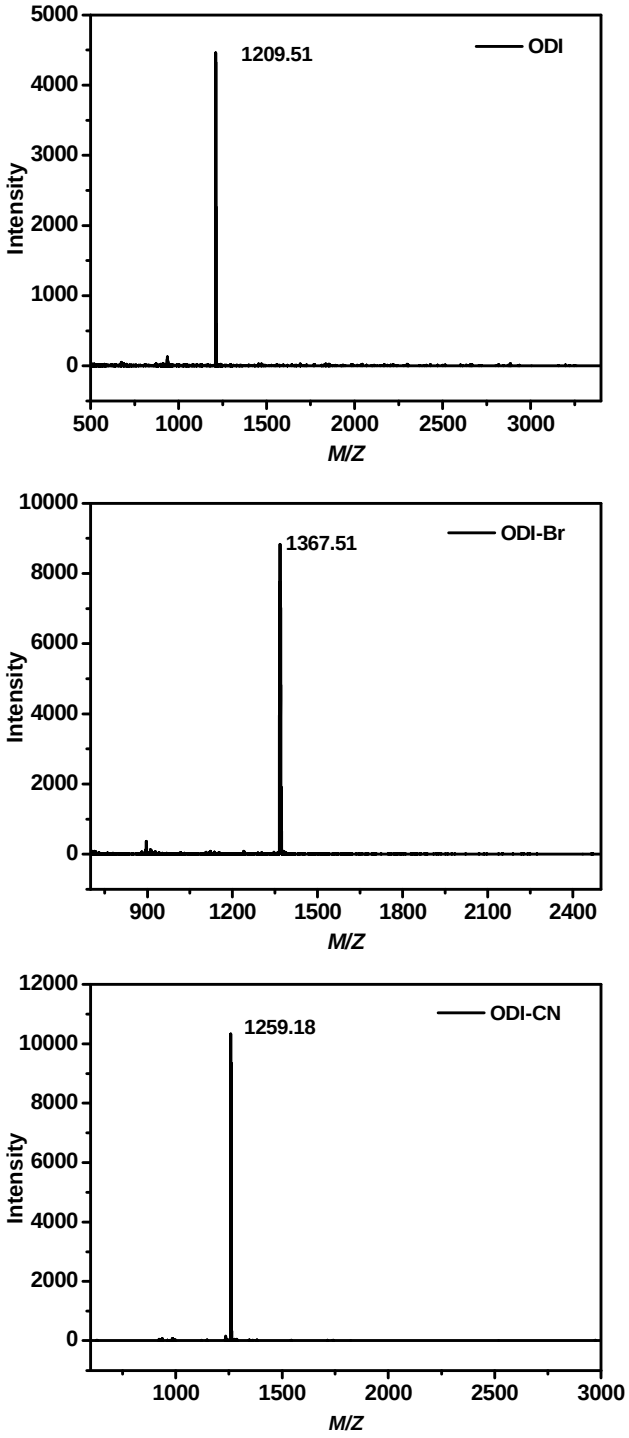

2. ^{1}H NMR (500 MHz), ^{13}C NMR (125 MHz) spectra of ODI, ODI-Br and ODI-CN recorded at 100 ^{o}C in $CDCl_2CDCl_2$.

^{1}H NMR spectrum of **ODI** recorded at 100 ^{o}C in $CDCl_2CDCl_2$ (500 MHz)

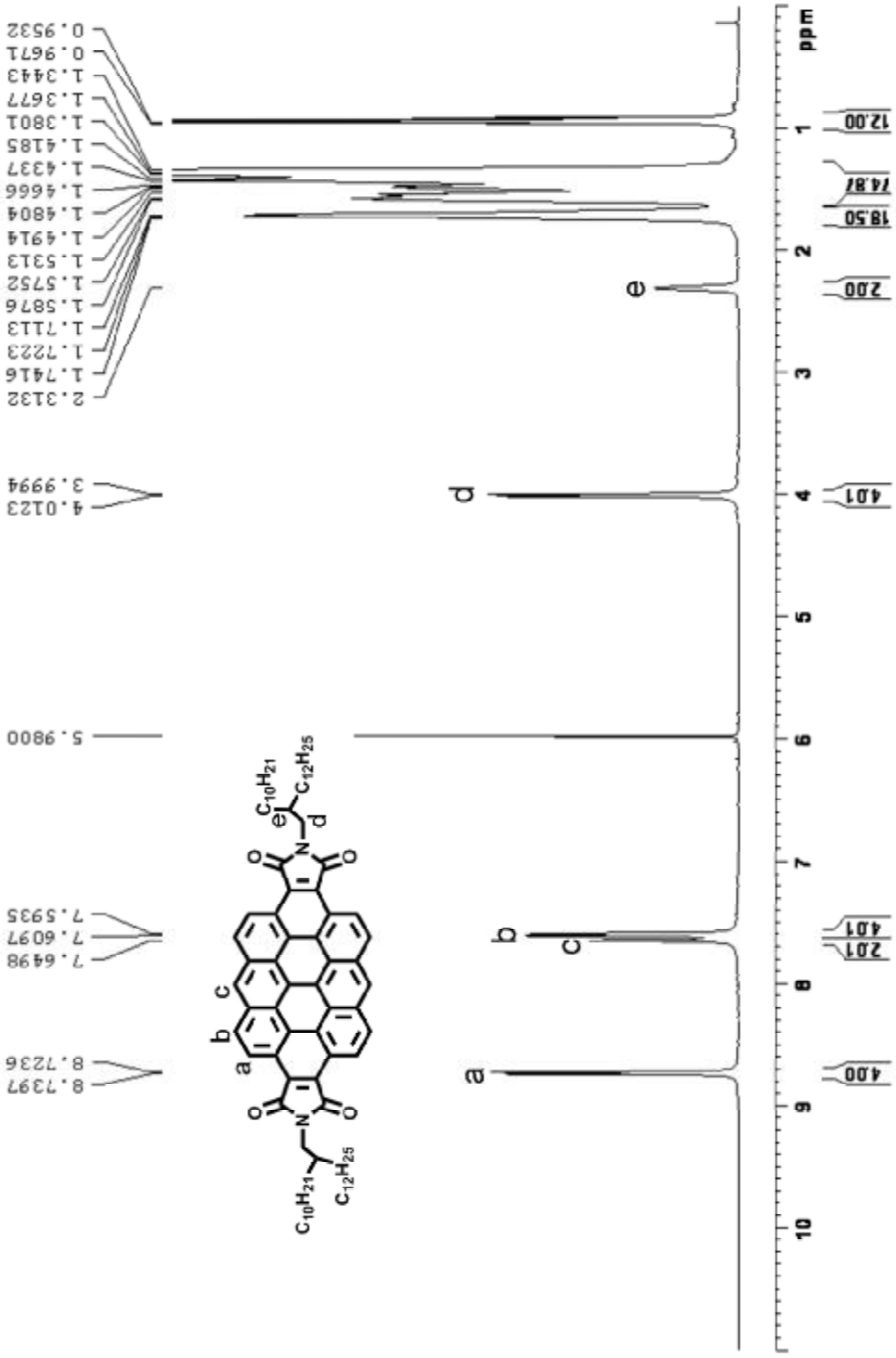

^{13}C NMR spectrum of **ODI** recorded at 100 ^{o}C in $CDCl_2CDCl_2$ (125 MHz)

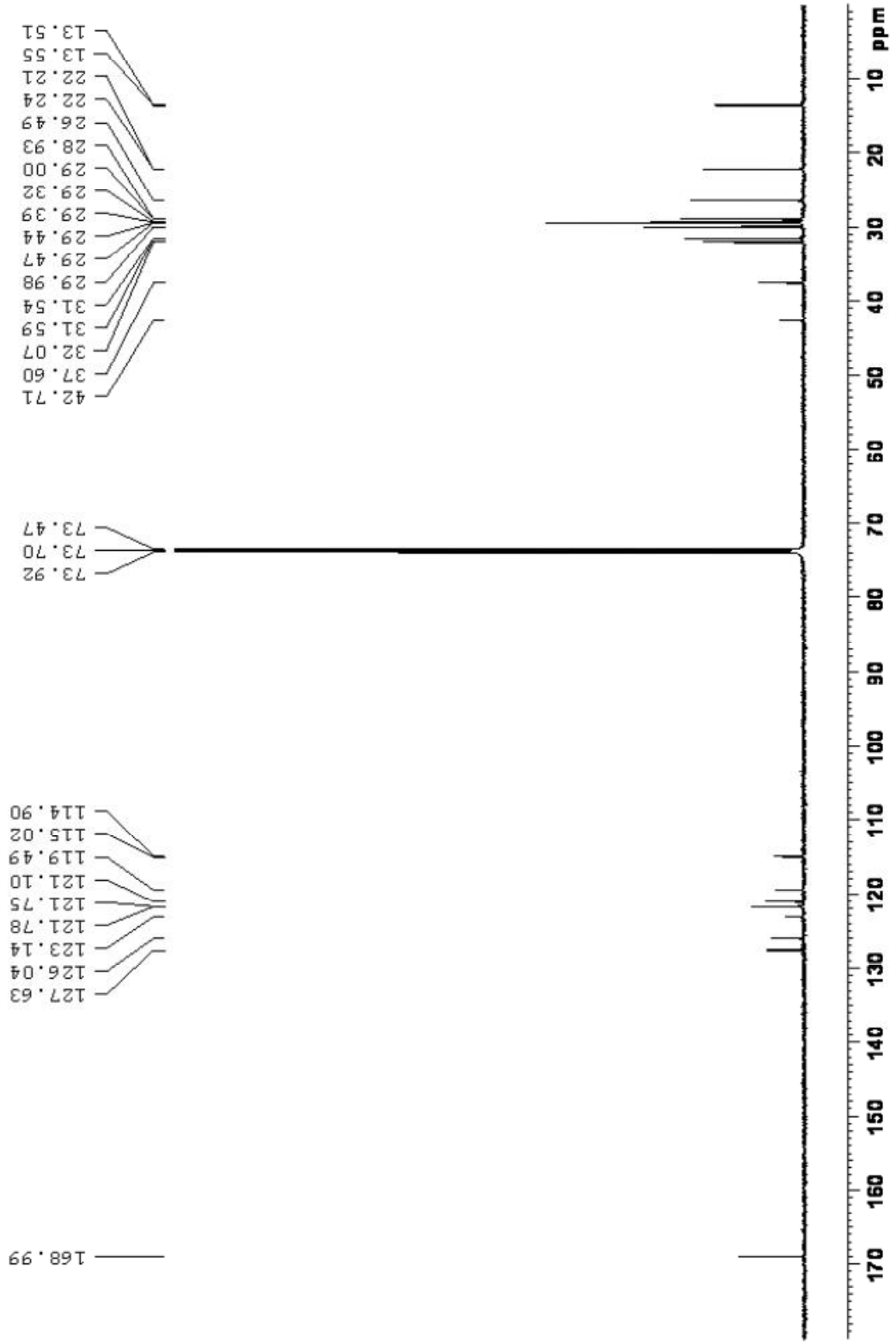

^{1}H NMR spectrum of **ODI-Br** recorded at 100 ^{o}C in $CDCl_2CDCl_2$ (500 MHz)

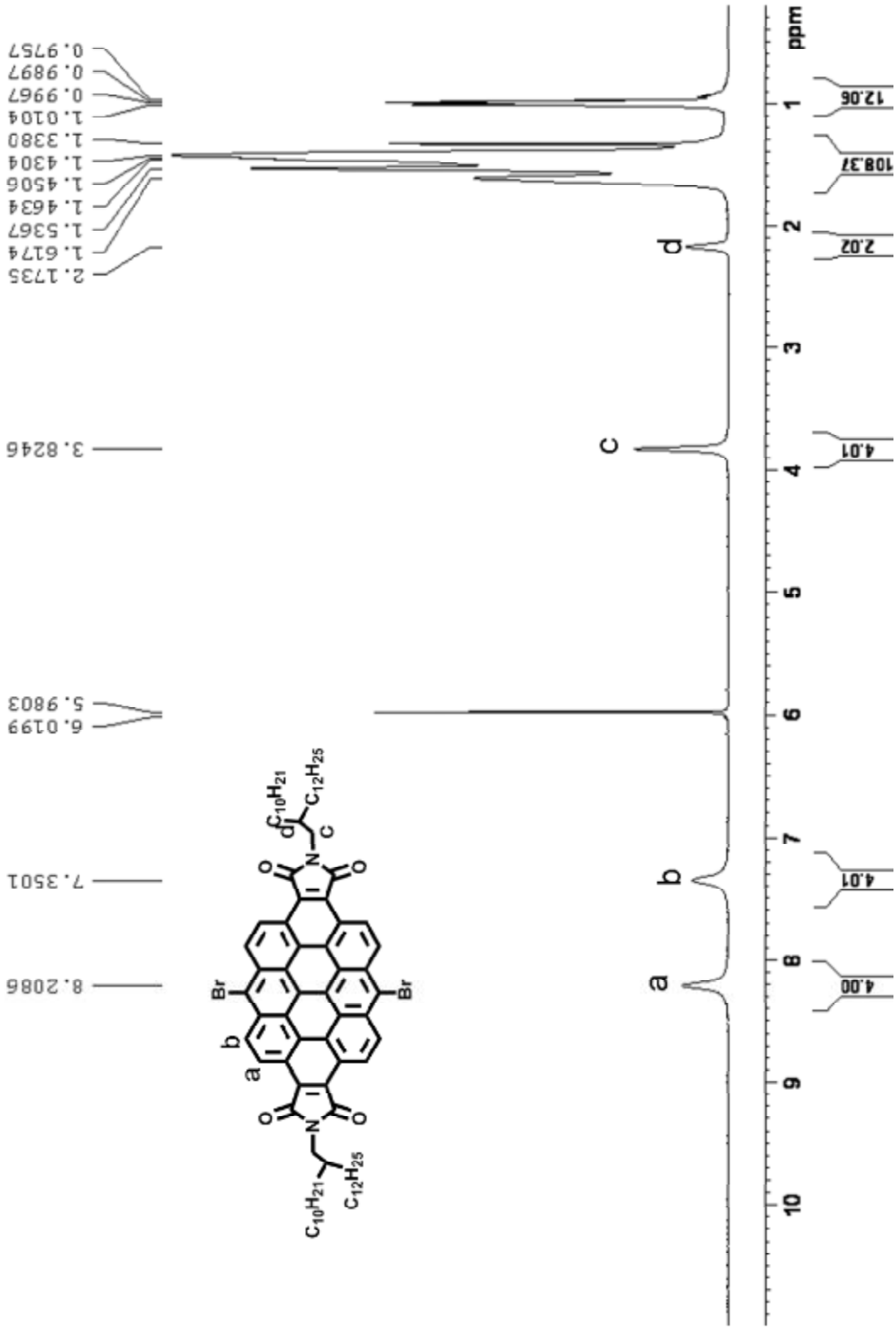

^{13}C NMR spectrum of **ODI-Br** recorded at 100 ^{o}C in $CDCl_2CDCl_2$ (125 MHz)

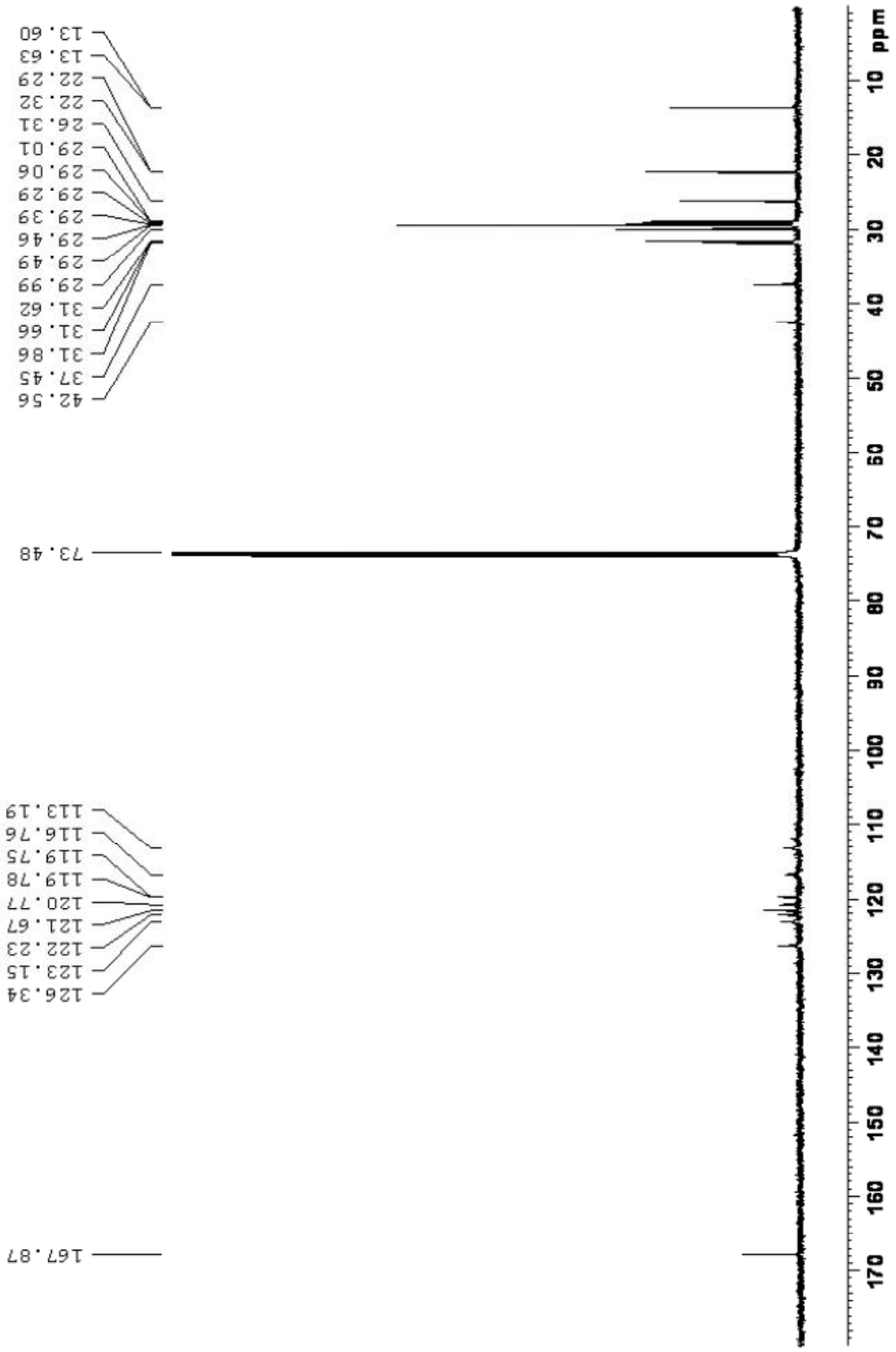

^{1}H NMR spectrum of **ODI-CN** recorded at 100 ^{o}C in $CDCl_2CDCl_2$ (500 MHz)

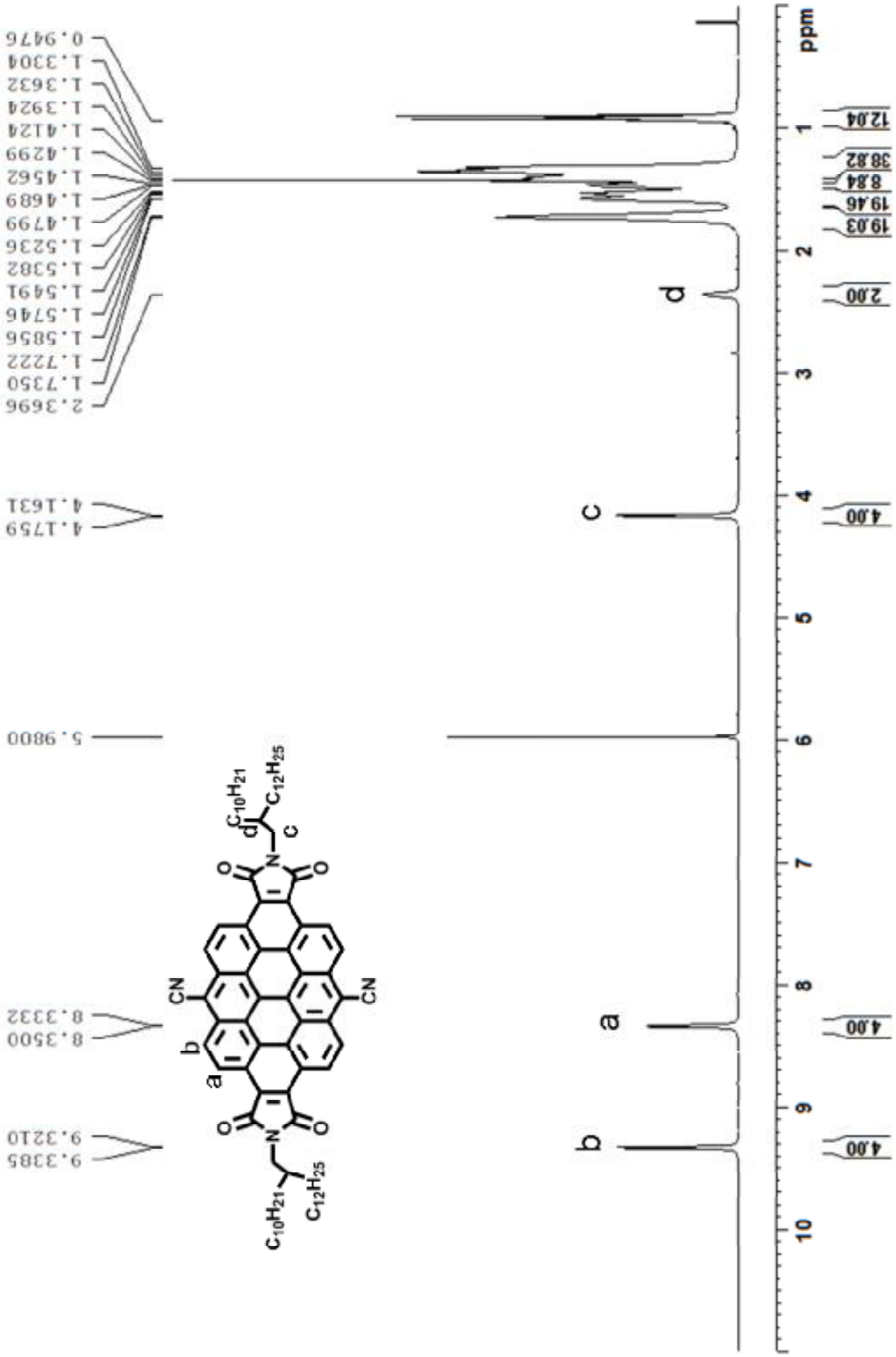

^{13}C NMR, spectrum of **ODI-CN** recorded at 100 ^{o}C in $CDCl_2CDCl_2$ (125 MHz)

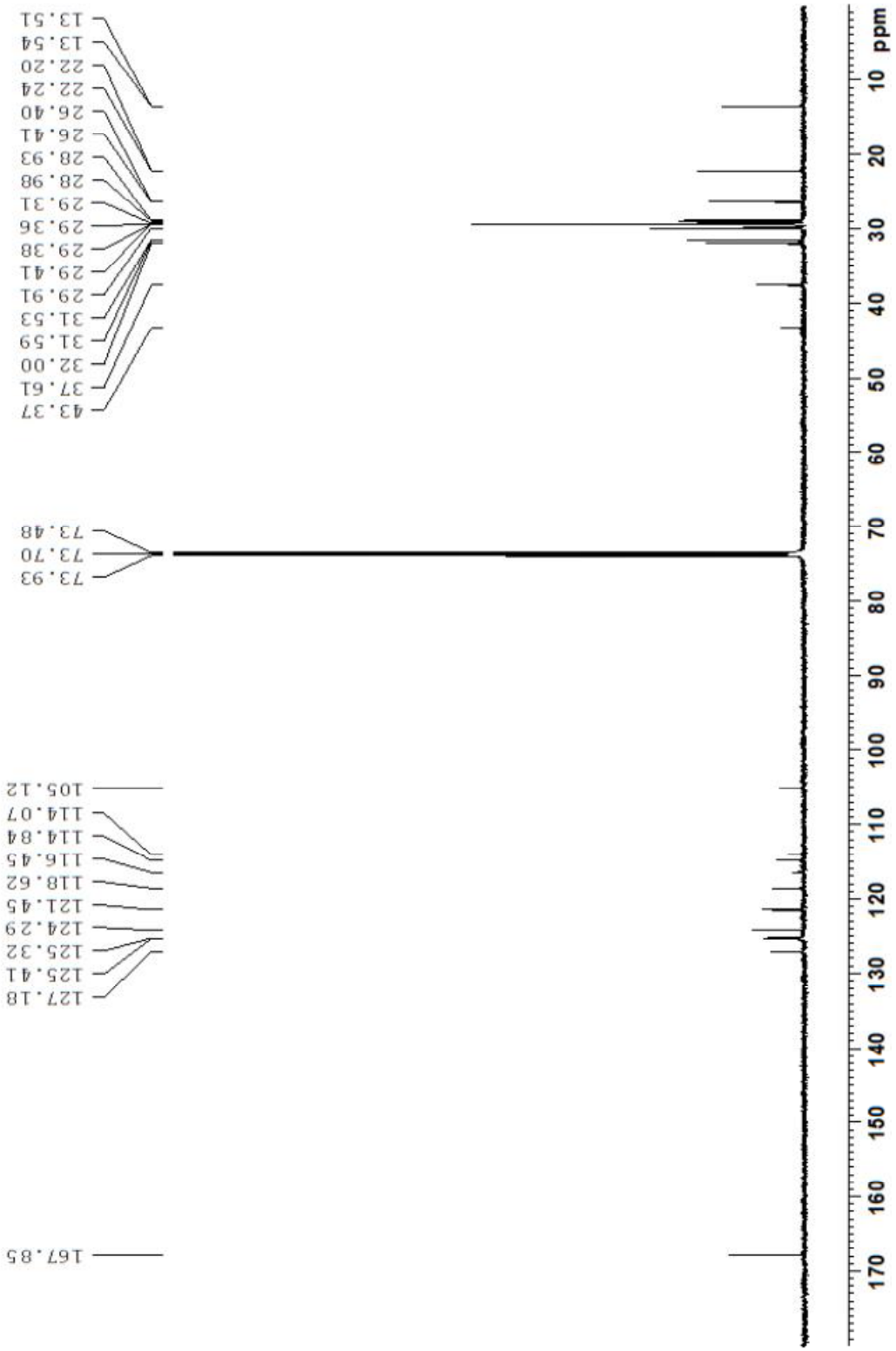

References

1. a) Dimitrakooulos, C. D.; Malenfant, P. R. L. *Adv. Mater.* **2002**, *14*, 99; b) Wen, Y.; Liu, Y. *Adv. Mater.* **2010**, *22*, 1331; c) Anthony, J. E.; Facchetti, A.; Heeney, M.; Marder, S. R. *Adv. Mater.* **2010**, *22*, 3876.

2. a) Anthony, J. E.; *Angew. Chem. Int. Ed*. **2008**, *47*, 452; b) Dong, H.; Wang, C.; Hu, W. *Chem. Commun*. **2010**, *46*, 5211.

3. a) Sakamoto, Y.; Suzuki, T.; Kobayashi, M.; Gao, Y.; Fukai, Y.; Inoue, Y.; Sato, F.; Tokito, S. *J. Am. Chem. Sc.* **2004**, *126*, 8138; b) Ando, S.; Nishida, J. I.; Fujiwara, E.; Tada, H.; Inoue, Y.; Tokito, S.; Yamashita, Y. *J. Am. Chem. Soc*. **2005**, *127*, 5336; c) Zheng, Q.; Huang, J.; Sarjeant, A.; Katz, H. E. *J. Am. Chem. Soc*. **2008**, *130*, 14410.

4. a) Babel, A.; Jenekhe, S. A. *J. Am. Chem. Soc*. **2003**, *125*, 13656; b) Letizia, J. A.; Salata, M. R.; Tribout, C. M.; Facchetti, A.; Ratner, M. A.; Marks, T. J. *J. Am. Chem. Soc.* **2008**, *130*, 9679; c) Chen, Z.; Zheng, Y.; Yan, H.; Facchetti. A. *J. Am. Chem. Soc*. **2009**, *131*, 8.

5. a) Facchetti, A.; Deng, Y.; Wang, A.; Koide, Y.; Sirringhaus, Y.; Marks, T. J.; Friend, R. H. *Angew. Chem. Int. Ed.* **2000**, *39*, 4547; b) Facchetti, A.; Mushrush, M.; Yoon, M.-H.; Hutchison, G. R.; Ratner, M. A.; Marks, T. J. *J. Am. Chem. Soc.* **2004**, *126*, 13859.

6. Letizia, J. A.; Salata, M. R.; Tribout, C. M.; Facchetti, A.; Ratner, M. A.; Marks, T. J. *J. Am. Chem. Soc.* **2008**, *130*, 9679.

7. Swartz, C. R.; Parkin, S. R.; Bullock, J. E.; Anthony, J. E.; Mayer, A. C.; Malliaras, G. G. *Org. Lett.* **2005**, *7*, 3163.

8. Ando, S.; Murakami, R.; Nishida, J.; Tada, H.; Inoue, Y.; Tokito, S.; Yamashita, Y. *J. Am. Chem. Soc.* **2005**, *127*, 14996.

9. a) Laschat, S.; Baro, A.; Steinke, N.; Giesselmann, F.; Hägele, C.; Scalia, G.; Judele, R.; Kapatsina, E.; Sauer, S.; Schreivogel, A.; Tosoni, M. *Angew. Chem. Int. Ed*. **2007**, *46*, 4832; b) Sergeyev, S.; Pisulab, W.; Geerts, Y. H. *Chem. Soc. Rev*. **2007**, *36*, 1902.

10. Adam, D.; Schuhmacher, P.; Simmerer, J.; Häussling, L.; Siemensmeyer, K.; Etzbach, K. H.; Ringsdorf, H.; Haarer, D. *Nature* **1994**, *371*, 141.

11. Wu, J.; Pisula, W.; Müllen, K. *Chem. Rev.* **2007**, *107*, 718.

12. Kimura, M.; Saito, Y.; Ohta, K.; Hanabusa, K.; Shirai, H.; Kobayashi, N. *J. Am. Chem. Soc.* **2002**, *124*, 5274.

13. Chandrasekhar, S. *Mol. Cryst. Liq. Cryst.* **1981**, *63*, 171.

14. a) Jones, B. A.; Facchetti, A.; Marks, T. J.; Wasielewski, M. R. *Chem. Mater.* **2007**, *19*, 2703; b) Shukla, D.; Nelson, S. F.; Freeman, D. C.; Rajeswaran, M.; Ahearn, W. G.; Meyer, D. M.; Carey, J. T. *Chem. Mater*. **2008**, *20*, 7486; c) Jung, B. J.; Sun, J. Lee, T.; Sarjeant, A.; Katz, H. E. *Chem. Mater.* **2009**, *21*, 94.

15. a) Jones, B. A.; Ahrens, M. J.; Yoon, M. H.; Facchetti, A.; Marks, T. J.; Wasielewski, M. R. *Angew. Chem. Int. Ed.* **2004**, *43*, 6363; b) Ling, M.; Erk, P.; Gomez, M.; Koenemann, M.; Locklin, J.; Bao, Z. *Adv. Mater.* **2007**, *19*, 1123; c) Weitz, R. T.; Amsharov, K.; Zschieschang, U.; Villas, E. B.; Goswami, D. K.; Burghard, M.; Dosch, H.; Jansen, M.; Kern, K.; Klauk, H. *J. Am. Chem. Soc.* **2008**, *130*, 4637; d) Piliego, C.; Jarzab, D.; Gigli, G.; Chen, Z.; Facchetti, A.; Loi, M. A. *Adv. Mater.* **2009**, *21*, 1573; e) Schmidt, R.; Oh, J. H.; Sun, Y.; Deppisch, M.; Krause, A.;

Radacki, K.; Braunschweig, H.; Könemann, M.; Erk, P.; Bao, Z.; Würthner, F. *J. Am. Chem. Soc.* **2009**, *131*, 6215.

16. An, Z.; Yu, J.; Domercq, B.; Jones, S. C.; Barlow, S.; Kippelen, B.; Marder, S. R. *J. Mater. Chem*. **2009**, *19*, 6688.

17. Debije, M. G.; Piris, J.; de Haas, M. P.; Warman, J. M.; Tomović, Ž.; Simpson, C. D.; Watson, M. D.; Müllen, K. *J. Am. Chem. Soc*. **2004**, *126*, 4641.

18. van de Craats, A.; Warman, J. M. *Adv. Mater*. **2001**, *13*, 130.

19. Clar, E. *Nature,* **1948**, *161*, 238.

20. Saidi-Besbes, S.; Grelet, E.; Bock, H. *Angew. Chem. Int. Ed.* **2006**, *45*, 1783.

21. Arabei, S. M.; Pavich, T. A. *J. Appl. Spectr.* **2000**, *67*, 236.

22. Jones, B. A.; Facchetti, A.; Wasielewski, M. R.; Marks, T. J. *J. Am. Chem. Soc.* **2007**, *129*, 15259.

23. Katz, H. E.; Johnson, J.; Lovinger, A. J.; Li, W. J. *J. Am. Chem. Soc.* **2000**, *122*, 7787.

Chapter 4: Lateral Extension of π-Conjugation along the Bay Regions of Bisanthene *via* Diels-Alder Cycloaddition Reaction

4.1 Introduction

Polycyclic aromatic hydrocarbons (PAHs) with largely extended π-conjugation and small band gap possess promising applications as organic semiconductors[1] for electronic devices and as organic dyes[2] for solar cells and bio-imaging. The physical property and chemical reactivity of a PAH is largely determined by arrangement of the benzenoid rings in the π-system and the extent of π-conjugation. Linear fusion of benzene rings leads to oligoacenes among which both the band gap and stability quickly decreases with increase of the number of benzene ring.[3] Anthracene,[4] tetracene[5] and pentacene derivatives[6] have been successfully applied in organic field effect transistors (OFETs) and organic light-emitting diodes (OLEDs). Higher order acenes (> pentacene) with low band gaps turned out to be extremely unstable and appropriate substitution by aryl, alkyne, arylthio- groups or electronegative halogen atoms have to be done to obtain relatively stable hexacene,[7] heptacene,[7d, 8] and nonacene.[9] Alternative approach to stabilize oligoacenes and to extend π-conjugation is benzannulation around acene framework and various benzannulated pentacene and higher order homologues have been reported.[10] Introduction of phenyl rings in these benzannulated acene fragments usually results in puckering the molecules, e.g., twisting, and gives a family of contorted molecules called as "twistacenes".[11] Another type of interesting PAH molecule is rylene, in which two or more naphthalene units

are *peri*-condensed together on a top-on-top mode. Similar to oligoacenes, rylene molecules show a convergence of band gap with increase of the number of naphthalene units from perylene to terrylene, quaterrylene, pentarylene and hexarylene.[12] Rylene derivatives have been studied in details as important dyes for many practical applications.[13]

The third type of interesting PAH molecule is called *periacene*, in which two acene units (anthracene, tetracene or pentacene) are *peri*-condensed together with a similar mode to that for perylene and the molecules are called bisanthene, peritetracene and peripentacene, respectively.[14] As predicted in chapter 1 and chapter 2, periacene molecules have been theoretically predicted to have very small band gaps with significant singlet biradical character and they are expected to be highly reactive due to their high lying HOMO energy levels.[14] So far, syntheses of peritetracene and peripentacene derivatives have never been successful although our group recently made some attempts.[15] Even the smallest member of the periacene family, i.e., bisanthene, is very sensitive to oxygen and light.[16] We recently developed different approaches[17] to prepare a series of soluble and stable bisanthene-based near infrared (NIR) dyes: (1) substitution by electron-withdrawing dicarboxylic imide groups at the zigzag edges; (2) quinoidization along the short-axis, and (3) substitution by aryl or alkyne at the most reactive *meso*-positions, which were introduced in detail in chapter 1 and chapter 2 . Similar to perylene, the bay regions of bisanthene have a diene character as shown in compound **4-1** in **Figure 4.1** and this opens opportunities to do further functionalizations *via* Diels-Alder cycloaddition reaction at the bay positions of bisanthene. E. Clar *et al.* report that Diels-Alder cycloaddition of parent bisanthene with maleic anhydride gave ovalene dianhydride which was then successfully converted into ovalene by decarboxylation.[18] Liquid crystalline ovalene tetraesters

were also prepared by esterification of ovalene dianhydride.[19] Recently, Scott *et al.* reported that nitroethylene could be used as a masked acetylene and underwent Diels-Alder reaction at the bay regions of bisanthene to give ovalene derivatives.[20] This method implied the possibility to synthesize single-chirality carbon nanotubes *via* a metal-free approach from a suitable cylindrical template. Diels-Alder reaction between a diene and a dienophile such as 1,4-benzoquinone, 1,4-naphthoquinone and 1,4-anthraquinone have been frequently used to construct extended acenequinones and higher order acenes.[3] In this work, we report the cycloaddition reactions between bisanthene and these quinones and the subsequent synthesis towards a series of aryl-annulated bisanthene compounds with laterally extended π-conjugation (e.g. compounds **4-2** to **4-5** in **Figure 4.1**). In all target molecules **4-2** to **4-5**, bulky 3,5-di-*tert*-butylphenyl groups are attached onto the zigzag edges to increase their stability and solubility. These molecules are expected to have a contorted structure due to steric congestion induced by the phenyl substituents and can be also regarded as anthryl-annulated twistacenes. Herein, synthetic chemistry, structure, photophysical properties, electrochemical properties and photostability of these laterally expanded bisanthene compounds are fully investigated and we are interested in understanding the fundamental structure-property relationship.

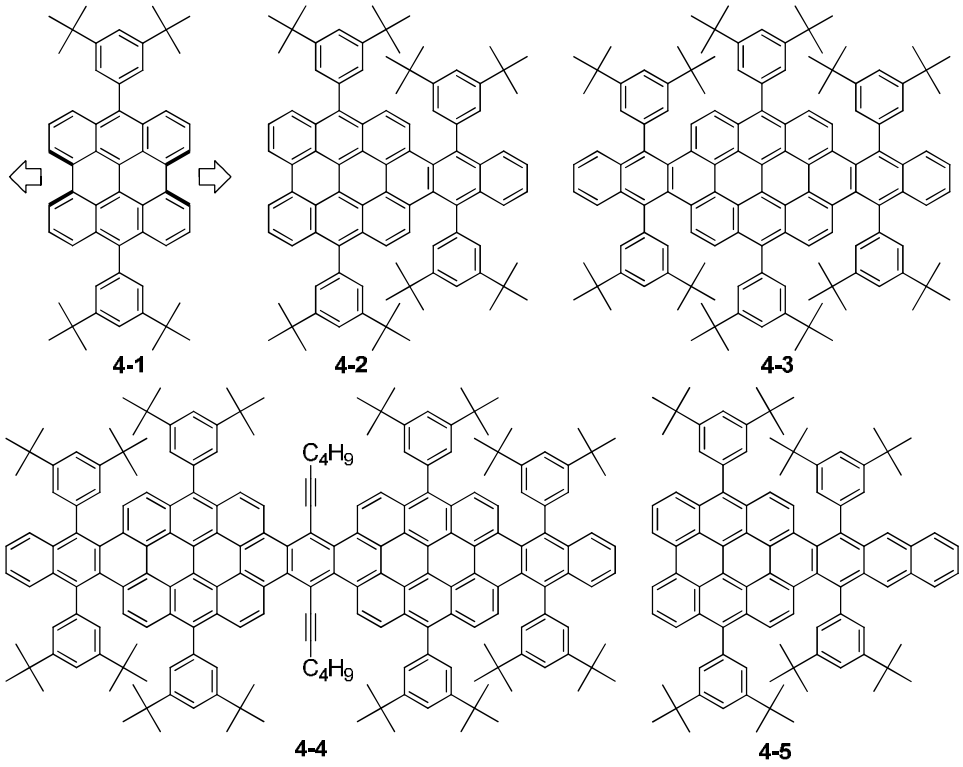

Figure 4.1 Structures of compounds **4-1**, **4-2**, **4-3**, **4-4** and **4-5**.

4.2 Results and Discussions

4.2.1 Synthesis

The synthesis of compounds **4-2** and **4-3** is depicted in **Scheme 4.1**. The 3,5-di-*tert*-butylphenyl-substituted bisanthene **4-1** was first prepared according to our previous report.[17c] Diels-Alder reaction between **4-1** and large excess of 1,4-naphthaquinone (20 equiv.) in refluxing nitrobenzene (240 ^{o}C) afforded the mono-addition product **4-6** and bis-addition product **4-7** and the ratio of **4-6**/**4-7** is dependent on the reaction time. Compound **4-6** was obtained as dominant product after refluxing for 24 h but compound **4-7** was yielded as major product after refluxing for two days. The nitrobenzene serves as high boiling point solvent as well as oxidant to convert the Diels-Alder product to the dyhydrogenated final products **4-6** and **4-7**. Compound **4-6**

reacted with the Grignard reagent of 3,5-di-*tert*-butylbromobenzene in anhydrous THF/toluene to give the diol **4-8** in 52% yields, which was followed by dehydroxylation and reductive aromatization with NaI/NaH_2PO_2 to afford the target compounds **4-2** in nearly quantitative yield. Compound **4-2** continued the Diels-Alder reaction with 1,4-naphthaquinone (20 equiv.) to give compound **4-10** in 85% yield, which underwent similar nucleophilic addition reaction with 3,5-di-*tert*-butyl-phenyl magnesium bromide, dehydroxylation and reductive aromatization, to yield the target compound **4-3** in 76% yield. Alternatively, compound **4-3** also can be prepared from quinone **4-7**. Addition reaction of **4-7** with 3,5-di-*tert*-butyl-phenyl magnesium bromide gave tetraol **4-9** and subsequent dehydroxylation/reductive aromatization afforded the final compound **4-3** in a moderate yield.

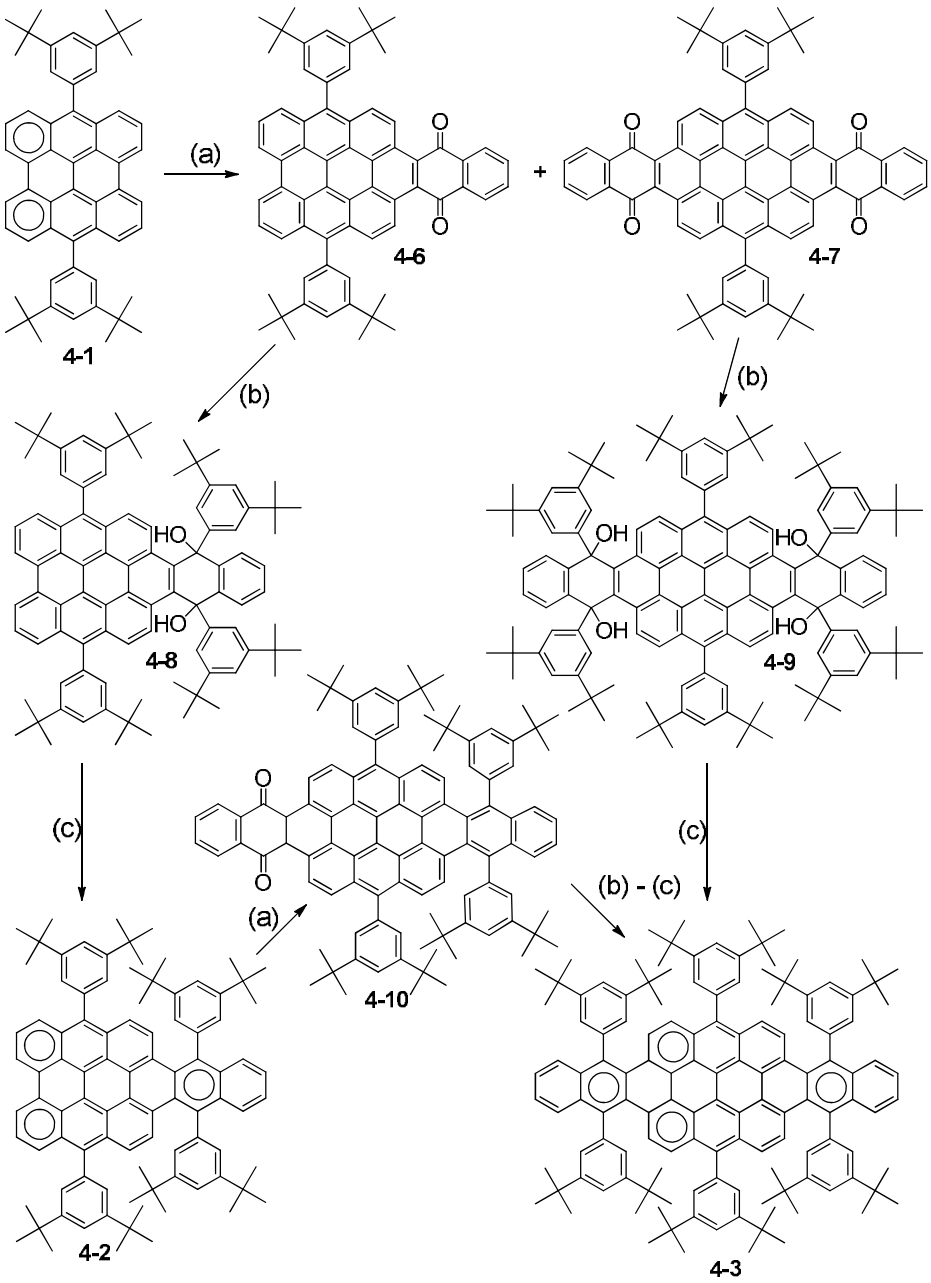

Scheme 4.1 Synthetic route to compounds **4-2** and **4-3**: (a) 1, 4-naphthoquinone (20 equiv.), nitrobenzene, reflux, 1 day (**4-6** as major product) or 2 days (**4-7** as major product); (b) 3,5-di-*tert*-butyl-phenyl magnesium bromide, THF/toluene, rt; (c) $NaH_2PO_2 \cdot H_2O$, NaI, acetic acid, reflux, 2h.

Scheme 4.2 outlines the synthetic route to the largely extended π-system **4-4**. Diels-Alder reaction took place between compound **4-2** and excessive 1,4-benzoquinone (20 equiv.) in refluxing nitrobenzene to give compound **4-11** in 85%

yield. A second Diels-Alder cycloaddition reaction between **4-2** and **4-11** produced quinone **4-12** in 40% yield. We also attempted one-step Diels-Alder reaction between two equiv of **4-2** and one equiv of 1,4-benzoquinone, however, no desired product **4-12** was formed. The nucleophilic addition of **4-12** with triisopropylsilyl (TIPS) acetylene Grignard reagent turned out to be challenging as there was no addition product even under heating in THF, presumably due to the steric hindrance between the TIPS groups and the core. Thus, the less bulky hexynyl group was used and addition of **4-12** with hexynylmagnesium bromide in anhydrous THF/toluene worked smoothly and afforded the intermediate compound **4-13**. The resulting diol **4-13** was used for subsequent dehydroxylation and reductive aromatization with the intension to prepare our target compound **4-4**. Surprisingly, a hydrogenated product **4-4-H_2** instead of **4-4** was obtained which was confirmed high resolution MALDI-TOF mass spectrometry. A peak at m/z = 2685.6657 ([M]) (calculated exact mass for $C_{206}H_{212}$: 2685.6589) was observed, which is 2 Da higher than that for **4-4** (calculated exact mass for $C_{206}H_{210}$: 2683.6433). The product **4-4-H_2** is in red color with the longest absorption maximum at 595 nm (**Figure 4.3**), which is much shorter than that for **4-2** and **4-3** (both at 700 nm, *vide infra*) as well as **4-12** (674 nm, **Figure 4.3**). This indicates that the π-conjugation in **4-4** was broken by dihydrogenation. This unexpected hydrogenation may be caused by the largely extended π-delocalization and a strongly twisted structure of **4-4** which makes the lateral acene fragment very reactive and thus dihydrogenation took place under the reductive condition (NaH_2PO_2/NaI, acetic acid). However, the exact structure of **4-4-H_2** was not confirmed due to complexity of its ^{1}H NMR spectrum and lack of single crystal suitable for crystallographic analysis.

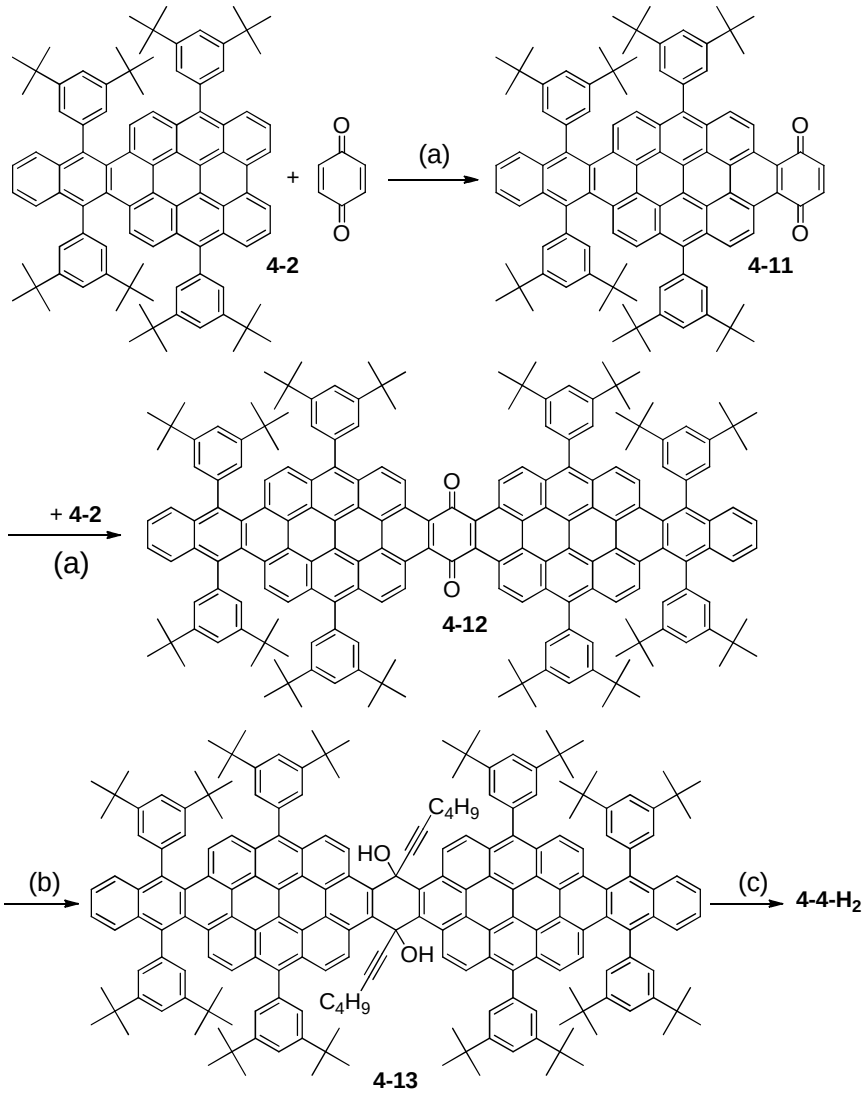

Scheme 4.2 Synthetic route to **4-4**: (a) nitrobenzene, reflux, 2 days; (b) *n*-C_4H_9-C≡C-MgBr, THF/toluene, 60 ^oC, overnight; (c) $NaH_2PO_2 \cdot H_2O$, NaI, acetic acid, reflux, 2h.

To achieve further lateral extension of π-conjugation along the bisanthene core, similar Diels-Alder cycloaddition reaction between compound **4-2** and large excess of 1,4-anthraquinone (20 equiv.) was performed and mono-addition product **4-14** was obtained together with trace amount of compound **4-15** after 1 day refluxing in nitrobenzene (**Scheme 4.3**). Extension of the reaction time does not help to generate more **4-15** presumably due to the relatively low reactivity and low solubility of **4-14** for further Diels-Alder reaction. Nucleophilic addition of compound **4-14** with excess

Grignard reagent of 1-bromo-3,5-di-*tert*-butylbenzene in anhydrous THF/toluene was then tested. Interestingly, a diaryl-substituted compound **4-17** was obtained in 54% yield after standard acidification workup and column chromatography in air, suggesting that the aryl Grignard reagent attacked onto the benzene rings instead of the carbonyl groups in **4-14**. The structure of **4-17** was unambiguously confirmed by NMR spectroscopy and high resolution mass spectrometry. Such an unusual addition reaction is similar to the Michael 1,4-addition of α, β-unsaturated ketone.[21] Similar Michael addition reaction took place on a fused bispentacenequinone as recently reported in our group.[15b] Herein, Michal addition reactions happen on the benzene rings adjacent to the ketone groups and subsequent acidification should give the intermediate compound **4-16**, which undergo simultaneous dehydrogenation in air to afford the title product **4-17** (**Scheme 4.3**). It is also worthy to note that only two, instead of four, hydrogen atoms are removed during the dehydrogenation process, giving a partially dehydrogenated product. We also attempted to do further dehydrogenation of **4-17** with *p*-chloranil in refluxing toluene, however, no reaction happened.

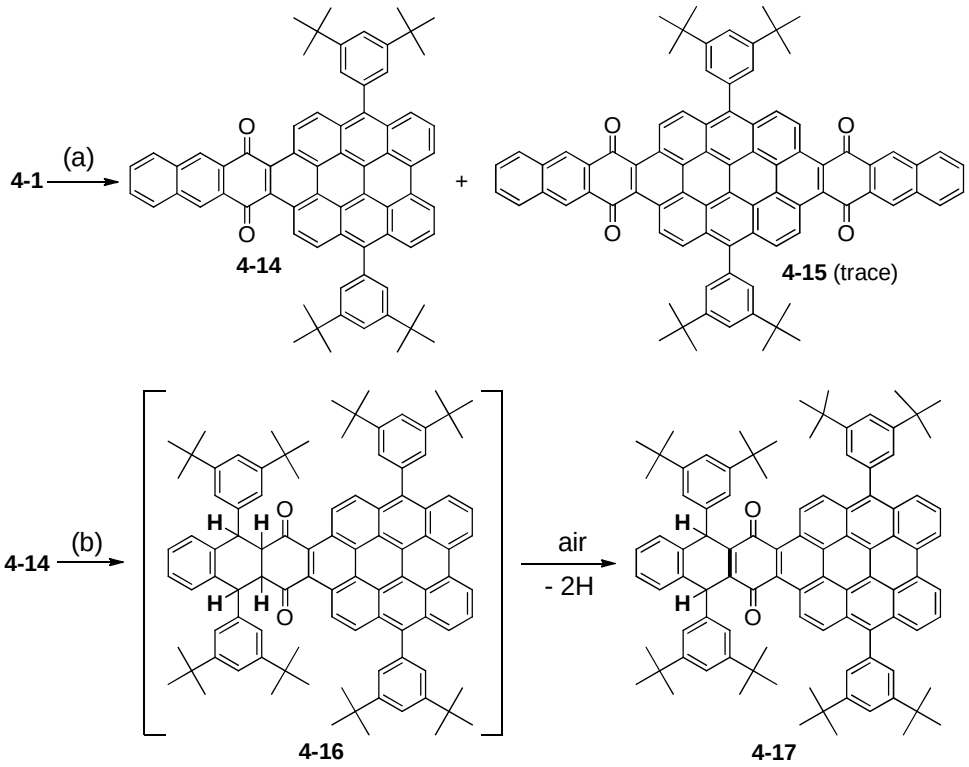

Scheme 4.3 Reagents and conditions: (a) 1, 4-anthraquinone (20 equiv.), nitrobenzene, reflux, 1 day; (b) 3,5-di-*tert*-butyl-phenyl magnesium bromide, THF/toluene, rt, 2 days; and then quenched by water.

4.2.2 Photophysical Properties

The attachment 3,5-di-*tert*-butylphenyl groups makes the final products and most intermediate compounds easily soluble in common organic solvents. The UV-vis-NIR absorption and fluorescence spectra of compound **4-1**, **4-2**, and **4-3** recorded in toluene are shown in **Figure 4.2(a)** and the data are collected in **Table 4.1**. The optical spectra of **4-2** and **4-3** in toluene show two major absorption bands, one at 300-500 nm (β-band) and another at 550-750 nm (*p*-band). The absorption maximum of **4-3** (409 nm) displays obvious bathochromic shift with respect to **4-2** (375 nm) as a result of annulation of an additional naphthalene unit at the bay region. The long-wavelength absorption bands of **4-1, 4-2** and **4-3** has a similar shape and the maxima

at located at 687, 697 and 697 nm, respectively. Such a small shift of the absorption band can be explained by Clar's aromatic rule.[22] Molecules **4-2** and **4-3**, although have larger molecular sizes, they possess more Clar's aromatic sextet rings than **4-1**, i.e., three for **4-2**, four for **4-3**, and two for **4-1**, as labeled as circle rings in **Scheme 4.1**. In addition, compound **4-2** and **4-3** are expected to show a contorted structure (*vide infra*) and deviation from planarity could also result in a blue shift of absorption spectrum. Compound **4-2** and **4-3** showed fluorescence with the emission maximum at 708 nm (**Figure 4.2(b)** and **Table 4.1**), which is 7 nm bathochromic shift with respect to compound **4-1**. Their photoluminescence quantum yields (Φ) were determined according to an optical dilute method (optical density A<0.05) by using cardiogreen dye (λ_{abs} (max) = 780 nm, Φ = 0.13 in DMSO) as a standard.[23] The Φ values of 0.45 and 0.38 were obtained for **4-2** and **4-3**, respectively, and these values are lower than compound **4-1** (0.81) presumably due to their twisted structures. The UV-vis-NIR absorption spectra of **4-12**, **4-4-H$_2$** and **4-17** were also recorded in toluene (**Figure 4.3**). Compound **4-12** and **4-17** showed typical intramolecular charge transfer bands at 674 and 648 nm, respectively, due to the existence of electron-withdrawing quinone units. Compound **4-4-H$_2$** exhibited a *p*-band at much shorter wavelength (450-620 nm) due to interruption of π-conjugation in **4-4**.

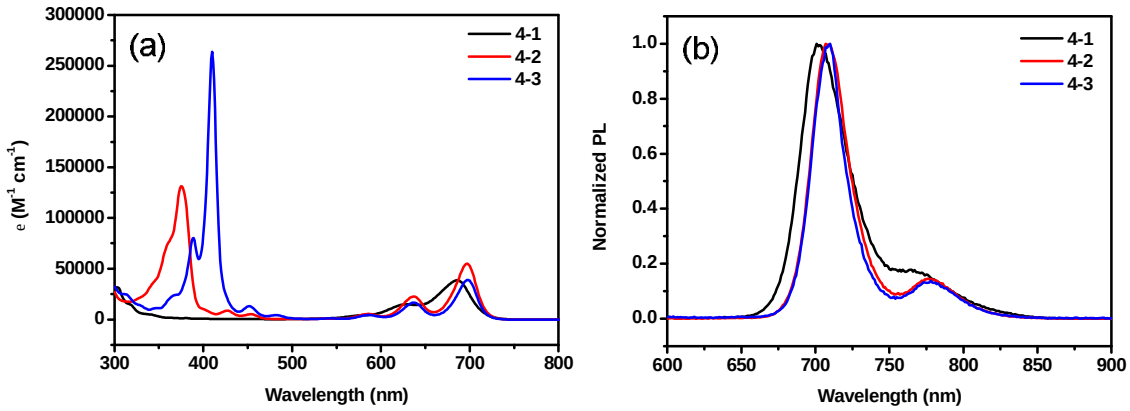

Figure 4.2 UV-vis-NIR absorption (a) and fluorescence spectra (b) of compounds **4-1**, **4-2** and **4-3** in dilute toluene solutions (concentration = $1x10^{-5}$ M for absorption spectra and $1x10^{-7}$ M for emission spectra).

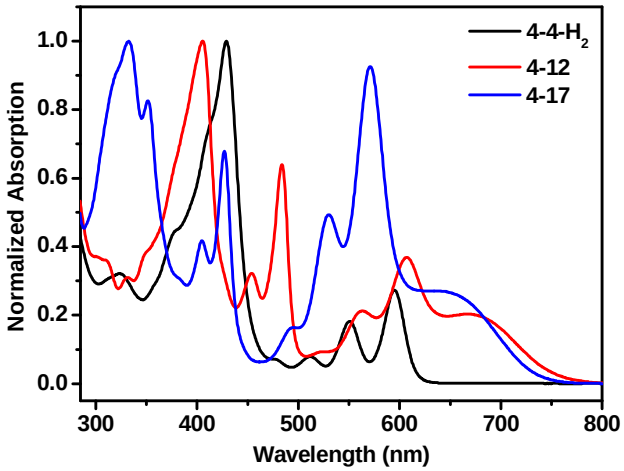

Figure 4.3 Normalized UV-vis-NIR absorption spectra of **4-4-H$_2$**, **4-12** and **4-17** recorded in toluene.

4.2.3 Theoretical Calculations

The geometric and electronic structures of molecules **4-2** and **4-3** are studied by density function theory (DFT) calculations at B3LYP/6-31G** level. The optimized geometric structure and the frontier molecular orbital profiles of **4-2** and **4-3** are

shown in **Figure 4.4**. As predicted, molecules **4-2** and **4-3** have non-planar twisted structures due to the steric congestion and the center-to-end distortion angle is around 41^{o} for both. In both cases, the HOMO and LUMO are mainly delocalized in the bisanthene unit, and partially delocalized along the naphthalene units although there is significant twist between the bisanthene and the naphthalene units. Time-dependent DFT (TDDFT) calculations also predict that both molecules have two major absorption bands with maxima at 372 and 748 nm for **4-2** (**Figure 4.5**), and 410 and 758 nm for **4-3** (**Figure 4.6**). These two bands can be correlated to the *β*-band and *p*-band, respectively, and the tendency agrees well with the experimental results.

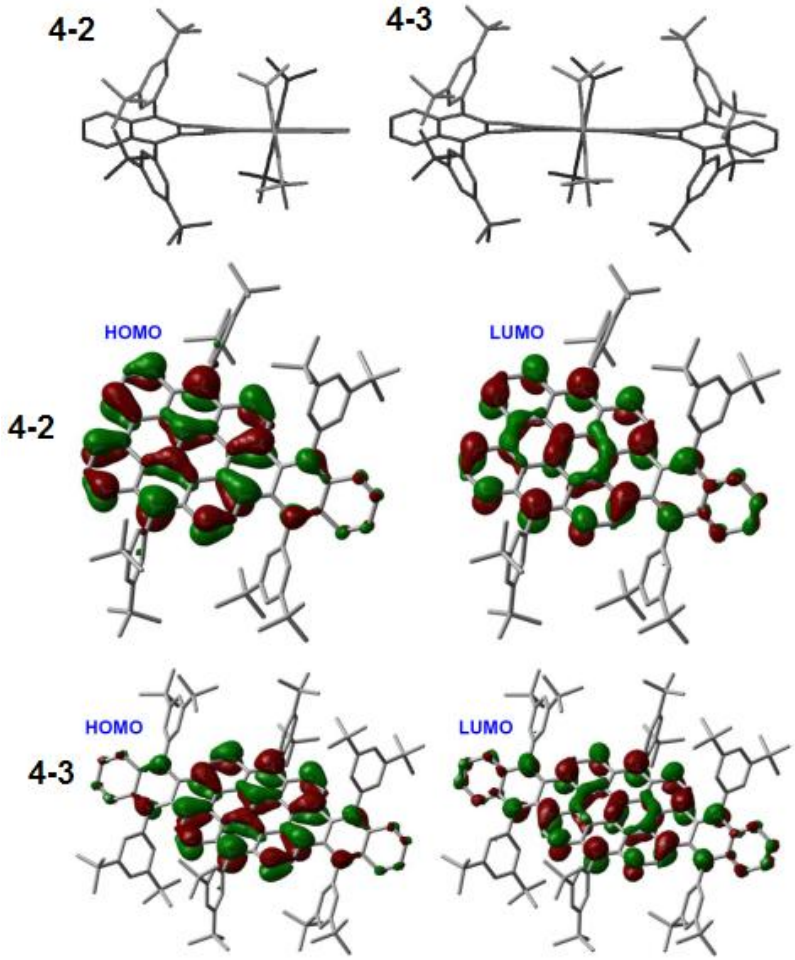

Figure 4.4 Optimized geometric structure and frontier molecular orbital profiles of **4-2** and **4-3**. The hydrogen atoms are omitted for clearance.

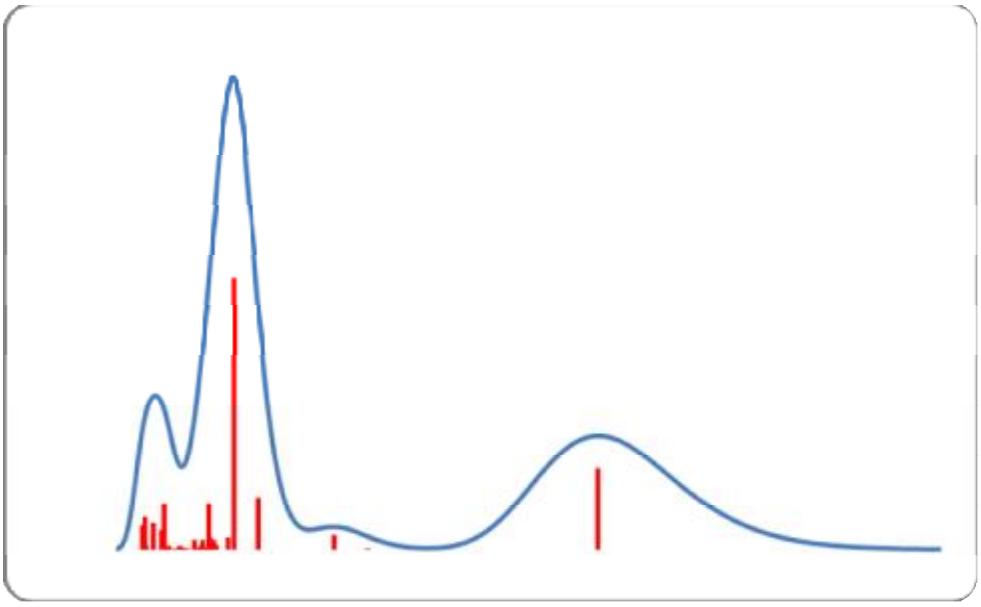

Figure 4.5 Calculated absorption spectrum for **4-2**.

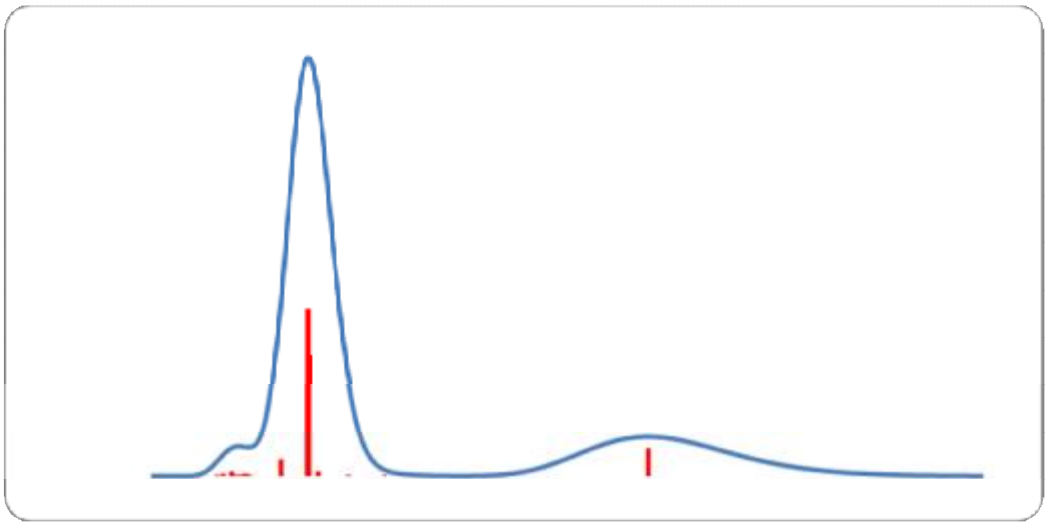

Figure 4.6 Calculated absorption spectrum for **4-3**.

4.2.4 Photostability

In contrast to the very unstable parent bisanthene, the solutions of **4-1**, **4-2** and **4-3** in toluene are relatively stable under ambient conditions. The photostabilities of these three compounds were also tested by irradiation with white light bulb (60 W) and UV-

lamp (254 nm, 4W). Upon irradiation of white light, the solutions gradually decomposed with a decrease of the optical intensity at the longest absorption band and appearance of new absorption band at short wavelength as depicted by arrows in **Figure 4.7**. The half-times ($t_{1/2}$) of around 1100, 405, and 279 min were estimated for **4-1**, **4-2** and **4-3**, respectively, by plotting the optical density at the longest absorption λ_{max} with the irradiation time (**Figure 4.7**). Upon irradiation by UV lamp (4 W), the decomposition process became faster, and the compounds displayed $t_{1/2}$ of about 404, 73, and 129 min, respectively (**Figure 4.8**). These results revealed that the photostability of compound **4-2** and **4-3** is lower than compound **4-1** and this difference can be explained by the strongly twisted structure in **4-2** and **4-3** as well as their slightly high lying HOMO energy levels, which makes them sensitive to light and oxygen.

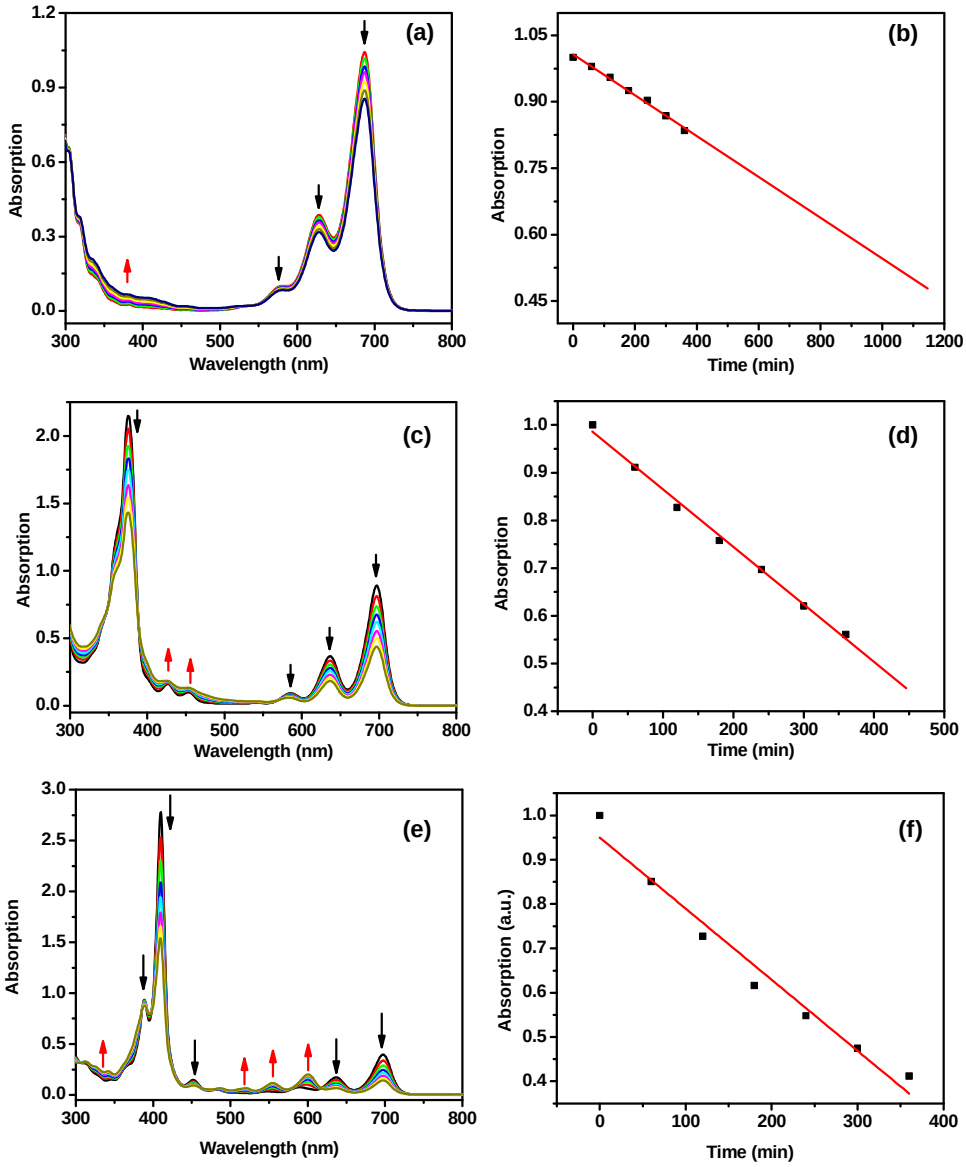

Figure 4.7 Photostability test of compounds **4-1**, **4-2** and **4-3** in toluene upon irradiation by 60 W white light bulb. Left: UV-vis-NIR absorption spectra of **4-1** (a), **4-2** (c), and **4-3** (e) in toluene recorded during the irradiation. The arrows indicate the change in the spectra. Right: change of optical density of **4-1** (b), **4-2** (d), and **4-3** (f) at the longest absorption maximum wavelength with the irradiation time. The original optical density before irradiation was normalized at the absorption maximum.

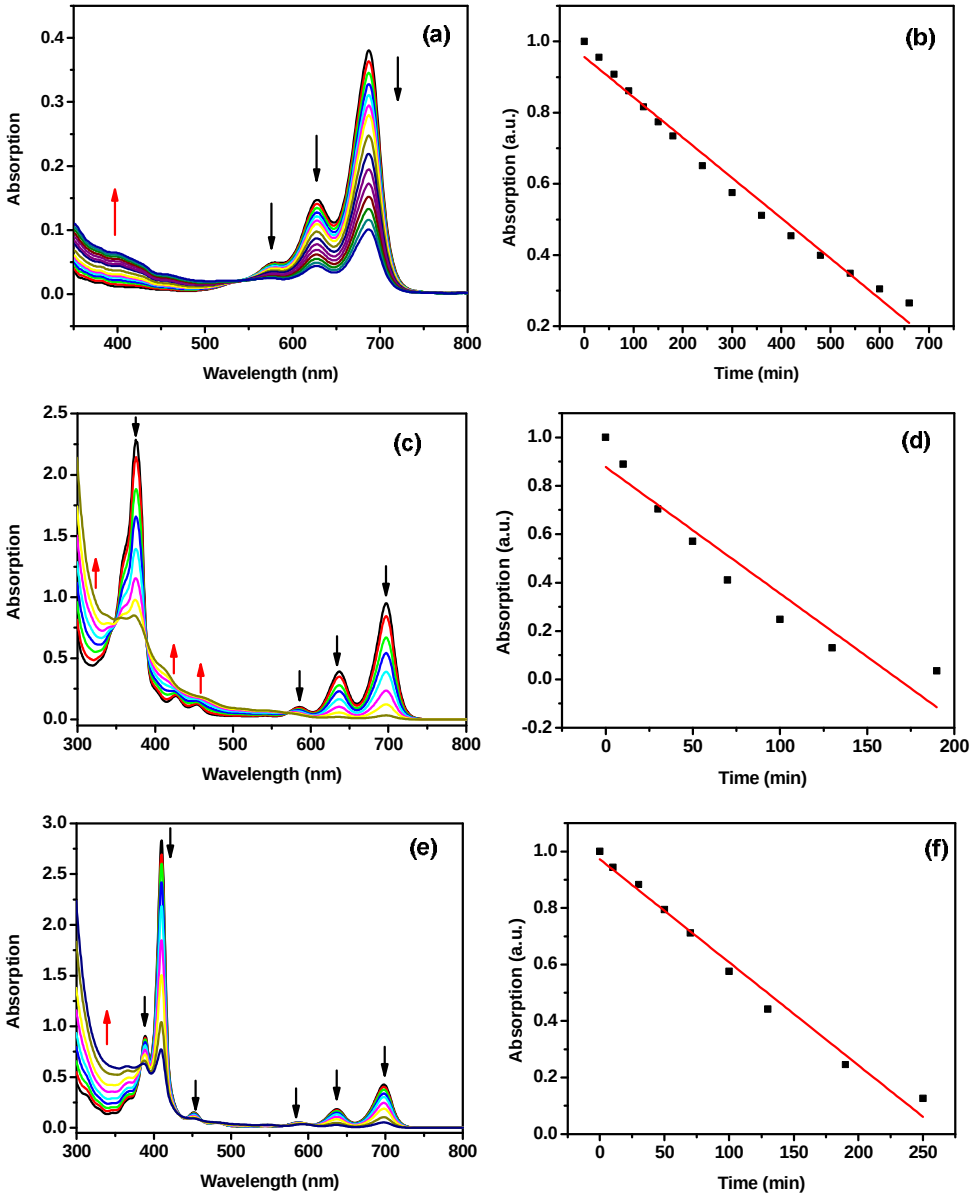

Figure 4.8 Photostability test of compounds **4-1**, **4-2** and **4-3** in toluene upon irradiation by 4 W UV lam (254 nm). Left: UV-vis-NIR absorption spectra of **4-1** (a), **4-2** (c), and **4-3** (e) in toluene recorded during the irradiation. The arrows indicate the change in the spectra. Right: change of optical density of **4-1** (b), **4-2** (d), and **4-3** (f) at the longest absorption maximum wavelength with the irradiation time. The original optical density before irradiation was normalized at the absorption maximum.

4.2.5 Electrochemical Properties and Chemical Oxidation

The electrochemical properties of compounds **4-2** and **4-3** were investigated by cyclic voltammetry (CV) in dry dichloromethane (DCM) and compared with **4-1**

(**Figure 4.9** (a) and **Table 4.1**). The cyclic voltammograms of **4-2** and **4-3** exhibited two reversible oxidation waves with half-wave potentials (E_{ox}^{n}) at -0.02 and 0.58 V for **4-1** and -0.04 and 0.57 V for **4-2**, while three oxidative waves were observed for **4-3**, with E_{ox}^{n} at -0.04, 0.49, and 1.20 V (vs Fc/Fc^{+}). Compound **4-1** also showed two quasi-reversible reduction waves with the half-wave potential of the first reductive waves (E_{red}^{1}) at -1.68 V, while compound **4-2** and **4-3** exhibited one reversible reduction wave with the half-wave potential (E_{red}^{1}) at -1.72 and -1.80 V, respectively. Such an amphoteric redox behavior suggests that compounds **4-1**, **4-2** and **4-3** can be reversibly oxidized into respective cationic species (e.g., radical cations and dications) and reduced into corresponding anionic species (e.g., radical anion and dianion) and the charged species can be stabilized by the largely delocalized π-system.

The HOMO and LUMO energy levels were deduced from the onset potentials of the first oxidation (E_{ox}^{onset}) and the first reduction wave (E_{red}^{onset}), according to the following equations: HOMO = - (4.8 + E_{ox}^{onset}) and LUMO = - (4.8 + E_{red}^{onset}), where the potentials are calibrated to $E_{Fct/Fc}$.[24] Compared with the precursor **4-1**, compounds **4-2** and **4-3** have slightly higher HOMO and LUMO energy levels. In agreement with the small optical band gap (E_{g}^{Opt}) determined from the absorption spectra, the electrochemical band gaps are also small due to a convergence of the HOMO and LUMO energy levels.

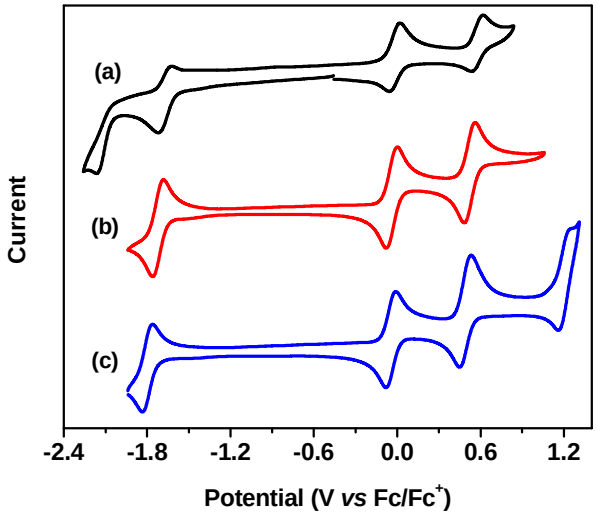

Figure 4.9 Cyclic voltammograms of **4-1** (a), **4-2** (b), and **4-3** (c) in dichloromethane (1 mM) with 0.1 M Bu_4NPF_6 as supporting electrolyte, AgCl/Ag as reference electrode, Au disk as working electrode, Pt wire as counter electrode, and scan rate at 50 mV/s.

Table 4.1 Photophysical and electrochemical data of compounds **4-1**, **4-2**, **4--3**.[a]

Compounds	λ_{abs} (nm)	λ_{em} (nm)	QY	E_{ox}^{1} (V)	E_{ox}^{2} (V)	E_{ox}^{3} (V)	E_{red}^{1} (V)	E_{red}^{2} (V)	HOMO (eV)	LUMO (eV)	E_g^{EC} (eV)	E_g^{Opt} (eV)
1	582, 628, 687	701	0.81	-0.02	0.58	-	-1.68	-2.10	-4.71	-3.20	1.51	1.73
2	375, 427, 453, 586, 637, 697	708, 778	0.45	-0.04	0.57	-	-1.72	-	-4.69	-3.14	1.55	1.72
3	388, 409, 451, 586, 637, 697	708, 778	0.38	-0.04	0.49	1.20	-1.80	-	-4.69	-3.07	1.62	1.72

[a]. The redox potentials are calibrated by Fc/Fc^+. HOMO and LUMO energy levels were deduced from the onset potentials of the first oxidation (E_{ox}^{onset}) and the first reduction wave (E_{red}^{onset}), according to the following equations: HOMO = - (4.8 + E_{ox}^{onset}) and LUMO = - (4.8 + E_{red}^{onset}), where the potentials are calibrated to $E_{Fc+/Fc}$. E_g^{EC} is electrochemical band gap deduced from the LUMO-HOMO. E_g^{Opt} is optical band gap estimated from the lowest energy absorption onset.

Chemical oxidation titrations of compounds **4-2** and **4-3** were conducted in DCM by using $SbCl_5$ as oxidant and the process was followed by UV-vis-NIR absorption spectroscopy. Like compound **4-1**,[17c] these two compounds can be reversibly oxidized by $SbCl_5$ into stable radical cations with the appearance of two new characteristic absorption bands at the shorter and longer wavelength (**Figure 4.10**). Such a phenomenon is common due to the redistribution of frontier molecular orbital energy

level in the energy gap, and one electron transition state at the higher energy and one electron transition state at lower energy are allowed in the new energy diagram. It is worthy to note that the longest absorption maximum for the radical cation exhibited obvious bathochromic shift from **4-1** (782 nm) to **4-2** (1276 nm) and **4-3** (1324 nm). The oxidized species can also be reversibly reduced into the neutral state by adding Zn dust to the solution containing oxidized species. Similar reversible process can be observed for **4-2** and **4-3** when iodine was used as oxidant.

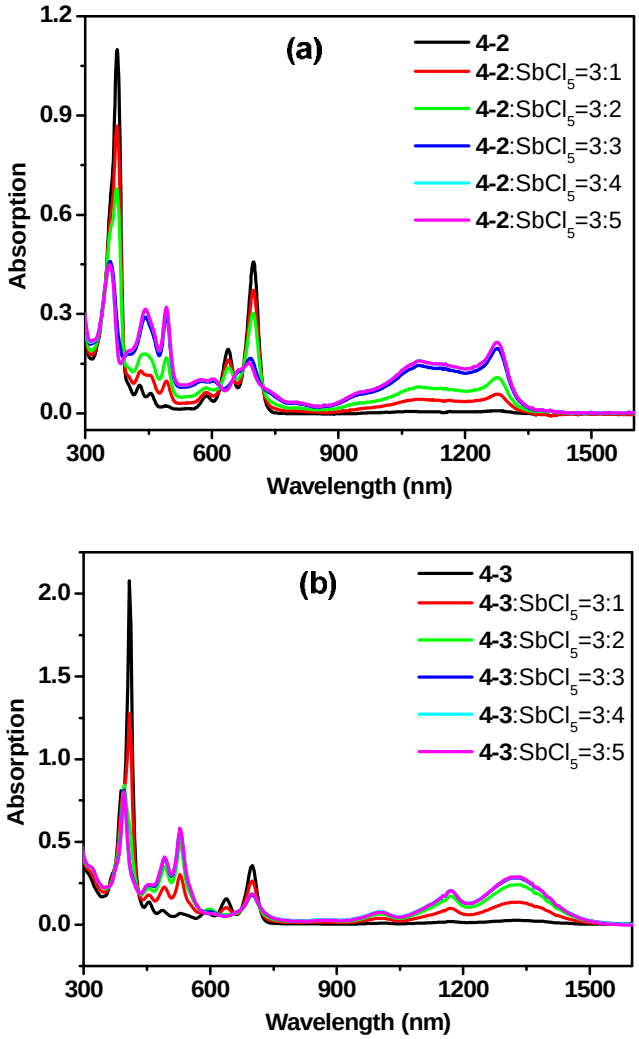

Figure 4.10 UV-vis-NIR absorption spectra of **4-2** (a) and **4-3** (b) during titration with $SbCl_5$ in dry DCM. The arrows show the changes of the spectra during the titration.

4.3 Conclusions

In summary, we have investigated the synthesis of a series of laterally expanded bisanthene compounds *via* Diels-Alder cycloadditon reaction at the bay regions of bisanthene. The naphthalene-annulated bisanthenes **4-2** and **4-3** have been successfully prepared, but synthetic efforts towards more extended π-systems **4-4** and **4-5** met unexpected hydrogenation or Michael addition reaction. Nevertheless, compounds **2** and **4-3** represent new members of largely extended PAHs with small band gap and near infrared absorption/emission. Our detailed studies on their geometric and electronic structure, photophysical properties, electrochemical properties and photostability revealed that the twisted geometry structure and the number of Clar's sextet rings all played important roles on their physical properties and chemical reactivity. Synthesis of large size expanded bisanthene with planar geometry is underway in our lab, which can be potentially used in organic electronic devices such as OFETs.

4.4 Experimental Section

4.4.1 General Experimental Methods

All reagents and starting materials were obtained from commercial suppliersand used without further purification. Tetrahydrofuran (THF) and toluene was purified by routine procedure and distilled over sodium under nitrogen before using. Column chromatography was performed on silica gel 60 (Merck 40-60 nm, 230-400 mesh). All NMR spectra were recorded on a Bruker AMX500 or AMX300 spectrometers at room temperature. All chemical shifts are quoted in ppm, relative to tetramethylsilane, using the residual solvent peak as a reference standard. High resolution mass spectra

were recorded on a Finnigan MAT95XL-T with FAB ionization source or recorded a Bruker Autoflex MALDI-TOF instrument, using 1,8,9-trihydroxyanthracene as a matrix. UV-vis absorption and fluorescence spectra were recorded in toluene solution on Shimadzu UV-1700 spectrometer or Lambda 750 spectrometer. Fluorescence spectra were recorded on RF-5301 fluorometer. Cyclic voltammetry measurements of compounds **4-2** and **4-3** in dichloromethane (1 M) was performed on a CHI 620C electrochemical analyzer with a three-electrode cell, using 0.1 M Bu_4NPF_6 as supporting electrolyte, $AgNO_3$/Ag as reference electrode, gold disk as working electrode, Pt wire as counter electrode, and scan rate at 50 mV/s.

4.4.2 Material Synthesis and Characterization Data

Synthesis of compound 4-6 and 4-7: Compound **4-1** (100 mg, 0.14 mmol) was heated under reflux (240 ^oC) with 1,4-naphthoquinone (435 mg, 2.75 mmol) in de-oxygen nitrobenzene (50 ml) and a color changed from deep blue to black-brown slowly. In the end, methanol was added into the cooled solution, and green precipitate was filtered off, washed with acetone and dried under vacuum to yield a mixture of compounds **4-6** and **4-7**. When the reaction time is 24 h, the major product is **4-6** together with trace amount of **4-7**. However, when the reaction was conducted for two days, the major product is **4-7** together with trace amount of **4-6**. The mixture was used directly for next step.

Synthesis of compound 4-8: Magnesium (3 mg, 0.13 mmol) and a piece of iodine crystal were placed in dry THF (1 mL). To the mixture, 1-bromo-3,5-di-*tert*-butylbenzene (305.5 mg, 1.13 mmol) in dry THF (4 mL) was added dropwise and the mixture was stirred at room temperature for 2 h to generate Grignard reagent. The as-prepared Grignard reagent was transferred into a suspension of crude compound **4-6**

(100 mg) in dry toluene (20 mL) and the mixture was stirred at room temperature for two days. The reaction was quenched with water (100 mL) and extracted with hexane. The organic layer was washed by water and dried over anhydrous Na_2SO_4. After removal of solvent, the residue was further purified by column chromatography on silica gel with $CHCl_3$: hexane = 2:1 (v/v) as eluent to afford compound **4-8** (72 mg, 52 %) as black-purple solid. ^{1}H NMR (300 MHz, $CDCl_3$), δ ppm = 1.11 (s, 36 H, *t*-Bu), 1.41 (s, 18 H, *t*-Bu), 1.45 (s, 18 H, *t*-Bu), 3.27 (s, 2 H, OH), 7.12 (s, 2 H, Ph), 7.23 (dd, ^3J = 6.09 Hz, ^4J = 3.3 Hz, 2 H, Ph), 7.35 (s, 2 H, Ph), 7.43 (s, 4H, Ph), 7.47 (s, 2 H, Ph), 7.60 (m, 4 H, Ar), 7.70 (m, 2H, Ar), 7.90 (t, *J* = 8.0 Hz, 2H, Ar), 8.09 (d, *J* = 8.4 Hz, 2H, Ar), 8.88 (d, *J* = 10.0 Hz, 2H, Ar), 9.02 (d, *J* = 7.2 Hz, 2H, Ar). ^{13}C NMR (75 MHz, $CDCl_3$), δ ppm = 32.09, 32.33, 32.36, 35.48, 35.72, 35.77, 120.08, 120.93, 121.26, 121.75, 123.16, 124.48, 125.46, 125.78, 126.26, 126.64, 126.74, 127.29, 128.25, 128.72, 129.05, 129.15, 129.41, 132.26, 132.41, 135.45, 137.79, 138.64, 140.11, 149.83, 150.85. HRMS (FAB): m/z = 1260.77196 ([M]), calculated for $C_{94}H_{100}O_2$ exact mass: 1260.77178 (error = 0.14 ppm).

Synthesis of compound 4-2: In absence of light, a mixture of compound **4-8** (100 mg, 0.079 mmol), NaI (119 mg, 0.79 mmol), $NaH_2PO_2 \cdot H_2O$ (152.8 mg, 1.185 mmol) and acetic acid (20 mL) was heated to reflux for 2 h. After cooling to room temperature, the precipitate was collected by filtration, washed with water, and purified by a flush column chromatography with hexane as eluent to afford compound **4-2** quantitatively as a deep blue solid. ^{1}H NMR (300 MHz, $CDCl_3$), δ ppm = 1.29 (s, 36 H, *t*-Bu), 1.42 (s, 36 H, *t*-Bu), 7.23 (m, 2 H, Ar), 7.37 (d, *J* = 1.65, 4 H, Ph), 7.46 (d, *J* = 1.62, 4 H, Ph), 7.53 (s, 2 H, Ph), 7.57 (s, 2 H, Ar), 7.60 (m, 4H, Ar), 7.72 (m, 4H, Ar), 7.93 (m, *J* = 8.55 Hz, 2H, Ar), 8.36 (m, 2H, Ar), 8.76 (d, *J* = 7.41 Hz, 2H, Ar). ^{13}C NMR (125 MHz, $CDCl_3$), δ ppm =32.16, 32.30, 35.63, 35.76, 120. 65, 121.37, 121.41, 123.91,

124.49, 125.68, 125.79, 126.00, 126.19, 126.78, 126.98, 127.26, 127.36, 127.54, 128.38, 128.81, 129.85, 129.98, 130.27, 132.41, 132.85, 136.50, 137.30, 138.56, 141.67, 151.37, 152.03. HRMS (FAB): m/z = 1226.7640 ([M]), calculated for $C_{94}H_{98}$ exact mass: 1226.7663 (error = -1.88 ppm).

Synthesis of compound 4-10: Compound **4-2** (100 mg, 0.08 mmol) was heated at reflux for 2 days with 1,4-naphthoquinone (253 mg, 1.6 mmol) in de-oxygen nitrobenzene (30 mL) and a color changed from green to black-green slowly. In the end, nitrobenzene was distilled under vacuum, the leaving green solid was washed with acetone and further purified by column chromatography on silica gel with $CHCl_3$: hexane = 2:1 (v/v) as eluent to afford compound **4-10** (96 mg, 85 %) as black-green solid. ^{1}H NMR (500 MHz, $CDCl_3$), δ ppm = 1.29 (s, 36 H, *t*-Bu), 1.52 (s, 36 H, *t*-Bu), 7.56 (s, 4 H, Ph), 7.61 (s, 2 H, Ph), 7.62 (br, 2 H, Ar), 7.67 (d, *J* = 1.5, 4 H, Ph), 7.72 (m, 2 H, Ar), 7.75 (s, 2H, Ph), 8.18 (d, *J* = 9.5 Hz, 2H, Ar), 8.20 (br, 2H, Ar), 8.48 (m, 2H, Ar), 8.61 (d, *J* = 9.5 Hz, 2H), 8.71 (d, *J* = 9.5 Hz, 2H, Ar), 10.04 (d, *J* = 10 Hz, 2H, Ar). ^{13}C NMR (125 MHz, $CDCl_3$), δ ppm = 32.17, 32.42, 35.68, 35.92, 121.31, 121.67, 121.93, 122.80, 123.69, 124.38, 124.68, 126.53, 126.69, 126.73, 127.05, 127.14, 127.31, 127.63, 127.73, 128.62, 128.74, 128.85, 128.92, 129.52, 130.04, 130.71, 130.94, 133.54, 135.54, 137.30, 138.44, 138.61, 141.71, 151.50, 152.42, 188.07. HRMS (MALDI-TOF, positive): m/z = 1380.7691 ([M]), calculated for $C_{104}H_{100}O_2$ exact mass: 1380.7718 (error = -1.98 ppm).

Synthesis of compound 4-3: Magnesium (19.3 mg, 0.80 mmol) and a piece of iodine crystal were placed in dry THF (1 mL). To the mixture, 1-bromo-3,5-di-*tert*-butylbenzene (194.7 mg, 0.72 mmol) in dry THF (4 mL) was added dropwise and the mixture was stirred at room temperature for 2 h to generate Grignard reagent. The as-

prepared Grignard reagent was transferred into a suspension of compound **4-10** (100 mg, 0.07 mmol) in dry toluene (20 mL) and the mixture was stirred at room temperature for 2 days. The reaction was quenched with water (100 mL) and extracted with hexane. The organic layer was washed by water and dried over anhydrous Na_2SO_4. The solvent was removed by evaporation and the residue was dried under vacuum. In absence of light, a mixture of the crude product diol (123 mg, 0.07 mmol), NaI (105 mg, 0.7 mmol), $NaH_2PO_2 \cdot H_2O$ (135.4 mg, 1.05 mmol) and acetic acid (20 mL) was heated to reflux for 2 h. After cooling to room temperature, the deep green precipitate was collected by filtration, washed with water and acetone, and purified by column chromatography on silica gel with $CHCl_3$: hexane = 1:5 (v/v) as eluent to afford compound **4-3** (92 mg, 76%) as a green solid. Alternatively, compound **4-3** can be prepared from the qunione **4-7** by a similar approach via an intermediate compound **4-9**. ^{1}H NMR (500 MHz, d_6-benzene), δ ppm = 1.27 (s, 72 H, *t*-Bu), 1.54 (s, 36 H, *t*-Bu), 7.45 (m, 4 H, Ar), 7.74 (s, 4 H, Ph), 7.75 (s, 8 H, Ph), 7.84 (s, 2 H, Ph), 7.96 (s, 4 H, Ph), 8.34 (d, *J* = 9.5 Hz, 4H, Ar), 8.56 (d, *J* = 9.5 Hz, 4H, Ar), 8.66 (m, 4H, Ar). ^{13}C NMR (125 MHz, d_6-benzene), δ ppm = 32.28, 32.57, 35.72, 36.11, 121.53, 121.61, 124.33, 124.40, 125.72, 126.28, 126.53, 127.95, 128.08, 128.61, 128.99, 129.52, 129.84, 130.28, 131.26, 136.76, 137.12, 139.55, 142.92, 151.51, 152.63. HRMS (MALDI-TOF, positive): m/z = 1727.1037 ([M]), calculated for $C_{132}H_{142}$ exact mass: 1727.1106 (error = -4.00 ppm).

Synthesis of compound 4-11: Compound **4-2** (100 mg, 0.08 mmol) was heated at reflux for 2 days with benzoquinone (173 mg, 1.6 mmol) in de-oxygen nitrobenzene (30 mL) and a color changed from green to black-green slowly. In the end, nitrobenzene was distilled under vacuum, the leaving green solid was washed with acetone and further purified by column chromatography on silica gel with $CHCl_3$:

hexane = 1:1 (v/v) as eluent to afford compound **4-11** (90 mg, 85%) as a black-green solid. ^{1}H NMR (500 MHz, $CDCl_3$), δ ppm = 1.30 (s, 36 H, *t*-Bu), 1.51 (s, 36 H, *t*-Bu), 6.72 (s, 2 H, quinone), 7.57 (d, *J* = 1 Hz, 4 H, Ph), 7.62 (s, 2 H, Ph), 7.65 (s, 4 H, Ph), 7.72 (m, 2 H, Ar), 7.74 (s, 2H, Ph), 8.17 (d, *J* = 9.5 Hz, 2H, Ar), 8.48 (m, 2H, Ar), 8.61 (d, *J* = 9.5 Hz, 2H), 8.65 (d, *J* = 9 Hz, 2H, Ar), 9.86 (d, *J* = 10 Hz, 2H, Ar). ^{13}C NMR (125 MHz, $CDCl_3$), δ ppm = 32.17, 32.42, 35.71, 35.90, 121.24, 121.73, 122.00, 122.89, 123.65, 124.50, 124.66, 124.88, 126.22, 126.45, 126.58, 127.32, 127.54, 127.76, 128.48, 128.55, 128.92, 129.07, 129.58, 130.12, 131.07, 131.28, 137.45, 138.38, 138.89, 139.36, 141.73, 151.52, 152.48, 189.69. HRMS (FAB): m/z = 1330.75594 ([M]), calculated for $C_{100}H_{98}O_2$ exact mass: 1330.75613 (error = -0.15 ppm).

Synthesis of compound 4-12: Compound **4-11** (100 mg, 0.07 mmol) was heated at reflux for 2 days with compound **4-2** (184 mg, 0.15 mmol) in de-oxygen nitrobenzene (30 mL) and a color changed from green to black-green slowly. In the end, nitrobenzene was distilled under vacuum, the leaving green solid was washed with acetone and further purified by column chromatography on silica gel with $CHCl_3$: hexane = 3:1 (v/v) as eluent to afford compound **4-12** (142 mg, 40 %) as black-green solid. ^{1}H NMR (500 MHz, $CDCl_3$), δ ppm = 1.29 (s, 72 H, *t*-Bu), 1.54 (s, 72 H, *t*-Bu), 7.56 (d, *J* = 1.5 Hz, 8 H, Ph), 7.61 (t, *J* = 2 Hz, 4 H, Ph), 7.68 (d, *J* = 2 Hz, 8 H, Ph), 7.72 (m, 4 H, Ar), 7.77 (t, *J* = 2 Hz, 4 H, Ph), 8.19 (d, *J* = 9.5 Hz, 4H, Ar), 8.49 (m, 4H, Ar), 8.62 (d, *J* = 9.5 Hz, 4H), 8.83 (d, *J* = 9.5 Hz, 4H, Ar), 10.05 (d, *J* = 9.5 Hz, 4H, Ar). ^{13}C NMR (125 MHz, $CDCl_3$), δ ppm = 32.16, 32.42, 35.67, 35.91, 121.65, 121.93, 121.96, 122.98, 123.88, 124.33, 124.77, 126.47, 126.49, 126.60, 127.12, 127.32, 127.54, 127.71, 128.81, 128.99, 129.05, 129.49, 130.01, 130.42, 130.79, 130.88, 137.21, 138.53, 138.56, 141.70, 151.57, 152.38, 193.37. HRMS (MALDI-

TOF, positive): m/z = 2553.4978 ([M]), calculated for $C_{194}H_{192}O_2$ exact mass: 2553.4917 (error = 2.39 ppm).

Synthesis of compound 4-4-H_2: Ethylmagnesium bromide (3 M in ether, 0.13 ml, 0.39 mmol) was added dropwise to a solution of 1-hexyne (32 mg, 0.39 mmol) in anhydrous THF (1 ml) at room temperature with stirring and this mixture was maintained at 60 ^oC for 2 h. Compound **4-12** (100 mg, 0.039 mmmol) was dissolved under nitrogen in anhydrous toluene (10 ml) and then added dropwise to the as-prepared Grignard reagent and the mixture was stirred at 60 ^oC for one night. The reaction was quenched with water (100 mL) and extracted with hexane. The organic layer was washed by water and dried over anhydrous Na_2SO_4. The solvent was removed by evaporation and the residue was dried under vacuum. In absence of light, a mixture of the crude product diol **4-13** (62 mg, 0.39 mmol), NaI (105 mg, 0.7 mmol), $NaH_2PO_2 \cdot H_2O$ (68 mg, 0.78 mmol) and acetic acid (20 ml) was heated to reflux for 2 h. After cooling to room temperature, the dark purple precipitate was collected by filtration, washed with water and acetone, and purified by column chromatography on silica gel with $CHCl_3$: hexane = 1:4 (v/v) as eluent to afford compound **4-4-H_2** which is a hydrogenated form of **4-4**. HRMS (MALDI-TOF, positive): m/z = 2685.6657 ([M]), calculated for $C_{206}H_{212}$ exact mass: 2685.6584 (error = 2.73 ppm).

Synthesis of compound 4-14: Compound **4-1** (100 mg, 0.14 mmol) was heated at reflux for 2 days with 1,4-anthraquinone (573 mg, 2.75 mmol) in de-oxygen nitrobenzene (50 mL) and a color changed from deep blue to black-brown slowly. In the end, methanol was added into the cooled solution, and green precipitate was filtered off, washed with acetone and dried under vacuum to yield the compound **4-15**

with trace amount of compound **4-16** as confirmed by MALDI-TOF mass spectrometry. The mixture was used directly for the next step.

Synthesis of compound 4-17: Magnesium (3 mg, 0.13 mmol) and a piece of iodine crystal were placed in dry THF (1 mL). To the mixture, 1-bromo-3,5-di-*tert*-butylbenzene (305.5 mg, 1.13 mmol) in dry THF (4 mL) was added dropwise and the mixture was stirred at room temperature for 2 h to generate Grignard reagent. The as-prepared Grignard reagent was transferred into a suspension of crude compound **4-14** (100 mg, 0.11 mmol) in dry toluene (20 mL) and the mixture was stirred at room temperature for 2 days. The reaction was quenched with water (100 mL) and extracted with hexane. The organic layer was washed by water and dried over anhydrous Na_2SO_4. After removal of solvent, the residue was further purified by column chromatography on silica gel with $CHCl_3$: hexane = 1:8 (v/v) as eluent to afford compound **4-17** (77 mg, 54 %) as black-purple solid. ^{1}H NMR (300 MHz, $CDCl_3$), δ ppm = 1.24 (s, 36 H, *t*-Bu), 1.47 (s, 36 H, *t*-Bu), 5.70 (s, 2 H, CH), 7.13 (m, 2 H, Ar), 7.24 (m, 8 H, Ar, Ph), 7.48 (m, 4 H, Ph), 7.69 (t, *J* = 2 Hz, 2 H, Ph), 7.94 (d, *J* = 10 Hz, 2 H, Ar), 8.03 (t, *J* = 7.5 Hz, 2H, Ar), 8.2 (d, *J* = 8.5 Hz, 2H, Ar), 9.04 (d, *J* = 10 Hz, 2H, Ar), 9.16 (d, *J* = 7.5 Hz, 2H, Ar). ^{13}C NMR (125 MHz, $CDCl_3$), δ ppm = 35.50, 35.83, 45.99, 121.13, 122.03, 122.16, 122.92, 123.93, 125.07, 125.53, 126.53, 126.69, 126.91, 127.18, 127.45, 127.53, 128.15, 129.18, 129.45, 129.96, 130.81, 132.24, 132.75, 137.08, 138.26, 139.62, 144.12, 147.01, 151.53, 151.72, 151.78, 189.68. HRMS (MALDI-TOF, positive): m/z = 1308.7718 ([M]), calculated for $C_{98}H_{100}O_2$ exact mass: 1308.7668 (error = -3.81 ppm).

Appendix: ^{1}H NMR and ^{13}C NMR spectra of 4-2, 4-3, and 4-17.

^{1}H NMR spectrum of compound **4-2** in $CDCl_3$ (500 MHz):

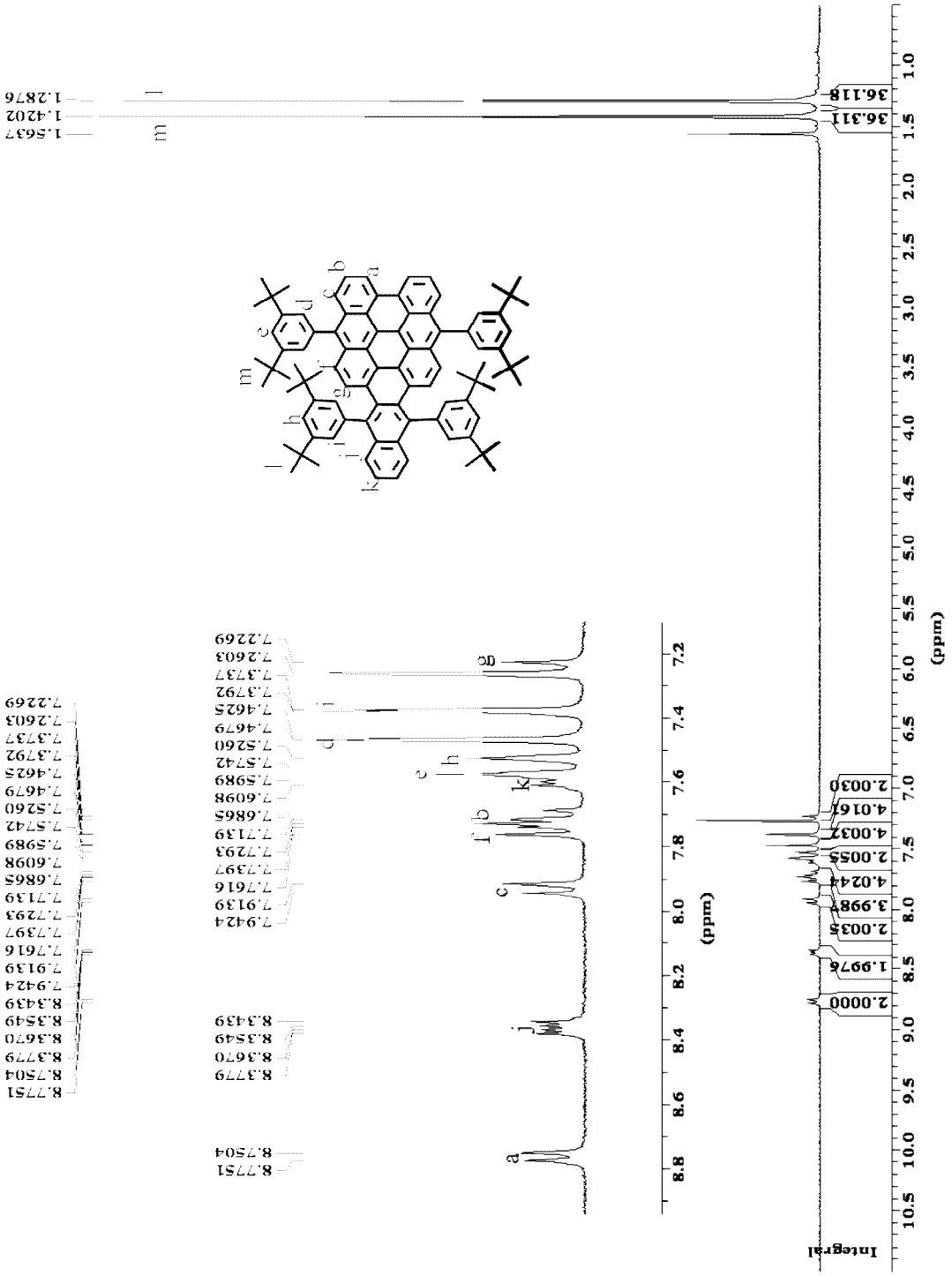

^{13}C NMR spectrum of compound **4-2** in $CDCl_3$ (125 MHz):

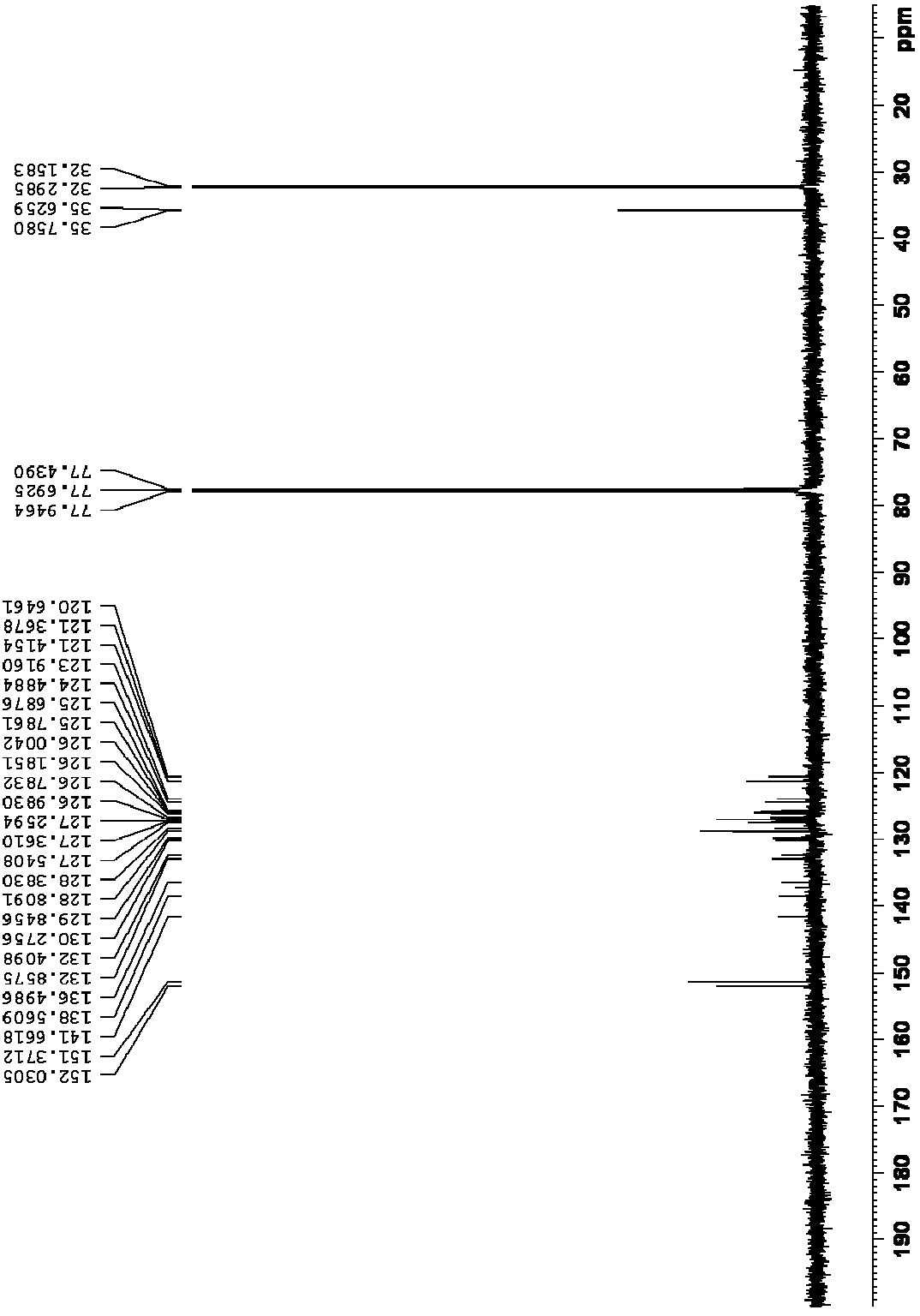

^{1}H NMR spectrum of compound **4-3** in *d*-benzene (500 MHz):

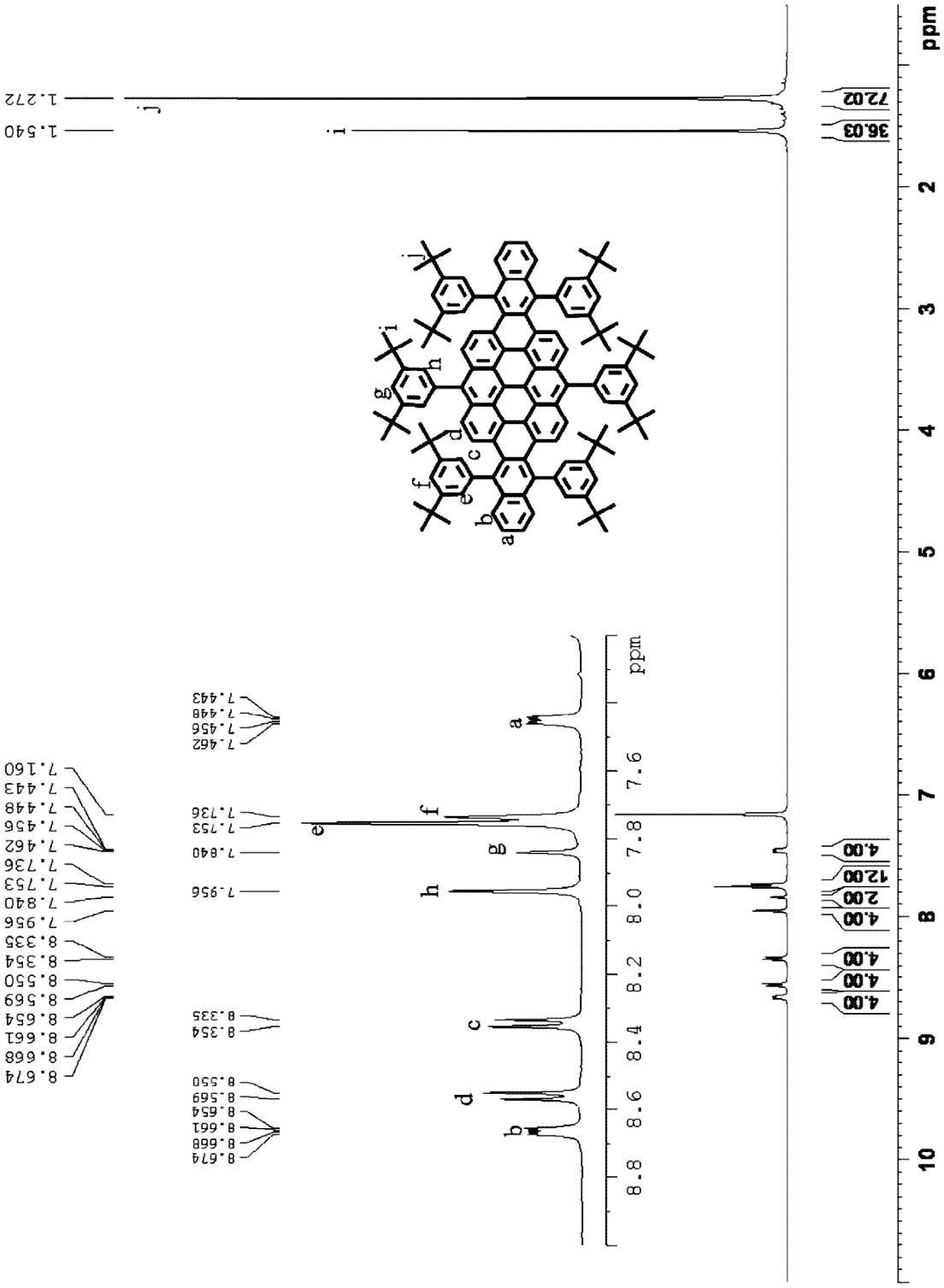

^{13}C NMR spectrum of compound **4-3** in *d*-benzene (125 MHz):

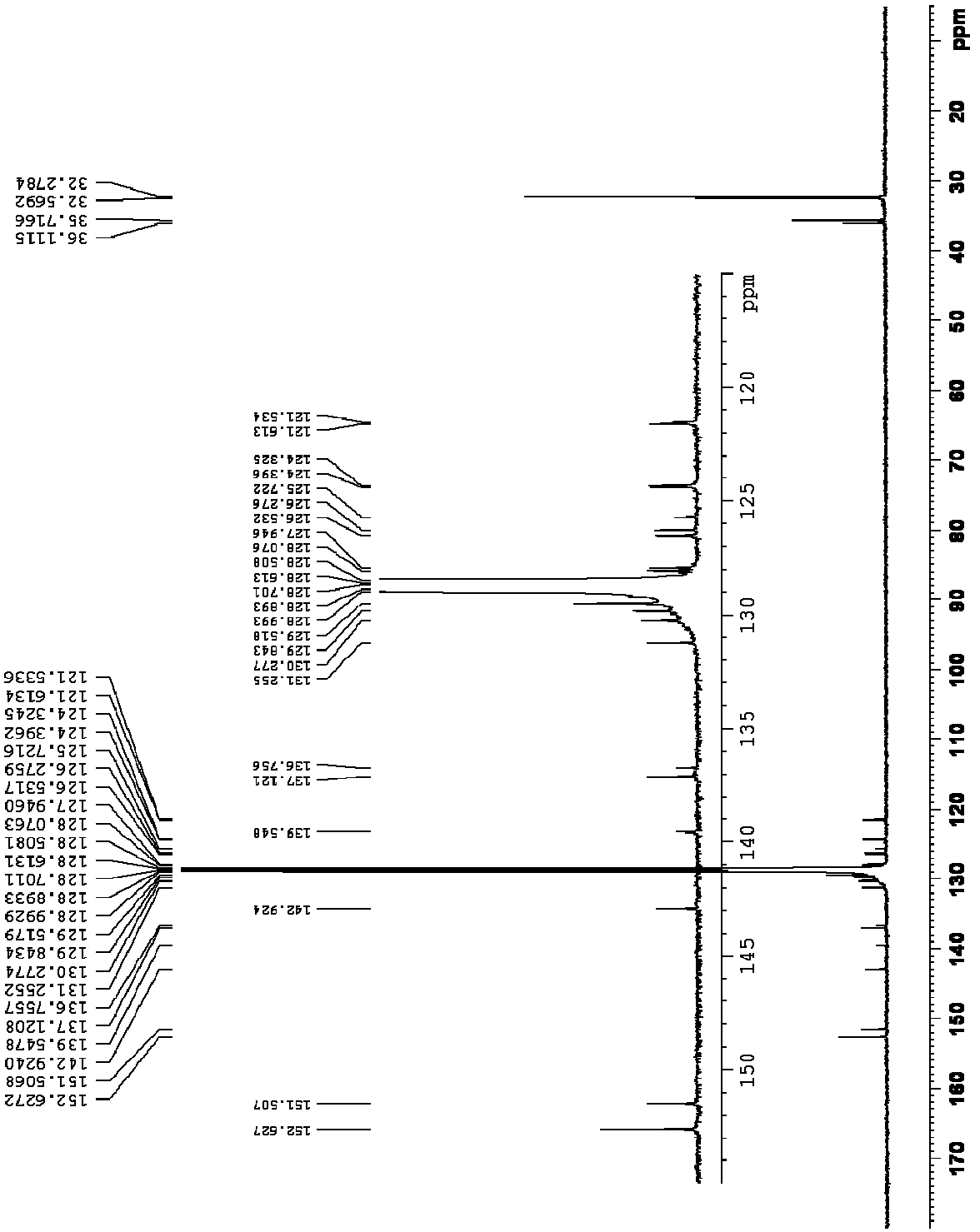

^{1}H NMR spectrum of compound **4-17** in $CDCl_3$ (500 MHz):

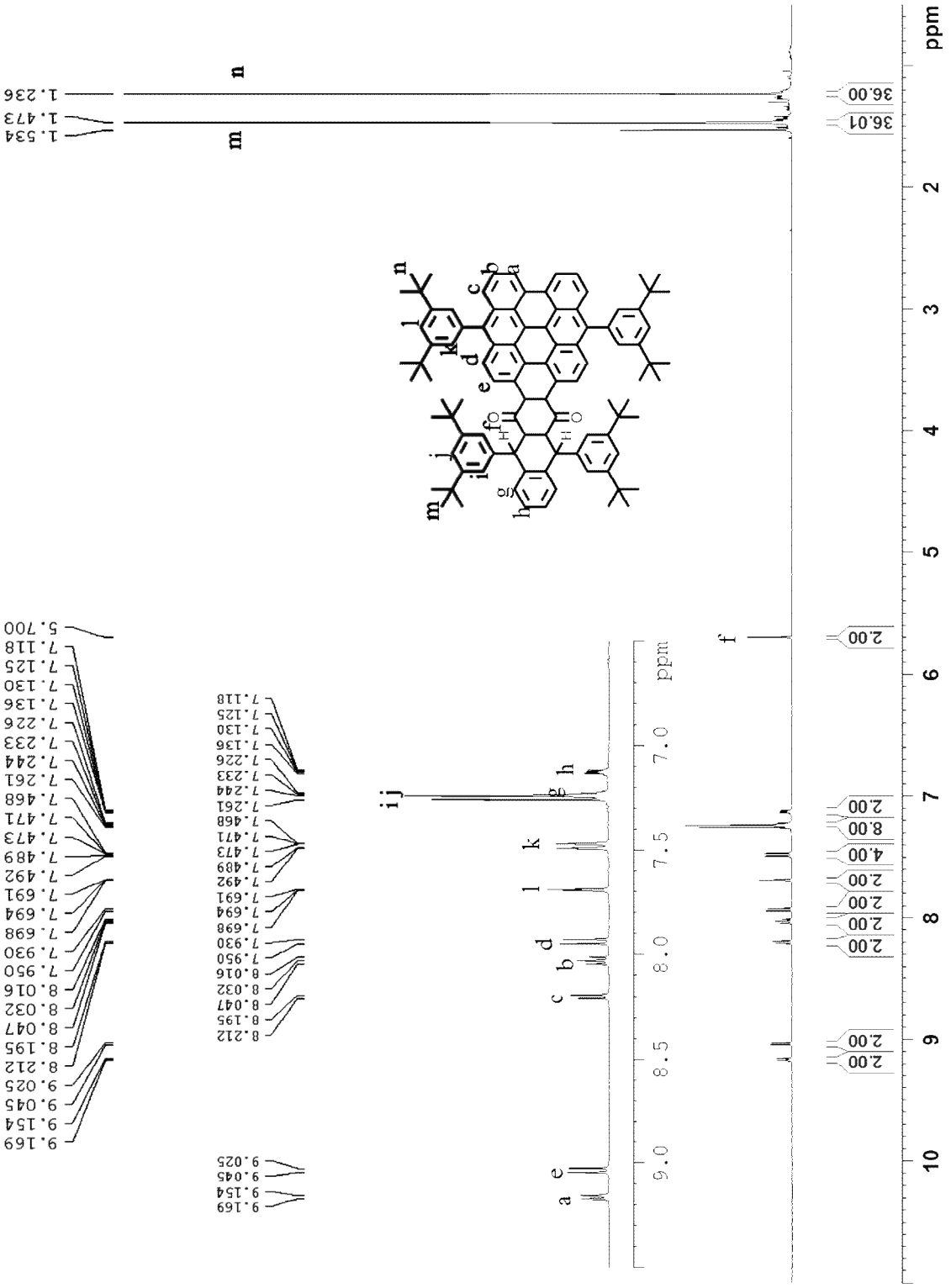

^{13}C NMR spectrum of compound **4-17** in $CDCl_3$ (125 MHz):

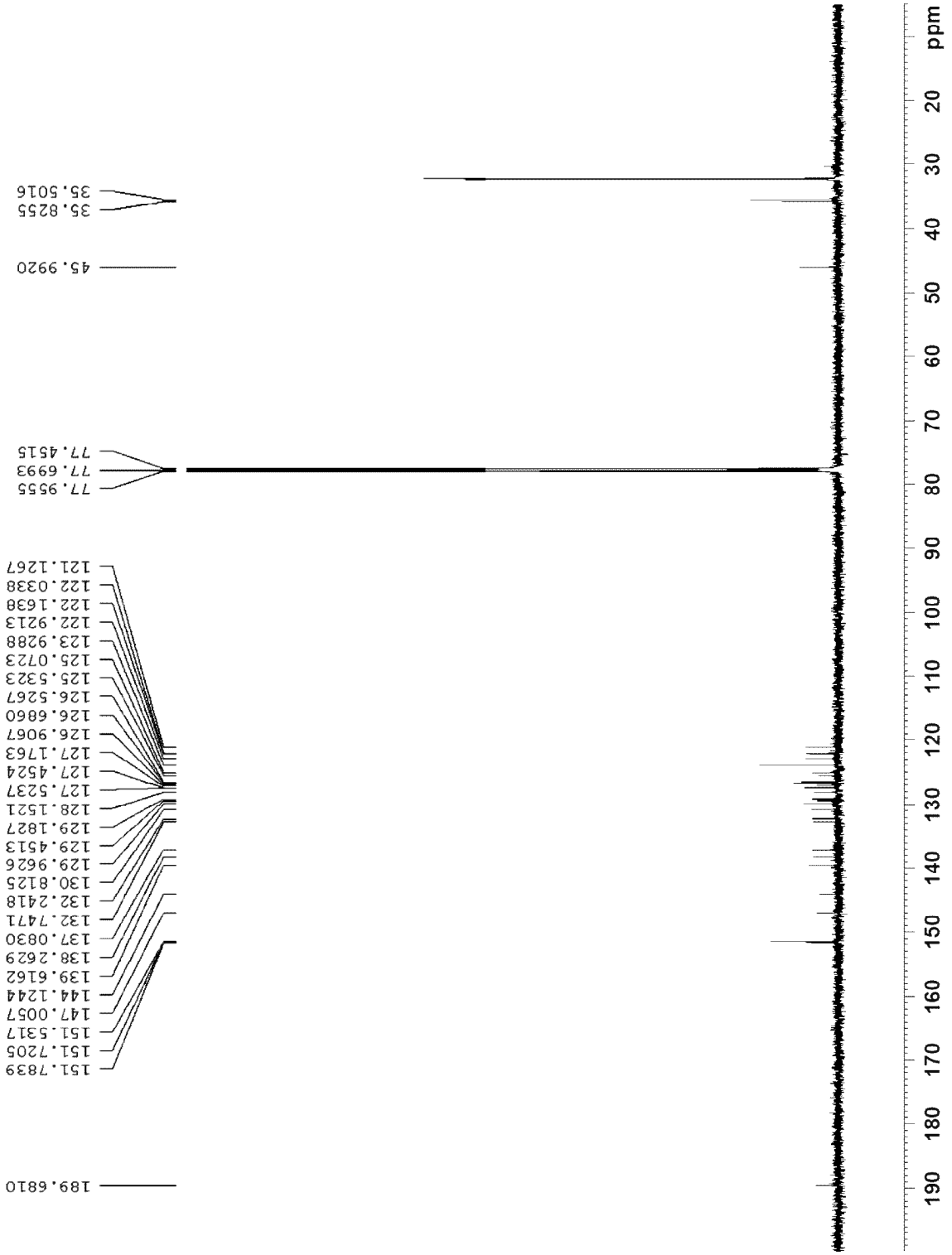

References

1. a) Wu, J.; Pisula, W.; Müllen, K. *Chem. Rev.* **2007**, *107*, 718–747. b) Dong, H.; Wang, C.; Hu, W. *Chem. Commun.*, **2010**, *46*, 5211–5222. c) Wen, Y.; Liu, Y. *Adv. Mater.* **2010**, *22*, 1331–1345. d) Anthony, J. E.; Facchetti, A.; Heeney, M.; Marder, S. R. *Adv. Mater.* **2010**, *22*, 3876–3892.

2. a) Fabian, J.; Nakanzumi, H.; Matsuoka, M. *Chem. Rev.* **1992**, *92*, 1197–1226; b) Qian, G.; Wang, Z. *Chem. Asian J.* **2010**, *5*, 1006–1029; c) Jiao, C.; Wu, J. *Curr. Org. Chem.* **2010**, *14*, 2145–2168.

3. a) Bendikov, M.; Wudl, F.; Perepichka, D. F. *Chem. Rev*. **2004**, *104*, 4891–4945. b) Anthony, J. E. *Chem. Rev.* **2006**, *106*, 5028–5048. c) Anthony, J. E. *Angew. Chem. Int. Ed.* **2008**, *47*, 452–483. d) Würthner, F.; Schmidt, R. *ChemPhysChem.* **2006**, *7*, 793–797.

4. a) Ito, K.; Suzuki, T.; Sakamoto, Y.; Kubota, D.; Inoue, Y.; Sato, F.; Tokito, S. *Angew. Chem. Int. Ed.* **2003**, *42*, 1159–1162. b) Meng, H.; Sun, F.; Goldfinger, M. B.; Jaycox, G. D.; Li, Z. G.; Marshall, W. J.; Blackman, G. S. *J. Am. Chem. Soc.* **2005**, *127*, 2406–2407. c) Meng, H.; Sun, F.; Goldfinger, M. B.; Gao, F.; Londono, D. J.; Marshall, W. J.; Blackman, G. S.; Dobbs, K. D.; Keys, D. E. *J. Am. Chem. Soc.* **2006**, *128*, 9304–9305.

5. a) Podzorov, Pudalov, V. M.; Gershenson, M. E. *Appl. Phys. Lett.* **2003**, *82*, 1739. b) Hepp, A.; Heil, H.; Weise, W.; Ahles, M.; Schmechel, R.; von Seggern, H. *Phys. Rev. Lett.* **2003**, *91*, 157406. c) Odom, S. A.; Parkin, S. R.; Anthony, J. E. *Org. Lett.* **2003**, *5*, 4245–4248. d) Sundar, V. C.; Zaumseil, J.; Podzorov, V.; Menard, E.; Willett, R. L.; Someya, T.; Gershenson, M. E.; Rogers, J. A. *Science* **2004**, *303*, 1644–1646.

e) Moon, H.; Zeis, R.; Borkent, E.-J.; Besnard, C.; Lovinger, A. J.; Siegrist, T.; Kloc, C.; Bao, Z.; *J. Am. Chem. Soc.* **2004**, *126*, 15322–15323. f) da Silva Filho, D. A.; Kim, E.-G.; Brédas, J.-L. *Adv. Mater.* **2005**, 17, 1072–1076.

6. a) Horowitz, G.; Fichou, D.; Peng, X.; Garnier, F.; *Synth. Met.* **1991**, *41*, 1127–1130. b) Lin, Y. Y.; Gundlach, D. J.; Nelson, S.; Jackson, T. N.; *IEEE Trans. Electron Devices* **1997**, *44*, 1325–1331. c) Herwig, P. T.; Müllen, K. *Adv. Mater.* **1999**, *11*, 480–483. d) Gruhn, N. E.; da Silva Filho, D. A.; Bill, T. G.; Malagoli, M.; Coropceanu, V.; Kahn, A.; Brédas, J.-L. *J. Am. Chem. Soc.* **2002**, *124*, 7918–7919. e) Afzali, A.; Dimitrakopoulos, C. D.; Breen, T. L. *J. Am. Chem. Soc.* **2002**, *124*, 8812–8813. f) Sakamoto, Y.; Suzuki, T.; Kobayashi, M.; Gao, Y.; Fukai, Y.; Inoue, Y.; Sato, F.; Tokito, S. *J. Am. Chem. Soc.* **2004**, *126*, 8138–8138. g) Park, S. K.; Anthony, J. E.; Mourey, D. A.; Jackson, T. N. *Appl. Phys. Lett.* **2007**, *91*, 063514. h) Jurchescu, D.; Popinciuc, M.; van Wees, B. J.; Palstra, T. T. M. *Adv. Mater.* **2007**, *19*, 688–692.

7. a) Marschalk, C. *Bull. Soc. Chim. Fr.* **1939**, *6*, 1112. b) Clar, E. *Ber. Dtsch. Chem. Ges. B* **1939**, *72*, 2137. c) Bailey, W. J.; Liao, C.-W. *J. Am. Chem. Soc.* **1955**, *77*, 992–993. d) Payne, M. M.; Parkin, S. R.; Anthony, J. E. *J. Am. Chem. Soc.* **2005**, *127*, 8028–8029.

8. a) Chun, D.; Cheng Y.;, Wudl, F. *Angew. Chem. Int. Ed.* **2008**, *47*, 8380–8385. b) Kaur, I.; Jia, W.; Kopreski, R. P.; Selvarasah, S.; Dokmeci, M. R.; Pramanik, C.; McGruer, N. E.; Miller, G. P. *J. Am. Chem. Soc.* **2008**, *130*, 16274–16275. c) Kaur, I.; Stein, N. N.; Kopreski, R. P.; Miller, G. P. *J. Am. Chem. Soc.* **2009**, *131*, 3424–3425. d) Qu, H.; Chi, C.; *Org. Lett.* **2010**, *12*, 3360–3363.

9. a) Tönshoff, C.; Bettinger, H. F. *Angew. Chem. Int. Ed.* **2010**, *49*, 4125-4128. b) Kaur, I.; Jazdzyk, M.; Stein, N. N.; Prusevich, P.; Miller, G. P. *J. Am. Chem. Soc.*

2010, *132*, 1261–1263. c) Purushothaman, B.; Bruzek, M.; Pakin, S. R.; Miller, A.-F.; Anthony, J. E. *Angew. Chem. Int. Ed.* **2011**, *50*, DOI:10.1002/anie.201102671.

10. a) Clar, E. *Polycyclic Hydrocarbons*, Academic Press: London, 1964; Vols. 1 and 2. b) Havey, R. G. *Polycyclic Aromatic Hydrocarbons*; Wiley-VCH: New York, 1997.

11. a) Pascal, R. A., Jr.; McMillan, W. D.; Engen, V. D.; Eason, R. G. *J. Am. Chem. Soc.* **1987**, *109*, 4660–4665. b) Smyth, N.; Engen, V. D.; Pascal, R. A., Jr. *J. Org. Chem.* **1990**, *55*, 1937–1940. c) Qiao, X.; Ho, D. M.; Pascal, R. A., Jr. *Angew. Chem. Int. Ed. Engl.* **1997**, *36*, 1531–1532. d) Schuster, I. I.; Cracium, L.; Ho, D. M.; Pascal, R. A., Jr. *Tetrahedron.* **2002**, *58*, 8875–8882. e) Duong, H. M.; Bendikov, M.; Steiger, D.; Zhang, Q.; Sonmez, G.; Yamada, J.; Wudl, F. *Org. Lett.*, **2003**, *5*, 4433–4436. f) Zhang, Q.; Divayana, Y.; Xiao, J.; Wang, Z.; Tiekink, E. R. T.; Doung, H. M.; Zhang, H.; Boey, F.; Sun, X. W.; Wudl, F. *Chem. Eur. J.* **2010**, *16*, 7422-7426.

12. Pschirer, N. G.; Kohl, C.; Nolde, F.; Qu, J.; Müllen, K. *Angew. Chem. Int. Ed.* **2006**, *45*, 1401–1404.

13. a) Herrmann, A.; Müllen, K. *Chem. Lett.* **2006**, *35*, 978–985. b) Weil, T.; Vosch, T.; Hofkens, J.; Peneva, K.; Müllen, K. *Angew. Chem. Int. Ed.* **2010**, *49*, 9068–9093. c) Zhan, X.; Facchetti, A.; Barlow, S.; Marks, T. J.; Ratner, M. A.; Wasielewski, M. R.; Marde, S. R. *Adv. Mater.* **2011**, *23*, 268–284.

14. a) Jiang, D.-E.; Sumpter, B. G.; Dai, S. *J. Chem. Phys.* **2007**, *127*, 124703. b) Jiang, D.-E.; Dai, S. *Chem. Phys. Lett.* **2008**, *466*, 72–75.

15. a) Zhang, X.-J.; Jiang, X.-X.; Luo, J.; Chi, C.; Chen, H.-Z.; Wu, J. *Chem. Eur. J.* **2010**, *16*, 464–468. b) Zhang, X.; Li, J.; Qu, H.; Chi, C.; Wu, J. *Org. Lett.* **2010**, *12*,

3946–3949. c) Yin, J.; Zhang, K.; Jiao, C.; Li, J.; Chi, C.; Wu, J. *Tetrahedron Lett.* **2010**, *51*, 6313–6315. d) Sun, Z.; Wu, J. *Aust. J. Chem.* **2011**, *64*, 519–528.

16. a) Clar, E. *Chem. Ber.* **1948**, *81*, 52–63. b) Kuroda, H. *J. Chem. Soc.* **1960**, 1856–1857. c) Arabei, S. M.; Pavich, T. A. *J. Appl. Spectrosc.* **2000**, *67*, 236–244.

17. a) Yao, J.; Chi, C.; Wu, J.; Loh, K.-P. *Chem. Eur. J.* **2009**, *15*, 9299–9302. b) Zhang, K.; Huang, K.-W.; Li, J.; Chi, C.; Wu, J. *Org. Lett.*, **2009**, *11*, 4854–4857. c) Li, J.; Zhang, K.; Zhang, X.; Huang, K-W.; Chi, C.; Wu, J. *J. Org. Chem.* **2010**, *75*, 856–863.

18. Clar, E. *Nature*, **1948**, *161*, 238–239.

19. Saïdi-Besbes, S.; Grelet, É.; Bock, H. *Angew. Chem., Int. Ed.* **2006**, *45*, 1783–1786.

20. a) Fort, E. H.; Donovan, P. M.; Scott, L. T.; *J. Am. Chem. Soc.* **2009**, *131*, 16006–16007. b) Fort, E. H.; Scott, L. T. *Angew. Chem. Int. Ed.* **2010**, *49*, 6626-6628.

21. a) Allen, C. F. H.; Bell, A. *J. Am. Chem. Soc.* **1942**, *64*, 1253. b) Ikawa, M.; Stahmann, M. A.; Link, K. P. *J. Am. Chem. Soc.* **1944**, *66*, 902. c) Lippert, A. R.; Kaeobamrung, J.; Bode, J. W. *J. Am. Chem. Soc.* **2006**, *128*, 14738–14739.

22. Clar, E. *The Aromatic sextet*, Wiely; London, 1972.

23. Licha, K.; Riefke, B.; Ntziachristos, V.; Becker, A.; Chance, B.; Semmler, W. *Photochem. Photobiol.* **2000**, *72*, 392–398.

24. a) Pommerehne, J.; Vestweber, H.; Guss, W.; Mahrt, R. F.; Bassler, H.; Porsch, M.; Daub, J. *Adv. Mater.* **1995**, *7*, 551–554. b) Chi, C.; Wegner, G. *Macromol. Rapid Commun.* **2005**, *26*, 1532–1537.

CONCLUSIONS

In this dissertation, synthesis, physical properties and applications of a series of bisanthene-based PAHs have been investigated in details. These bisanthene derivatives not only enrich the family of PAHs, but also provide new materials for organic electronics.

Firstly, besides the substitution by electron-withdrawing dicarboxylic imide groups at the zigzag edges and quinoidization along the short-axis, substitution at the active *meso*-positions of the bisanthene with either aryl or alkyne group have approved to be also an efficient way to achieve soluble and stable bisanthenes. Furthermore, these *meso*-substituted bisanthene not only have red shift to NIR spectral region with high to moderate fluorescence quantum yields, but also to be good potential materials for OFETs because of their amphoteric redox behavior with multistep reversible redox processes.

Secondly, **ODI-CN** with DLC character have been synthesized in a high yield using bisanthene as a stating material and exhibited a high electron mobility up to 0.1 cm^2/Vs under ambient conditions on OFETs, which resulting from the ordered π-π aggregation between the planar large cores. Till now, the application of **ODI-CN** is confined to OFTEs in our lab, and applying this good material on organic solar cell or other device as electron accepter will be another important project.

Thirdly, the bay regions of bisanthene have a diene character and this opens opportunities to do further functionalizations *via* Diels-Alder cycloaddition reaction at the bay positions of bisanthene. Therefore, the synthesis of a series of lateral extended

bisnathenes has been investigated. The prepared naphthalene-annulated bisanthenes showed a red shift in to NIR spectral ragion with moderate fluorescent quantum yields, non-planar twisted structures and also amphoteric redox behavior with multistep reversible redox processes. These properties may give a chance for these molecules to be potential organic materials for NIR OLED.

PUBLICATIONS

- **Jinling Li**[+], Jing-Jing Chang[+], Pheobe Huei Shuan Tan, Hui Jiang, Xiaodong Chen, Zhikuan Chen, Jie Zhang, Jishan Wu*. "*Disc-like 7,14-Dicyano-ovalene-3,4:10,11-bis(dicarboximide) as Solution Processible n-Type Semiconductor for Air Stable Field-Effect Transistors*" *Chem. Sci.* **2012**, *3*, 846-850. ([+] **equal contribution**)

- **Jinling Li**, Chongjun Jiao, Kuo-Wei Huang, Jishan Wu*. "*Lateral Extension of π-Conjugation along the Bay Regions of Bisanthene via Diels-Alder Cycloaddition Reaction*". *Chem. Eur. J.* **2011**, *17*, 14672-14680.

- **Jinling Li**, Kai Zhang, Xiaojie Zhang, Kuo-Wei Huang, Chunyan Chi, and Jishan Wu*. "*Meso-Substituted Bisanthene as Soluble and Stable Near-infrared Dyes*". *J. Org. Chem.* **2010**, *75*, 856-863.

- Kai Zhang, Kuo-Wei Huang, **Jinling Li**, Jing Luo, Chunyan Chi, and Jishan Wu*. "*Soluble and Stable Quinoidal Bisanthene with NIR Absorption and Amphoteric Redox Behavior*". *Org. Lett.* **2009**, *11*, 4854-4857. (**Highlighted by T. M Swager *et al.* in *Synfacts*, 2010, *1*, 0050**)

- Xiaojie Zhang, **Jinling Li**, Hemi Qu, Chunyan Chi, and Jishan Wu*. "*Fused Bispentacenequinone and Its Unexpected Michael Addition*". *Org. Lett.* **2010**, *12*, 3946-3949. (**Highlighted by T. M Swager *et al.* in *Synfacts*, 2010, *11*, 1245**)

- Hemi Qu, Weibin Cui, **Jinling Li**, Jinjun Shao and Chunyan Chi*. "*6,13-Dibromopentacene [2,3:9,10]-Bis(dicarboximide): A Versatile Building Block for*

Stable Pentacene Derivatives". *Org. Lett.* **2011**, *13*, 924-927. (**Highlighted by T. M Swager *et al.* in *Synfacts*, 2011, *5*, 0492**)

- Jun Yin, Chongjun Jiao, Kai Zhang, **Jinling Li**, Chunyan Chi, and Jishan Wu*. "*Synthesis of Functionalized Tetracene Dicarboxylic Imides*". *Tetrahedron Lett.* **2010**, *51*, 6313-6315.